The United Graduate School of Agriculture Sciences, Iwate University (UGAS)
Yamagata University, Faculty of Agriculture

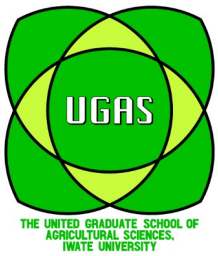

Doctoral Thesis

Evaluation And Identification Of Bark Beetle-Induced Forest Degradation Using RGB Acquired UAV Images And Machine Learning Techniques

Nguyen Ha Trang

Yamagata, Japan 2021

Table of Contents

Table of Figures

Index of Tables

List of Acronyms

CHM	Canopy Height Model
DL	Deep Learning
DSM	Digital Surface Model
DTM	Digital Terrain Model
ER	Error rate
FN	False negative
FP	False positive
GNSS	Global Navigation Satellite System
GPS	Global Positioning System
LR	Learning rate
nDSM	Normalized Digital Surface Model
RF	Random Forest
RGB	Red – Green – Blue
ROI	Region of Interest
SfM	Structure from Motion
TN	True negative
TP	True positive
UAV	Unmanned Aerial Vehicle

Acknowledgement

This thesis, and more importantly, my three year PhD, could not have been done without loads of support from professors, colleagues, family and friends. To achieve this milestone today, it is not only my effort but also the efforts, from everyone around me in supporting my research.

I would like to take this opportunity to express my gratitude to professor Larry Lopez, for his professional supervision on my academic work. There were numerous hours Larry spent advising me and keeping track with my research work and he often gave me invaluable guidance. His positive energy and professional support in research and in life made my three year PhD in Japan run smoothly and kept it interesting. The field trips I had with Larry and my lab-mates to many mountains and forests around Tohoku and Hokkaido will be forever in my memory. Special thanks to professor Yago Diez and his support in helping to develop the algorithm along with lots of discussion, patient and kindness, without which this work would not have the depth of results. I am thankful to Hase Shu sensei for always being supportive and kind since the first day I came to Yamagata University. Many thanks also to Tsu Ching-Ying sensei for listening to my research and professional suggestions. Thanks Arifa Rahman sensei for making effort to cease the problem of grading. Thanks to the UGAS dean Uemura sensei for keening listen to students and try to improve UGAS activities accordingly. Thanks to Gakumu staff, specially thanks to Sakuma san, for their friendly supports.

Many thanks to my colleague Herve for sharing the Autumn data and Sarah for helping to collect the Summer data of site 4 and 5. Thanks a lot to Nhung and Kohei for helping with the data annotation. Thanks to Mizuki for the Japanese translation of the summary and some scientific

papers. Thanks Moritake for helping with the algorithm. Thanks Cho kun for the first day waiting for me for six hours and picking me up from Sendai airport and for carrying all the furniture to get it ready before I came to the dormitory. I would also like to thank all of my lab-mates for cooking, eating, laughing, having fun and sharing unforgettable memories together during the last three years. Thanks a lot to all of friends in Tsuruoka (Tung, Luc, Thu and their families, Junko san and family, Shine chan, Bulbul, Ryoko san, Rosa, Agy, Marietta, Rahima, Kimani, Sarah, Alex) for never forgetting me in any gathering, it made me never felt lonely or bored even in this small city.

Special thanks to Rod Harbinson for helping with English correction in my paper and thesis, above all, for his countless efforts to support me during my study.

Last but not least, I would like to thanks my parents, my sister and my nephew for always loving me and giving me strong foundation to complete this study.

Summary in English

Recent increases in air temperature, high variability in precipitation, earlier springs and especially warmer winters, appear to be responsible for the increase in the frequency and virulence of insect outbreaks in forest ecosystems. Such a case has occurred in Zao Mountains between the prefectures of Yamagata and Miyagi in northeastern Japan, where an outbreak of bark beetle, that started in 2013, had by the year 2016, completely decimated fir (*Abies mariessi*) forest stands in areas close to the tree line and has slowly but steadily moved down the mountains to lower altitudes showing different degrees of infestation. The total area affected extends to hundreds of hectares that is impossible to evaluate in its entirety by field surveys. Satellite images provide an overview of the damage but because of its coarse resolution, it is not possible to observe in detail the infestation of single trees or the infestation patterns within the forest, hindering the understanding of insect outbreak spread within the forest, their rate of infestation and in general the evaluation of the spatial health status of forests within elevational gradients. However, with the recent advances in Unmanned Aerial Vehicles (UAV), it is now possible to obtain very high resolution of few centimeters, capable of detecting the shape of leaves or different levels of defoliation of branches of a single tree. Thus, based on the data collected from this new technology, this study is composed of two parts: tree health spatial evaluation using Random Forest technique and tree health identification using Deep Learning techniques.

In the first part, the impacts of terrain on the spread of bark beetles were evaluated using Random Forest technique to predict the occurrence of bark beetles and different health classes (healthy, sick, and dead) based on elevation, slope and aspect. Two predictive models were made:

the first model was used to predict two classes “healthy” and “infested” (“infested” includes sick fir and dead fir trees) to evaluate how the terrain characteristics can impact the spread of bark beetles in fir forests and the second model was used to predict three classes “healthy”, “sick” and “dead” in order to evaluate how the terrain affects sickness and mortality rate. The predictors from these models obtained high overall accuracy of 75% and 71% respectively, by considering only the terrain factors. This indicates that the terrain regulates the mountainous climate, and as such has strong influence on the emergence of bark beetle. The results illustrate that elevation which affects 60% of the accuracy of the predictive model is the most important factor that impacts the spread of bark beetles and leads to the mortality of trees. Slope and aspect were equally responsible for 20% each on the model accuracy. High elevation (1600 – 1700 m), steep slope (21.8^0 – 90^0), especially those facing west present the highest percentage of bark beetle infestation and faster mortality rate. This finding contributes to understanding the biological interaction between the host, the bark beetles and the habitat which may give some clues on future habitat selection of the host trees as a strategy to mitigate the impact of bark beetle infestation.

In the second part of the study, an automatic system was developed to classify all the fir trees in the forest into two classes, healthy and sick fir, based on UAV-acquired data and Deep Learning analysis. Considering detection alone, the results showed 85.70% success, while in terms of detection and classification, we were able to detect/classify correctly 78.59% of all tree classes (39.64% for sick fir). However, with data augmentation, detection/classification percentage of the sick fir class rose to 73.01% at the cost of the result accuracy of all tree classes that dropped 63.57%. Finally, the results of this study showed that the implementation of UAV, computer vision and DL techniques has the potential to significantly contribute to the development of a new

approach to evaluate the impact of insect outbreaks in forest. The methodologies and results from this study provide enhanced approach and opportunities for forest disturbance assessment which until now have been mainly based on field work and satellite images.

Summary in Japanese

（日本語）

近年の気温上昇、降水量の変動、春の始まりの早さ、とりわけ暖冬は森林生態系における昆虫の発生の頻度や病原性の増加の要因となっている。このような事例は日本北東部、山形県と宮城県の間に位置する蔵王山でも起こった。蔵王山では2013年から続いたキクイムシの発生により、2016年までに樹木限界付近におけるアオモリトドマツ(学名：*Abies mariessi*)が完全に枯死した。それ以来、昆虫のまん延度合いは異なるものの、ゆっくりだが着実に標高が低い位置まで影響が及んだ。影響が観察されたエリアの総面積は何百ヘクタールにも達し、全体を現地調査するのは不可能となっている。衛星画像は被害の概観を捉えることができる。しかし、その解像度は粗いことから、森林内や個体における被害状況を詳細に観察し解析するのは不可能で、昆虫の発生や被害の割合、標高における森林の空間的健康状態の全体評価を妨げている。しかし、近年無人航空機(UAV)により、センチメートル単位での高い解像度の画像を入手することが可能となった。それにより、葉の形状や各個体の落葉度合いを知ることができる。本研究論文は、この新しい技術により得られた情報に基づいて、①Random Forest技術を用いた木の健康状態の空間的評価、②ディープラーニング技術を用いた木の健康状態の同定、の2つの章を主体に構成された。これらはUAVから得られるRGB画像を用いて行った。

ひとつ目の章では、キクイムシの広がりに対する地形の影響をRandom Forest技術を用いて評価し，標高、傾斜、方位に基づき、キクイムシの発生と木の健康状態(健全・病気・枯死)を予測した。予測モデルを二つ作成し，一つ目のモデルは地形の特徴がどのようにアオモリトドマツの木におけるキクイムシの広がりに影響を与えるかを評価するために「健全木」と「被害木」（病気と枯死を含む。）の二つのクラスで予測した。二つ目のモデルは、地形がどのように昆虫の侵入割合と枯死率に影響を与えるのかを評価するために「健全」「病気」「枯死」の三つのクラスを予測するモデルを構成した。これらのモデルからの予測は地形要因だけを考慮して、各75%、71%の高い正確さを得ることができた。これは地形が山の天候を左右し、キクイムシの発生に強い影響を与えることを示唆する。これらの結果はキクイムシの広がりには標高が最も大きな要因であることを示し、また、これが木の枯死率を導き、予測モデルの正確性に60%寄与していることを示した。傾斜と方位はともに20%ずつ予想モデルに影響した。高い標高$(1600 - 1700\ \mathrm{m})$で急な斜面 $(21.8^0 - 90^0)$、特にこれらが西向きに面している場合においてキクイムシの被害が高く、枯死に至るまでのスピードが速い。この発見はキクイムシとその生息地との間の生物学的相互関係の解明に貢献する。これはキクイムシの被害を和らげる戦略として、今後のキクイムシの生息地の選択に何かしらのヒントを与えるかもしれない。

ふたつ目の章では、無人航空機により得られた情報とディープラーニングに基づき、森林内にある全てのアオモリトドマツの木を発見し、健全と病気の二つに分類分けするための自動システムが開発された。発見のみの正確性は87.50%であったが、発見と分類の正確性は78.59%で全ての木を発見して分類することができた$(病気の木に対しては39.64\%)$。しかしながら、データ量が増加すると病気の木の発見と分類の正確性は73.01%に上昇するものの、全ての木に対する分類の精度は63.57%にまで下がった。最終的にこの研究結果は、無人航空機技術とコンピュータ画像、ディープラーニング技術の導入は、森林における昆虫の発生による被害を評価するための新しい手法の確立に非常に大きく貢献することを示している。この研究結果は、今日まで主に現地調査と衛星画像によって行われている森林分布の伝統的評価手法を詳細さという観点において超えた。

Chapter 1

Introduction

1.1 Background

Bark beetles causing mass forest mortality have been seen in many fir and other coniferous forests for many centuries (Cole & Amman 1980; Pavlov et al., 2020). In recent years insect outbreaks in forests appear to be increasing in frequency and magnitude all over the world as a result of climate change (Agne et al., 2018; Jactel et al., 2019; Przepiora et al., 2020). Insect disturbed forests reported in 75 countries covering boreal, temperate and tropical regions reached 85.5 million hectares, of which 82% are found in temperate regions. This represents 3% of the total forest area in these countries (2807 million hectares) (van Lierop et al., 2015).

Forest worldwide has seen huge economical loss through timber values and tourism due to pest and insect infestations. Emerald ash borer on ash trees caused US$1 billion lost per year in the United States; cypress aphids killed trees in many countries around Asia, Africa and Europe that were worth more than US$50 million; European woodwasp costs Brazil about US$25 million yearly, etc, (FAO. 2011). From the ecosystem perspective, pests and insects are part of forest dynamics where all parts of forest interact with each other in beneficial ways. In fact, forest disturbance is considered as part of the forest ecosystem for forest succession and regeneration (Raffa, 2015; Linnakoski, 2019; Ciesla, 2001; Logan & Powell 2001). Especially in its native range, beetles usually infest fresh logs or trees that have already been weakened, contributing to the regeneration of new trees. Since the host trees usually play a crucial part of the forest ecosystem, providing food and habitat to nourish forest biodiversity (Keane & Arno 1993; Lanner, 1996; Keane, 2000; Logan & Powell 2001), aggressive insect outbreaks that lead to large mortality of healthy trees and rapid degradation on a large-scale, interrupt ecological habitats, disturb forest ecosystem and influence environmental functions (Arno and Hoff 1990; Keane, 2000). In some cases, the tree species could become extinct in some specific region or replaced by another species. For example, after fir disease in the 19th century, in the1880s and in the 1920s, silver fir (*Abies alba*) forest in central Europe (Saxony) and northeastern Bavaria became almost extinct in these habitats (Kandler, 1993). Beside that, the aesthetics and wilderness of forests often are destinations for diverse purposes for travelers such as sport, psychological health therapy, trekking and camping (Cole, 1990; Keane, 2000; Hansen et al., 2017). Thus pest infestation also places an adverse effect on the recreational functions of the forest regarding human health and the tourism economy. Therefore, it is important to understand the dynamic of forest degradation due to insect outbreaks. Identifying pest infestation in natural forest is not always for pest control. Sometimes chemical

treatments leave more negative effect than doing nothing due to various factors like personnel' skills, the characteristics of territories and the extent of infestation (Cole & Amman 1980). Quantifying the insect outbreaks is necessary to measure carbon emissions, biomass loss, biodiversity loss and economical loss and thus support strategies for pest prevention.

For that purpose, a feasible and economical method is required to assess pest infestation on a large scale at individual tree level. Unmanned Aerial Vehicle (UAV), commonly known as drone, have the advantage of providing data over a large coverage area with high resolutions up to centimeters can help to meet that demand. In recent years, UAV has become a popular remote sensing platform for data collection among forest managers and scientists due to its flexibility, time saving and low cost compared with field measurement and satellite based data. A commercial UAV can collect images over 100 hectares (Ha) of complex terrain forest in one to ten days with spatial resolutions up to centimeters, providing the ability to monitor every individual trees down to the detail of leaf structure. This makes it possible to monitor health conditions of trees based on the visualizations of canopies. Näsi et al., (2015), Safonova et al., (2000), Nguyen et al., (2021) pioneered using UAV visual data collection with deep learning techniques to classify tree health (healthy, sick, dead) based on different degrees of defoliation and obtained good results in term of accuracy. Another advantage of UAV is that the photos taken overlap each other, advancing 3D model of the forest with structure from motion (SfM) technique (Westoby et al., 2012; Frey et al., 2018) and calculate tree heights, making it a potential competitor to Lidar acquired data in terms of cost and processing (Zarco-Tejada et al., 2014; Mohan, 2017). Tree height measurement is essential for many studies to detect individual trees (Mohan, 2017; Brieger et al., 2019, Nguyen et al., 2021), calculate biomass (Lin et al., 2018; Jayathunga et al., 2019), estimate carbon emissions (Mlambo et al., 2017) and individual tree crown segmentation (Lim et al., 2015). With the easy on the mission characteristics, UAV has become an essential tool to collect data repeatedly assisting forest health change monitoring (Dash et al., 2017).

1.2 Objective

This thesis aims to explore the use of UAV images in combination with AI techniques and GIS in providing information and a better understanding on the patterns and dynamics of pest-induced forest disturbance. Through the thesis, I focus on the ecological behavior of *Polygraphus proximus,* how it has affected the forest structure and composition observed from a perspective different than the usual observation from the ground, in the case of this study a straight forward look from the top

of the canopies (so called nadir). From the imagery, the study aims to explore the possibility of AI techniques (i.e. deep learning and machine learning) and non-AI techniques (i.e. computer vision and GIS) to automatically convert remotely sensed data to annotated data for inventory, geographical analysis and visualization. Further I used the annotated data to analyze the pattern of infestation, in order to evaluate how the abiotic factors (i.e, elevation, slope, aspect) impact on the spread of bark beetles. The techniques and study frameworks I propose are intended to provide useful tools for forest experts and managers to actively manage the forest in ways that help to detect bark beetle infestation at an early stage and demand the least time and physical work. The study also provides a foundation for further studies on the automatic classification of the degree of infestation, forest health temporal change detection and early warning. Finally it will provide an insight about the pattern of infestation in Zao Mountain, Japan which is relevant to the ecological behavior of *P. proximus* bark beetles.

Thus the objectives of the thesis are the following:

1. To detect individual trees by means of Canopy height model (CHM) and computer vision techniques.

2. To classify healthy fir trees and sick fir trees using deep learning techniques.

3. To investigate the impact of terrain factors on the spread of beetles by means of GIS and Random Forest (RF) technique.

1.3 Structure of the Study

The study is composed of four main sections and illustrated in figure 1.1:

(I) The field work and the UAV data collection.

(II) The data pre-processing where all the structure from motion (SfM) data were created including dense point cloud, Digital Surface Model (DSM) and Orthomosaics.

(III) The data preparation where canopy height model (CHM), Digital Terrain Model (DTM), treetop annotation, tree crown annotation and GIS database of tree classes were created.

(IV) From the data prepared in the previous steps, the analysies were made and divided into two parts: chapter 2 where the evaluation of the impact of the terrain factors on the infestation of *P. proximus* using GIS and Random Forest were performed and chapter 3 where the individual tree detection and tree health classification using computer vision and deep learning were presented (**achieved with a publication:** Nguyen et al., 2021).

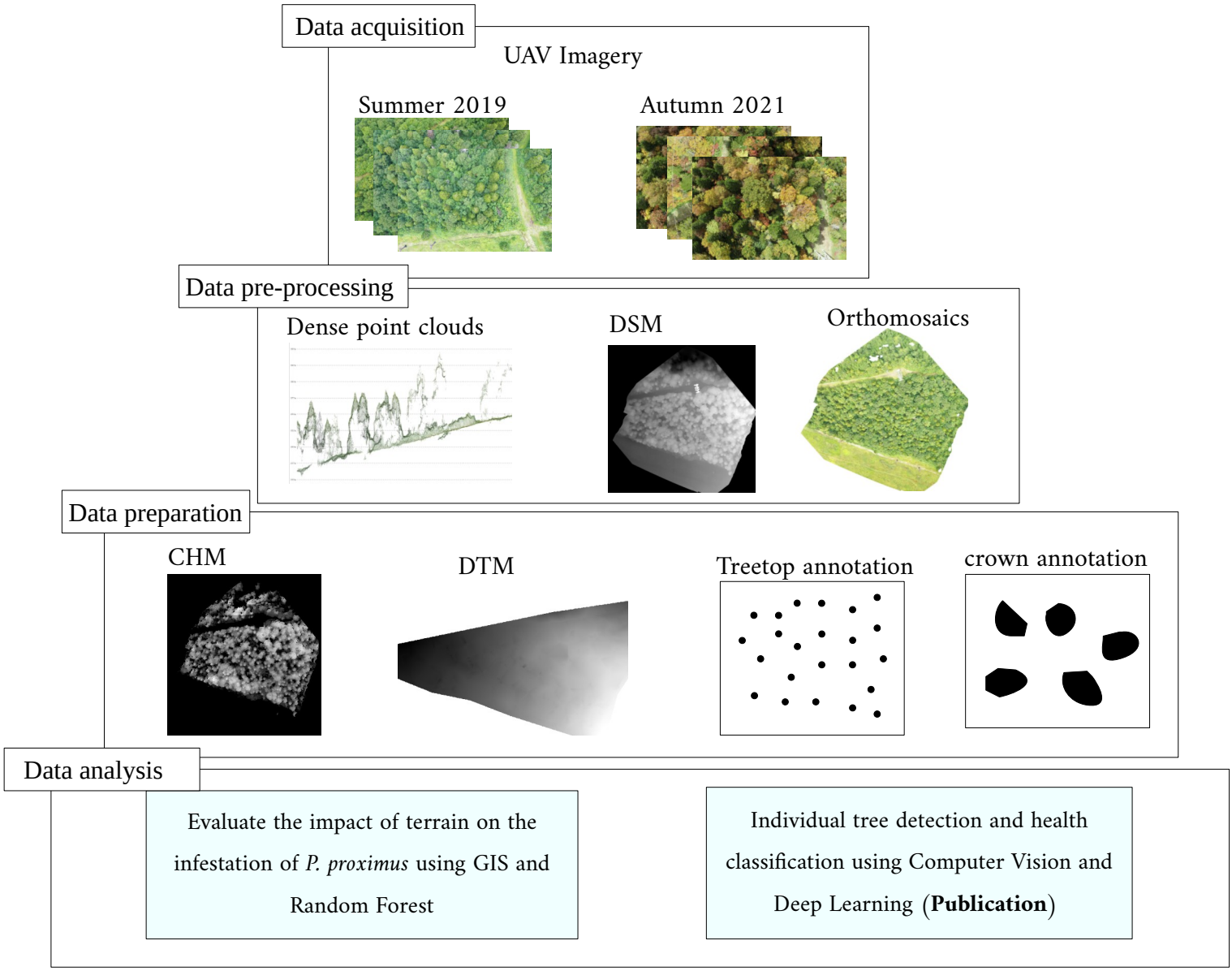

Figure 1.1: The structure of the study

1.4 Scope

The bark beetle induced tree mortality in Zao Mountains has been studied by the author through literature reviews and field work. Based on that perception, the study focused on the computational solutions for the automatic detection of sick trees through the visualization of its crown on the images and then to evaluate the forest health. These techniques are applicable and will assist forest staff and managers to manage the forest in an efficient and cost saving ways. However the scope of this study is not focusing on the identifying the biological/chemical causes of the tree mortality nor proposing solutions to stop or control the pests, but rather propose a sound methodology to evaluate forest health.

Chapter 2

Evaluate the Impact of Terrain on the Infestation of *Polygraphus Proximus* Using GIS and Random Forest

2.1 Introduction

2.1.1 Background Introduction

As a result of climate change, insect outbreaks are affecting forest ecosystems irreversibly around the world (Jactel et al., 2019; Agne et al., 2018; Przepióra et al., 2020). In Japan, *P. proximus* bark beetles (Nobuchi, 1979) have caused a big loss on the local economy in Northeastern provinces in term of timber production and tourism and has degraded the ecosystem of the forests which also host large mammal including Asiatic black bear and Sika deer. Since 2013, the Maries fir forests in Zao Mountain, Yamagata Prefecture, have been subjected to insect-induced disturbances. The mortality of the fir trees has been reported as the result of double insect attack. From 2013 to 2016, Tortrix moths (*Epinotia piceae*) infested trees and affected their capacity to perform photosynthesis. Since the trees had already been weakened by the previous attacks, *P. proximus* bark beetles colonized the trees and led to extensive tree mortality in 2016 (Saito & Chiba., 2017). This coniferous tree species has a high economic value for timber production but mainly as a local tourist attraction because of the way snow accumulates on its branches, creating giant shapes known as "Snow Monsters". The insect attacks led to tree mortality across an area of about 7 ha on the top of Zao mountain that has taken away the spectacular views of Snow Monsters (figure 2.1).

In its original habitats in Japan, *P. proximus* is known as a secondary pest, because it infests trees that are weakened from a primary pest species, from fire or from extreme environmental damage (EPPO, 2014). There have been several similar incidents of forest damages in Japan caused by this species of bark beetle. A *P. proximus* outbreak took place in 1955 in a Sakhalin fir forest stand in Hokkaido after a typhoon had wiped out the forest (Yamaguchi, 1963). In the period from 1998 to 1999, *Abies firma* forest in Mount Unzen, Kyushu island, witnessed a die-back after curculionid,

Parendaeus abietinus, weakened the trees in 1995. The process of die-back slowed down when the population of *P. abietinus* decreased from 1998 and *P. proximus* stopped colonizing healthy trees after that (Tokuda et al., 2008).

Figure 2.1: Dead trees on the top of Zao Mountains

Although the forest in Zao Mountain is a local tourist attraction and habitat of many tree species, plants and animal species, there is still not enough attention on the damage to the forest due to pest outbreaks here. Since the mortality only happens on some certain areas of the forest and at some certain ranges of elevation, it is worth understanding more thoroughly if there are any spreading patterns of the *P. proximus* regarding mountainous topography. The results will contribute to better understanding the relationship between the terrain and forest ecology. This will also place the first brick to build up a future early warning system of *P. proximus* in Japan.

The objectives of this chapter therefore include (1) to understand the infestation mechanism of *P. proximus* on fir trees particularly and of bark beetles on coniferous trees generally and; (2) to investigate the impact of elevation, slope and aspect on the spreading of *P. proximus.* These objectives will be fullfilled using a combination of (1) the review of literature and (2) GIS spatial analysis and machine learning technique (Random Forest) to find out how accurately the terrain factors solely can contribute to the prediction of *P. proximus* infestation in Zao Mountains.

2.1.2 The bark beetles - *Polygraphus proximus*

Four eye fir bark beetles *P. proximus* Blandford (*Coleoptera*: *Scolytidae*) is a bark beetle species fed on fir trees (*Abies*) and other conifers such as pine and spruce; however, only *Abies* species are being killed by this pest (EFSA, 2020). *P. proximus i*s distributed in all Japan's islands (Hokkaido, Honshu, Kyushu, Shikoku), the Korean peninsula, South-East China, Russia, West Siberia, East Siberia and the Far East (Tokuda et al., 2008; Baranchikov, 2010; Kerchev, 2014; EPPO, 2014; Kononov, 2016; EFSA, 2020). While *P. proximus* is considered as a secondary pest in its original habitats in East Asia and the Far East, it has been introduced into Russia via the trans-Siberian log transportation from the Far East and is classified as a high threat to healthy *Abies* forest stands in this region(Krivet and Kerchev, 2011; Kerchev, 2014; Kononov, 2016) (figure 2.2).

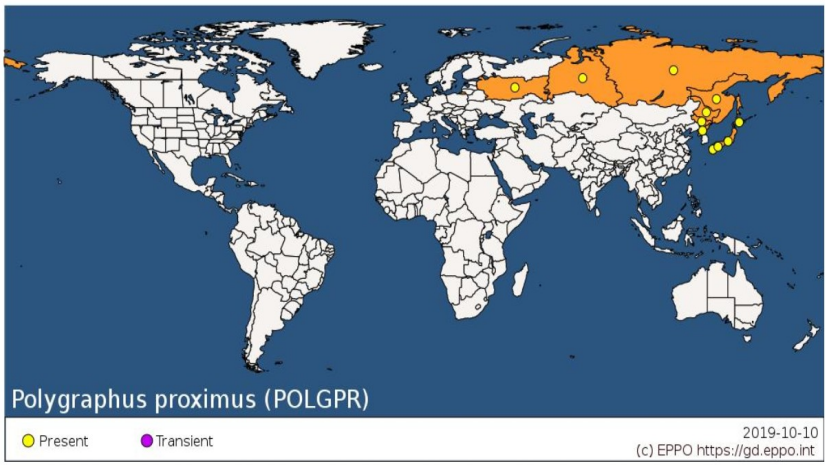

Figure 2.2: The distribution of P. proximus (Source: EPPO Global Database, https://gd.eppo.int/)

An average adult *P. proximus* has a broad body and is about 2.5-3.5 mm length. They are known as bivoltine species, which has 2 swarming periods per year. Every period begins when an adult beetle emerges from an infested tree and flies to infest another fresh log or weakened tree. The first emergence takes place in the early summer from May to July and the second emergence occurs at the end of summer from August to September (EPPO, 2014). A swarming cycle of a beetle begins when it lays eggs until a young adult emerges through the bark to fly off to another weakened tree. The ideal weather for the flights is when the average daily temperature in summer is above 15 ^{0}C, with calm wind and lack of precipitation (Krivets et al., 2019). During a long fly period, female beetles may lay eggs in several trees and the generations may overlap. Trees died within 2-4 years after the colonization (EFSA, 2020). In the early swarming period, male beetles pioneer fresh logs or weakened trees, bore entry holes and tunnels into the bark where they release pheromones to attract female beetles. The female beetles follow the pheromone, come into the tunnel, mate in the nuptial chamber and lay eggs in the maternal galleries (Kerchev, 2014; EFSA, 2020). Although it belongs to *Polygraphus* genus, *P. proximus* is a monogamous species. The mating system includes one

male and one female, which differs from many other species of the same genus (Kerchev, 2014; Köbayashi, 2020). Under the bark, the beetles construct egg (maternal) gallery systems that have double arms laying horizontally to the bark. In rare cases, one, three, four or five galleries of the same system are found (Kerchev, 2014; Köbayashi, 2020). Kerchev (2014) found 45.2 ± 15.3 eggs under each maternal system of *Abies Sibirica* while Yamaguchi (1963) showed that the average offspring of a female beetle on Shakhalin fir is 23. However Köbayashi (2020) suggests that it is actually 46 since there is only one female per gallery.

Trees infested by *P. proximus* show no specific sign in the early stage of the attack. Tree crown may appear healthy while its stems are covered by resin exuded at entry holes. In the early stage of the colonization, the crowns become partly defoliated in some branches showing a visual pale-green colour and when the whole crown turns red, the trees are completely colonized and die off (Baranchikov et al., 2010; EPPO, 2014; Krivets et al., 2015).

2.1.3 The host – Maries fir (*Abies Mariesii*)

Abies Mariesii (*A. mariesii*) is an evergreen tree of the Pinaceae family, Fir genus. It grows in subalpine zone(cold temperate rain forest) with high rainfall and heavy snow, providing more moisture to the soil which is important for the development of the trees. This fir species is native to Japan, known as "Aomori Todomatsu" (Aomori Abies Sachalensis), distributed in Northern Honshu island (1300 m to 1800 m) and in Central Honshu (1400 m – 2900 m) (Tanaka & Matsui, 2007) (figure 2.3). These trees usually grow from 10 to 20 m in height and occasionally can reach up to 30 m. The bark has a dark gray color and is smooth. The needles have round tips and fully cover the branches. *A. mariesii's* flower blooms around June, expressing visual bluish purple cylindrical

cones which grow upward while the male flowers grow downward. This species favours acid, neutral and moist soils. In Zao Mountains, *A. mariesii* provide the foundation which become a spectacular winter scenery of "snow monsters" (Juhyo in Japanese), attracting hundreds of thousands of tourists every year (figure 2.4).

Figure 2.3: *Abies Mariesii* distribution in Japan, the demonstration based on Iwaki & Totsuka (1959); Yoshihisa Suyama (2014)

Figure 2.4: Snow Monster in Zao Mountains (*source*: *https://www.thehiddenjapan.com/zao*)

2.1.4 The habitat – terrain (elevation, slope and aspect)

Since elevation, slope and aspect influence the forest composition and structure, so do the distribution of its dependents such as bark beetles. These factors are usually considered as important abiotic factors for the spread of bark beetles in literature.

Elevation

In their study about the outbreak of Mountain pine beetle, Logan and Powell (2001) showed the importance of elevation range in forming a suitable habitat for bark beetles. High elevation is home for many mountainous conifer species such as lodgepole pine, ponderosa pine and Douglas pine (Logan and Powell, 2001; Kurz et al., 2008; Safranyik and Carroll, 2007; Cole and Amman,

1980). The abundance of bark beetle, *P. proximus,* might be due to the increase in tree density at higher elevations. Lausch et al., (2011) through their 18 year models, concluded that elevation plays the most important role among other abiotic factors in the spreading of bark beetle *Ips. Typographus* in a Bavarian National Park where has the elevation rose from 700 m to 1450 m a.m.s.l. However Amman (1973) found that high elevation can become unsuitable for the survival of the beetles due to extreme cold weather. On the other hand Logan and Powell, (2001) stated that "high elevation" is a relative term since it can be high for an area but not for another. Since the dynamics of bark beetles depend on weather conditions, which vary in latitude and altitude. Therefore, it is important to find out at which elevation ranges of Zao Mountains, bark beetles *P. proximus* become more active and damaging.

Slope and aspect

The aspect toward the sun increase the abundance of bark beetles as the solar radiation helps to boost their productivity (Reid, 1962; Rasmussen, 1974). Additionally, the sun facing slopes dry the soil faster, which rots the roots and weakens the trees, making the trees become favorable hosts for bark beetles. Iwaki and Totsuka (1959) in their study in Mount Shimagare found that *A. mariesii* and *A. veitchii* trees on the gentle slopes facing south (SW-S-SE) in the elevation range from 2100 m – 2500 m a.m.s.l were more vulnerable to stripe withering. They found that the tall trees on this side of the slope exposed more to strong wind moving upward, which weakened the trees. This finding also agrees with the study of Yatoh (1958) (cited in Iwaki and Totsuka, 1959) in which the authors found the disease concentrated more on the SW slope of mount Myojo and mount Chosen. This latter study was conducted at the elevation of 1718 m, similar to Zao Mountains. Although

Lausch et al., (2011) found that elevation played an important role in the spreading of bark beetles in mountainous area through their 18 year models, they did not see the same effect for aspect and slope. Their conclusion also agreed with the study of Wulder et al., (2006) at the elevation range from 600 m to 800 m in which the author found that elevation, slope and aspect did not contribute to bark beetle infestation. However, these findings did not apply to the case of the national forest where the elevation range was 1000 m, in which the elevation, slope and aspect increase the accuracy of infestation model.

2.1.5 Study Sites

Zao Mountains is a volcanic mountain in Northern Honshu island, the main island in Japan, located on two prefectures Yamagata and Miyagi. The study sites are on the side of Yamagata prefecture (figure 2.5). The forests here are typical northern subalpine forests (Franklin et al., 1979; Okitsu, 2003) positioned on the latitude and longitude 38°09'10.5"N 140°25'18.4"E, covered by either pure conifer Maries's fir (*Abies Mariesii*) or mixed with other coniferous and deciduous species (*Acer tchonoskii, Acer japonicum, Acer nipponicum*, *Fagus crenata*, *Sorbaria sorbifolia*, and *Salix*) while the understory layer is covered by Sasa grass (a.k.a dwarf bamboo) which become an obstacle for the regeneration of the *A. mariesii* (Chiba et al., 2020) on the top of the Mountain. The average minimum and maximum annual temperature of the period from 2012 to 2014 was 9 degree and 14 degree respectively (Akihiko Sasaki, 2015).

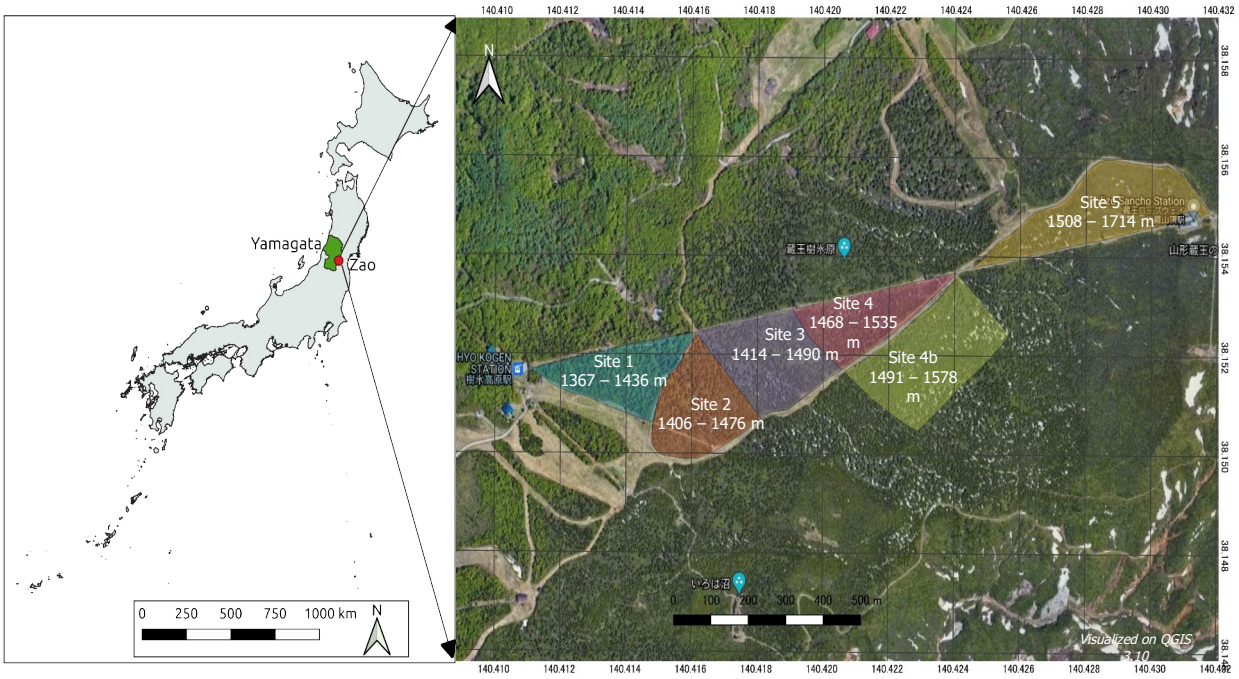

Figure 2.5: Study area

The study area covers an area of 24.5 ha of Zao Mountain, divided into 6 sites according to the paths within the forest following along the ropeway of cable cars which carry tourists to the top of the Mountain. The density of the forest is more than 280 trees per hectare. The altitude of terrain increases from 1367 m to 1714 m and witness an increase in the degrees of fir tree infestation, fir tree density and decrease in the deciduous density.

Site 1, approximately 4 hectares, has an elevation ranges from 1367 to 1436 meters above mean sea level (a.m.s.l) and has the highest composition of mixed forest, with a high proportion of deciduous trees. The forest on this site is dense with less space for fir trees to grow. The average canopy area of a deciduous tree in this site is about 50 m^2, but can reach up to 100 m^2 while the canopy of a full-grown healthy fir tree can reach18 ± 8 m^2.

A transition is observed in site 2 where the area near to the boundary with site 1 is mixed forest with big deciduous trees, while the rest of the site, the deciduous trees become smaller and fir

trees become dominant. On this site, a mature fir tree canopy is 30 ± 10 m^2. Site 2 covers an area of 4.77 hectares, altitude ranges from 1406 to 1476 meters a.m.s.l.

Site 3 covers 5.2 hectares of forest land, with elevation ranges from 1414 to 1490 meters a.m.s.l, completely dominated by fir trees. The deciduous trees are as small as bushes spread under canopy, lower than 4 meter height. An average mature fir tree on this site is about 20 ± 10 m^2.

Site 4 covers 4.0 hectares, the elevation ranges from 1468 to 1535 meters a.m.s.l, the forest composition is similar to site 3. However more sick fir trees are found in this site, especially in the group along the path under the ropeway. A full-grown fir at this site covers about 18 ± 10 m^2.

Site 4b is the largest site in the study covering more than 7 ha and presents the largest number of sick fir trees. Elevation ranges from 1491 to 1578 meters a.m.s.l. An adult fir tree on this site is about 14 ± 9 m^2.

Site 5 extends almost 7 hectares and the elevation ranges from 1551 to 1706 meters, it has the steepest slope, with the same forest structure as in site 3 and 4. This site separated from the other 5 sites by the intersection of the forest paths. More than 90% of fir trees here are dead. The trees at this site are known to be much smaller (Saito & Chiba, 2017) and much higher in density in comparison with the other lower sites. The forest composition and health condition of each site are presented in figure 2.6

Site 1

Site 2

Site 3

Site 4

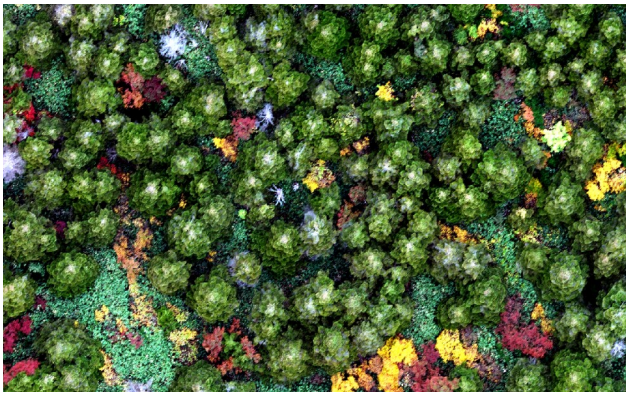

Site 4b

Site 5

Figure 2.6: Forest composition and health condition of each site

2.2 Material and Methods

2.2.1 UAV imagery collection and processing

Sets of images were collected using commercial RGB drone DJI Phantom RTK cameras at an altitude of 60 m in the autumn of 2021 on a cloudy day. The drone is equipped with Real Time Kinetic (RTK) GPS, providing a precise position in real time up to a centimeter level that helps all the orthomosaic images line up accurately while reducing Geo-referencing tasks for post processing. Before the flight, all the flight missions were pre-programmed on software DJI GS RTK (DJI Inc., Shenzhen, China). All the photos were captured with 90% side and front overlap, nadir view (the camera looks directly down). This setup provided post processing images with ground sampling distance from 1.3 – 1.5 cm/pixel for sites 2 to 5; 2.2 and 3.2 cm/pixel for site 1 and 4b respectively. which helps gather information on the detail of the crown.

The set of UAV raw photos were aligned to create dense point clouds and orthomosaics using structure from motion (SfM) technique (Ullman, 1979) on Metashape software (Agisoft) with batch process. The processing pipeline and corresponding parameters are described in table 2.1. The dense point clouds and orthomosaics were exported to *.las and *.tif extensions respectively projection UTM Zone 54N for Japan in order to prepare data for data pre-processing steps.

Table 2.1: UAV data processing in Metashape with corresponding parameters

Task	**Parameters**
Align photos	Accuracy: high
	Key point limit: 40,000
	Tie point limit: 4000
Build Dense Point Cloud	Quality: ultra high
	Depth filtering: mild
Build Mesh	Source data: dense cloud
	Surface type: Arbitrary
	Depth maps quality: ultra high
	Face count: high
	Depth filtering: high
Build Texture	Mapping mode: generic
	blending mode: mosaic
	texture size: 4,096
Build DEM	Source data: dense cloud
	Quality: ultra high
	Interpolation: enable
	Depth filtering: mild
	Reuse depth maps: yes
Build Orthomosaics	Surface: Mesh
	Blending mode: Mosaic
	Hole filling: yes

2.2.2 Data preprocessing

A layer "all_treetops.shp" was created in ArcGIS Pro to annotate all the treetops of six sites. All these treetops were then attributed with the site number, the orthomosaic number and the tree classes: healthy fir, sick fir, dead fir and deciduous. Since many deciduous trees from site 2 up to site 5 are too small and do not play the role of wind break or pest transmitting prevention, they were excluded from the annotation.

In order to calculate the tree density for the hotspot analysis, the study area was constructed into a grid of 30 m x 30 m fishnet. The grid size was chosen based on the distribution of infested trees. Smaller grid size results in only a few to zero infested trees in a grid cell while bigger grid size would result in too many trees within a cell and less cell unit for spatial pattern analysis.

2.2.3 Generate digital terrain model (DTM) for elevation, slope and aspect factors

2.2.3.1 *Generating digital terrain model*

The dense point clouds were used as input data in Fusion/LDV software (mcgaughey, 2009) to define ground points by function "GROUNDFILTER" was adapted from algorithm of Kraus and Pfeifer (1998). Table 2.2 describes an example script that was used to identify ground points from dense point cloud of site 5.

These bare-earth points were then interpolated to DTM in ArcGIS Pro using function "Las Dataset to Raster", serving as the medium to derive elevation, slope and aspect data across the site.

Table 2.2: Fusion script to identify the ground points for DTM generation

```
cd C:\
PATH C:\FUSION
set NOLASZIPDLL=



rem CATALOG
rem _____________________________
set input=E:\Work\STUDY\PhD\ZaoData\RTK\Z5
set output=E:\Work\STUDY\PhD\ZaoData\RTK\Catalog


catalog.exe /density:1,240,256 /coverage %input%\Z5_densecloud.las %output%\
Z5_catalog



rem GROUNDFILTER  #identify ground point
rem _____________________________
set input=E:\Work\STUDY\PhD\ZaoData\RTK\Z5
set output=E:\Work\STUDY\PhD\ZaoData\RTK\Ground


groundfilter.exe  /tolerance:0.0000001  /smooth:2  /median:3  /finalsmooth
%output%/Z5_ground.las 6 %input%/Z5_densecloud.las
```

2.2.3.2 *Generating elevation, slope and aspect*

After DTM was generated in Fusion/LDV software, elevation, slope and aspect was created in ArcGIS Pro software.

Elevation

In order to derive elevation data for each tree's location, the function "Extract Values to Points" in ArcGIS was used to extract values of DTM to all tree points of annotated layer "all_treetops.shp".

Slope

The "Slope" function in "3D Analyst" toolbox (ArcGIS) was used to create a Slope raster From the DTM. The results were chosen to be presented in degrees. The values of the raster were then extracted to tree points using function "Extract Values to Points".

Aspect

The "Aspect" function in "3D Analyst" toolbox (ArcGIS) was used to create an Aspect raster From the DTM. The values of the raster were then extracted to tree points using function "Extract Values to Points"

After the processing, the attribute table of the tree points includes the site number, the orthomosaic number, tree classes, elevation values, slope values and aspect values of each tree, as presented in figure 2.7

FID	Shape	tree_ID	Site	orthomosai	type_code	tree_type	AspectVal	Elev_Val	SlopeVal
1121	Point	8690	2	2	1	healthy fir	257.152	1471.82	10.1161
1122	Point	8691	2	2	1	healthy fir	252.989	1471.7	9.91113
1123	Point	8692	2	2	1	healthy fir	164.163	1472.14	41.4589
1124	Point	8693	2	2	1	healthy fir	245.124	1472.58	8.56064
1125	Point	8694	2	2	2	sick fir	339.382	1471.19	44.6531
1126	Point	8720	2	2	2	sick fir	236.997	1473.5	5.04295
1127	Point	8721	2	2	1	healthy fir	16.9275	1473.27	4.19623
1128	Point	8722	2	2	1	healthy fir	248.902	1473.24	5.9292
1129	Point	8723	2	2	1	healthy fir	250.514	1473.06	3.01122
1130	Point	8724	2	2	1	healthy fir	255.964	1473.18	1.44157
1131	Point	8729	2	2	1	healthy fir	337.484	1442.3	21.1324
1132	Point	8730	2	2	3	dead fir	337.459	1443.35	21.0123
1133	Point	8731	2	2	2	sick fir	323.711	1444.67	28.4315
1134	Point	8732	2	2	1	healthy fir	337.546	1439.18	21.0827
1135	Point	8733	2	2	1	healthy fir	337.484	1440.61	21.1324
1136	Point	8734	2	2	1	healthy fir	337.459	1442.08	21.0123
1137	Point	8735	2	2	3	dead fir	337.521	1440.29	20.9625
1138	Point	8736	2	2	2	sick fir	320.301	1440.81	22.8036
1139	Point	8737	2	2	2	sick fir	320.301	1442.18	22.8036
1140	Point	8738	2	2	4	deciduous	262.89	1441.53	19.3597
1141	Point	8739	2	2	1	healthy fir	262.536	1442.59	19.4131
1142	Point	8740	2	2	1	healthy fir	311.657	1435.57	32.1709
1143	Point	8741	2	2	1	healthy fir	303.551	1433.3	31.3322
1144	Point	8748	2	2	1	healthy fir	271.71	1445.81	5.83987
1145	Point	8750	2	2	1	healthy fir	256.409	1444.1	8.12999
1146	Point	8751	2	2	1	healthy fir	256.409	1443.71	8.12999
1147	Point	8884	2	2	2	sick fir	358.398	1438.67	23.5847
1148	Point	9175	2	2	1	healthy fir	257.768	1444.67	6.36981
1149	Point	9181	2	2	1	healthy fir	280.423	1435.21	29.2864
1150	Point	9183	2	2	1	healthy fir	297.639	1438.42	29.4272
1151	Point	9184	2	2	1	healthy fir	297.574	1436.99	29.3377

0 of 9,399 selected

Figure 2.7: The Attribute table of all trees presented in the study area

2.2.4 Climate data

The monthly climate data were downloaded from the website of Japan Meteorological Agency (https://www.data.jma.go.jp/obd/stats/data/en/smp/index.html) for Yamagata station (Station ID: 47588). The data include maximum and minimum temperature from 1889 to 2020, wind speed from 1951 to 2020, snow depth from 1953 to 2020 and precipitation from 1889 to 2020. The Yamagata meteorological station is located at an altitude of 153 meters a.m.s.l while the study sites on Zao Mountains has an altitude range of 1300 to 1800 meters, so the temperature of Zao Mountains is naturally lower than at Yamagata city. According to Watanabe (2015) the temperature difference between Yamagata city and Zao sancho ropeway station is 9 degrees. Thus the data were converted from Yamagata station (T_Y) to Zao Mountain (T_Z) based on the data provided in the literature of (Sasaki, 2015) in which the author provided monthly minimum and maximum temperature of Zao Mountain at 1350 m a.m.s.l from November 2011 to October 2014. The monthly difference in minimum and maximum temperature (d_T) between Zao Sancho ropeway station and Yamagata during the provided period were calculated as $d_T = T_Y - T_Z$ and the results are shown in table 2.3. The average difference ($avg.d_T$) in minimum and maximum temperature between Yamagata city and Zao Mountains were then calculated and presented in table 2.4. The monthly temperatures at Zao Sancho ropeway station were then calculated by subtracting the temperature at Yamagata station with the average difference between two stations $T_Z = T_Y - avg.d_T$. Table 2.4 shows that the difference in minimum and maximum temperature between two stations is 6.3^0C and 9.6^0C which is suitable with the conclusion of Watanabe (2015). The calculation was based on the assumption that the annual changes of temperature at two stations were linear. Since this study only used climate data to observe how it is regulated by the terrain factors and thus

factors and thus impact on the spread of bark beetles, I consider that this calculation is adequate. However an accurate measurement on different altitudes of Zao Mountain is recommended to satisfy the prediction results that are based on climatic conditions.

Since literature about the wind speed and snow depth data of Zao Mountain was not available, these data were used from Yamagata station to observe the trend from 1950 to 2020.

Table 2.3: Minimum and maximum temperature observed at Yamagata station (JMA) and Zao Mountain (Sasaki, 2015)

Year	Month	Zao Mountain (Sasaki, 2015)		Yamagata station (JMA)			
		Mean minimum temperature	Mean maximum temperature	Mean minimum temperature	Mean maximum temperature	Min difference	Max difference
2012	11	-2.7	2.2	4.3	11.7	7	9.5
	12	-8.4	-3.2	-1.6	4.2	6.8	7.4
2013	1	-10.6	-6.4	-4.4	2.2	6.2	8.6
	2	-11.3	-5.7	-4.6	2.4	6.7	8.1
	3	-6.9	1.3	-1.3	10	5.6	8.7
	4	-2.5	4.5	3.6	15.1	6.1	10.6
	5	5.1	13.0	10.1	22.8	5	9.8
	6	11.2	17.6	16.5	27.5	5.3	9.9
	7	14.9	18.5	20.6	28	5.7	9.5
	8	15.5	20.6	21.3	31.2	5.8	10.6
	9	11.6	17.8	16.4	26.7	4.8	8.9
	10	6.6	12.5	11.8	20.2	5.2	7.7
	11	-4.3	2.5	3.1	11.9	7.4	9.4
	12	-7.7	-4	-0.1	5.5	7.6	9.5
2014	1	-11.5	-6.2	-3.7	3.7	7.8	9.9
	2	-11.7	-7.1	-3.7	3	8	10.1
	3	-7.7	-2.2	0.1	7.9	7.8	10.1
	4	-2.9	5.1	3.8	17.1	6.7	12
	5	5.0	13.4	11.1	23.6	6.1	10.2
	6	10.8	16.9	17.2	27.1	6.4	10.2
	7	13.9	19.2	19.9	29.4	6	10.2
	8	15.6	20.6	21.3	30.2	5.7	9.6
	9	9.0	15.7	14.7	25.1	5.7	9.4
	10	4.5	11.7	8.7	19.2	4.2	7.5

Table 2.4: the average difference in minimum and maximum temperature between Yamagata city and Zao Mountain

Month	**1**	**2**	**3**	**4**	**5**	**6**	**7**	**8**	**9**	**10**	**11**	**12**	**Average**
Avg. min difference	7	7.4	6.7	6.4	5.6	5.9	5.9	5.8	5.3	4.7	7.2	7.2	6.3
Avg. max difference	9.3	9.1	9.4	11.3	10	10.1	9.9	10.1	9.2	7.6	9.4	9.5	9.6

2.2.5 Hotspot analysis

In order to analyse the hotspot of sick fir trees, The hotspot analysis – Getis-ord-Gi* statistics (Getis and Ord, 2010) was used. The method defines the clusters of high and low values based on the comparison of sick fir density within the neighbourhood area of a targeted grid cell with the whole study area (figure 2.8). In a monoculture of fir stand, the infestation was usually found within 50 m radius (Kerchev & Torchkova, 2018 (cited in EFSA, 2020)), thus a neighbourhood within 50 m from a targeted cell was chosen to identify hotspots of sick fir. The process was run on ArcGIS, with returning results in the form of its statistical significance at seven different levels.

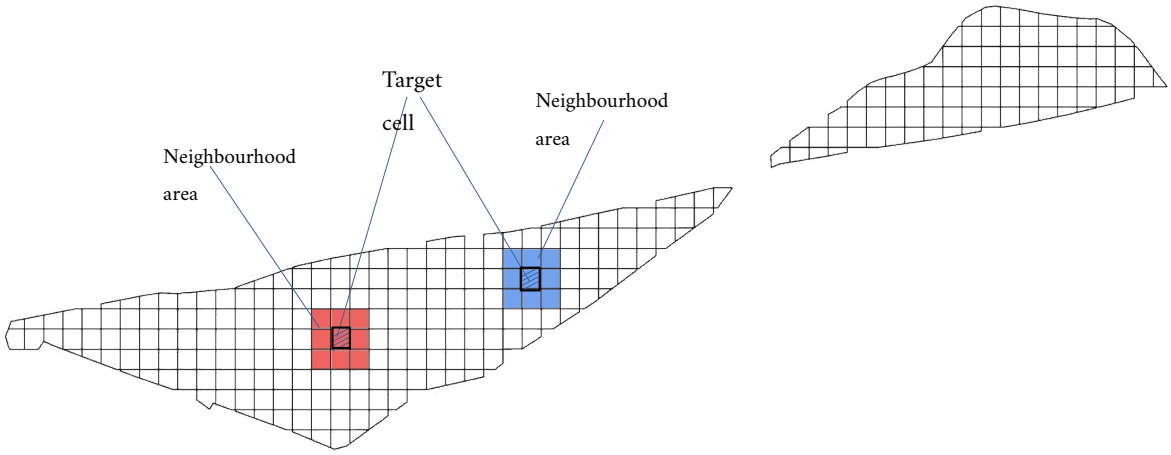

Figure 2.8: hotspot analysis with targeted grid cells and neighbourhood area

Table 2.5: interpretation the statistical levels of hotspots and coldspots

Gi_Bin	z-score and p-value	Interpretation
Hotspot – 99% Confidence	> + 2.58 and < 0.01	Cluster of high values with the probability less than 1%, 5% and 10% respectively the spatial pattern is a result of randomness
Hotspot – 95% Confidence	> +1.96 and < 0.05	
Hotspot – 90% Confidence	> +1.65 and < 0.10	
Not Significant		No statistical significant
Coldspot – 90% Confidence	> - 2.58 and < 0.01	Cluster of low values with the probability less than 1%, 5% and 10% respectively the spatial pattern is a result of randomness
Coldspot – 95% Confidence	> - 1.96 and < 0.05	
Coldspot – 99% Confidence	> - 1.65 and < 0.10	

2.2.6 Random forest

2.2.6.1 *Data preparation*

Random forest (RF) is a type of classification and regression model asembled from multi-decision trees. The model uses bootstrapping technique to randomly sample the dataset into many subsets of features (trees). The result is the average of all voting results from a large number of trees which helps to improve the model performance and prevent overfitting. RF has been used widely for its simplicity, ability to handle large datasets and accurate results most of the time (Breiman, 2001). By generating a large number of random trees from multiple variables, it aims to find the best model to perform the relationship between a dependent variable and independent variables. This relationship is illustrated through variable importance in which the role of each independent variable is permuted to evaluate how the permutation decreases the accuracy of the

model (Breiman, 2001). In this study, tree health conditions and the three terrain factors were used as dependent and independent variables.

The hypothesis of this study is that the topographic conditions promote or enhance the spread of *P. proximus* in the Mountain. Therefore, the study aims at predicting the fir tree health conditions from terrain factors using RF. For that, the random forest was used in two scenarios to predict tree health. The first scenario was to evaluate if there was an impact of terrain factors on the infestation of fir trees (figure 2.9). In this scenario, all the trees were classified into two classes: healthy fir and infested fir (*in this study infested fir is used to describe all fir trees that were and have been colonized by bark beetles including sick fir and dead fir*). The second scenario was to evaluate if there was a terrain pattern that enhanced the spreading – some places infested first showing the highest density of dead trees now while some places infested later and showing high density of sick trees. In this scenario, all the trees were classified into three classes: healthy fir, sick fir and dead fir (figure 2.10).

Besides that, two more scenarios that included deciduous trees were analysed to evaluate if there was an impact of terrain pattern on different tree types and health. These two scenarios are described in Appendix

Each scenario was run on python as the most popular platform for random forest algorithm and in ArcGIS with the function names "Forest-based Classification and Regression" to evaluate the potential of this software in this context of classification.

The data were split into two separate files for the training set (80 %) and test set (20 %). From the shape file of all the treetop points, the tool "Create Random Points" in ArcGIS was used to randomly select 7517 points out of 9399 points and exported them into a training and validation

set to build up a predictive model. The remaining 1882 points were then exported into a test set file. The voted predictive model was used to predict these 1882 points. The comparison of the prediction results and the ground truth was made in the form of a confusion matrix to evaluate the performance of the predictive model. Table 2.6 and 2.7 illustrate the percentage of each health class present in the training set and test set for each scenario. In this study RF algorithm was performed using the Scikit-learn library in Python, ensemble package (Pedregosa et al., 2011). For the detail of the Python code, refer to Appendix

Scenario 1: Two classes of tree health (healthy fir, infested fir)

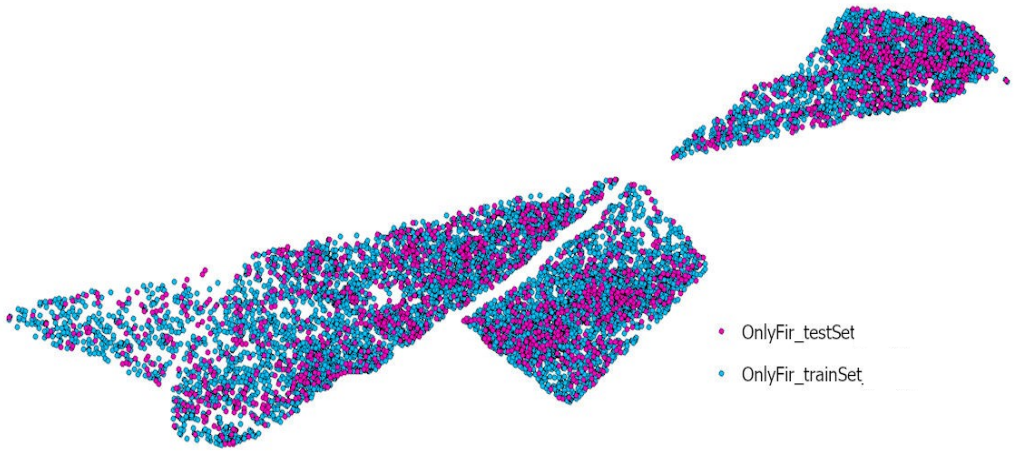

Figure 2.9: The distribution of training dataset and testing dataset for two classes of tree health (scenario 1)

Table 2.6: The percentage of each class of tree health contribute to training set and test set

	Training set (80 %)	**Test set (20 %)**
Healthy fir	3162 (45.2 %)	819 (46.8 %)
Infested fir	3834 (54.8 %)	932 (53.2 %)
Total	**6996**	**1751**

Scenario 2: Three classes of tree health (healthy fir, sick fir and dead fir)

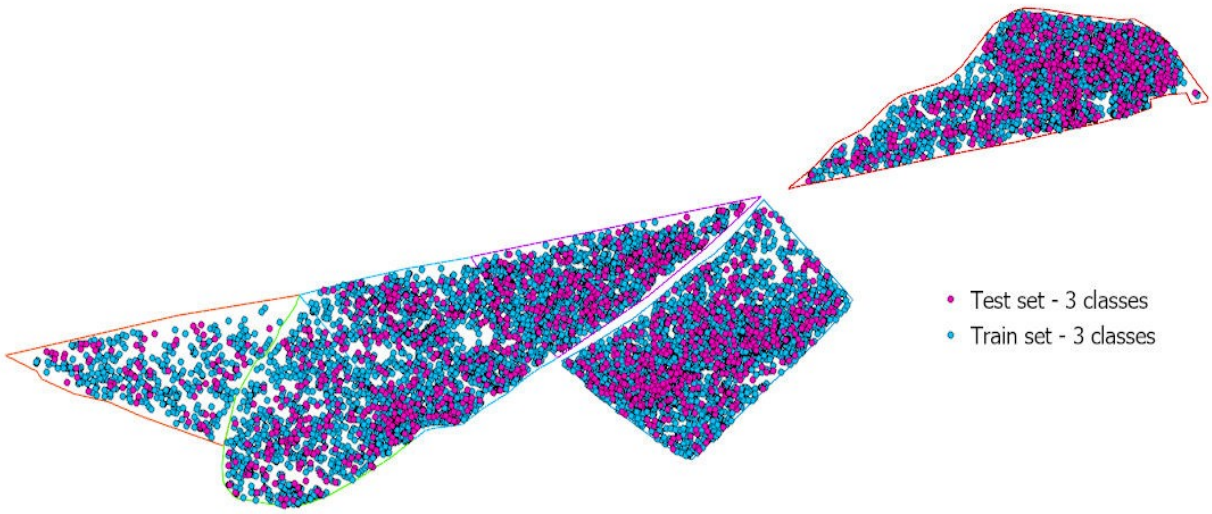

Figure 2.10: The distribution of training dataset and testing dataset for three classes of tree health (scenario 2)

Table 2.7: The percentage of each class of tree health contribute to training set and test set

	Training set (80%)	**Test set (20%)**
Healthy fir	3181 (45.5 %)	800 (45.7 %)
Sick fir	1714 (24.5 %)	431 (24.6 %)
Dead fir	2102 (30 %)	519 (29.7 %)
Total	**6997**	**1750**

2.2.6.2 *Validation*

The validation was performed on the test set using a confusion matrix (table 2.8) to compare the predicted result with the actual result. Three metrics of validation were used to evaluate the prediction result: precision, recall and F1-score. These metrics were calculated based on the number of true positive, false negative, false positive and true negative. Besides that, feature importance was calculated in order to evaluate the importance of each factor elevation, aspect and slope on the classification of tree types and health in Zao Mountains.

Table 2.8: Confusion matrix

		Predicted class	
		Tree	Not tree
Actual class	Tree	True positive (TP)	False negative (FN)
	Not tree	False positive (FP)	True negative (TN)

True positive: when the predicted result of a positive class is the same as actual class.

True negative: when the predicted result of a negative class is the same as actual class.

False positive: when the actual class is negative but the predicted result is positive.

False negative: when the actual class is positive but the predicted result is negative.

Accuracy: is the ratio of total correctly classified samples over the total samples. Accuracy is not a good indicator if the data is imbalanced.

$$\text{Accuracy} = (\text{TP}+\text{TN})/(\text{TP}+\text{FP}+\text{FN}+\text{TN})$$

Precision: is the ratio of true positive results over total positive results. The precision answer the question, for example: among all of the trees are predicted as sick, how many are actually sick?

$$\text{Precision} = \text{TP}/(\text{TP}+\text{FP})$$

Recall: Recall is also known as sensitivity, it is the ratio of true positive over the total of true positive and false negative. Recall help to answer the question, for example: of all the trees are actually sick, how many are predicted as sick? $\text{Recall} = \text{TP}/\text{TP}+\text{FN}$

F1-score: F1-score is a metric that works for both balance and imbalance data. The measurement is the weighted average of precision and recall. If both precision and recall are high, F1 is high; if

either precision and recall is low, F1 is low. F1 helps to answer how good the classifier can predict a class. Thus, F1-score is useful to compare the performance of different classifiers.

$$F1\ Score = 2*(Recall * Precision) / (Recall + Precision)$$

2.3 Result

2.3.1 Tree inventory

A total of 9399 trees in the forest were found from the images and were annotated to convert it into GIS data. These are trees which are full canopy and partial canopy visible, including seedling, sapling and mature fir trees. In a total of six sites there are 8747 fir trees and 652 deciduous trees presenting 93% and 7% of all trees respectively. This composition again confirms the dominance of Maries fir species in Zao Mountains. Of all the fir trees, 3981 are healthy, 2145 are sick and 2621 are dead (table 2.9), equal to 42.4%, 27.9% and 22.8% respectively (figure 2.11).

Table 2.9: Tree types inventory

Tree type	**Site 1 (4 ha)**		**Site 2 (4.77 ha)**		**Site 3 (5.2 ha)**		**Site 4 (4.04 ha)**		**Site 4b (7.05 ha)**		**Site 5 (6.9 ha)**		
	Number of trees	Density	Number of trees	Density	Number of trees	Density	Number of trees	Density	Number of trees	Density	Number of trees	Density	Total
Healthy fir	352	88.8	711	149	933	179.4	743	183.9	1227	174	15	2.2	3981
Sick fir	23	5.8	186	39	368	70.8	413	102.2	1017	144.3	138	20	2145
Dead fir	10	2.5	24	5.03	34	6.5	72	17.8	194	27.5	2287	331.4	2621
Deciduous	410	102.5	154	32.3	43	8.3	24	5.9	14	2	7	1	652
Total	**798**	**199.5**	**1075**	**225.4**	**1378**	**265**	**1252**	**309.9**	**2452**	**347.8**	**2447**	**354.6**	**9399**

Site 1 is a mixed forest, where more than 50% of trees are full-growth deciduous, there are only 385 fir trees in this site with the density at 97.1 trees/ha. Of which 352 trees are healthy fir, 23 trees are sick and 10 are dead.

Site 2, the number of fir trees on this site is 921 trees, 193 trees/ha, almost double site 1. While the density of healthy fir trees and dead fir trees increase doubles from site 1, the number of sick fir trees increase almost seven times up to 39 trees/ha.

Site 3, the density of fir trees also increases to compare with site 1 and site 2. This is because there are almost no deciduous trees now, only 43 small deciduous trees are found. Since fir trees become dominated, the risk of infestation is increased. The total number of fir trees is 1335 with a density of 256.7 trees/ha, among them 933 are healthy, 368 are sick and 34 are dead, this is equal to the density of 179.4, 70.8 and 6.5 trees/ha respectively.

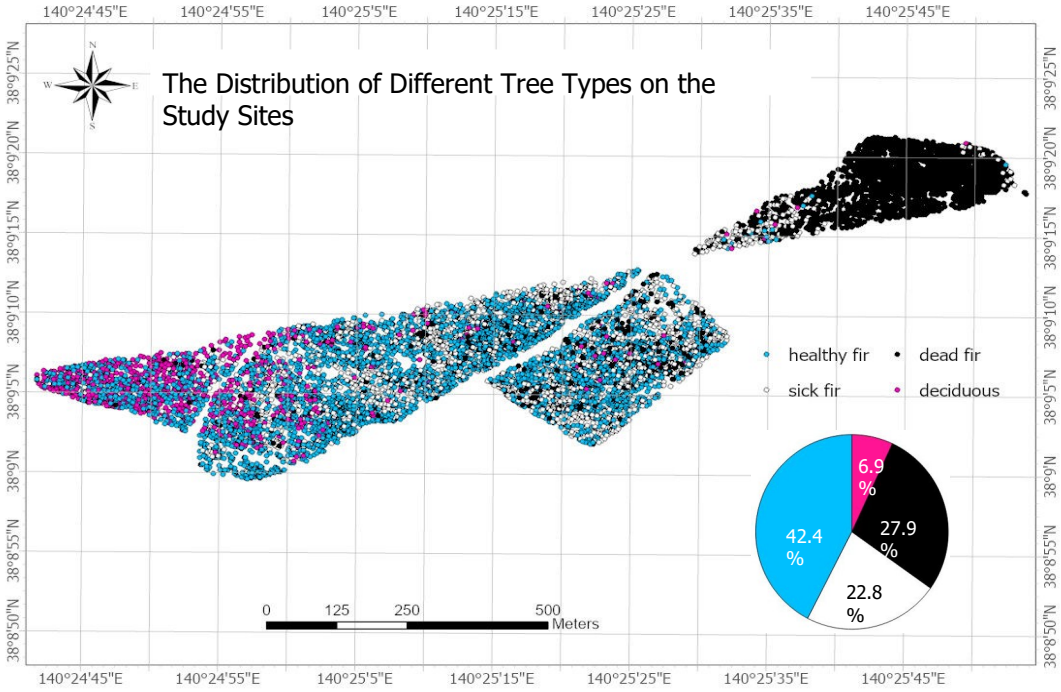

Figure 2.11: Map of the distribution of different tree types on the study sties

The density of fir trees in site 4 continues to increase to 310 trees/ha. The density of healthy, sick and dead fir is as high as 183.9, 102.2 and 17.8 trees/ha respectively.

Site 4b, while the density of sick fir and dead fir trees increases to 144.3 and 27.5 trees/ha respectively, the density of healthy fir trees slightly decreases to 174 trees/ha in comparision to site 4. This shows a sign of the decreasing tree health.

Site 5, the number of fir trees and density are almost similar to site 4b. However, this is a site with the highest density of dead trees in which the density of healthy and sick fir are only 2.2 and 20 trees/ha respectively while it is 331.4 trees/ha for dead fir.

While the density of healthy fir does not change much from site 2 to site 4b, a significant increase on sick fir and slight increase on dead fir among these sites show continuous degradation on forest health condition following the high mortality rate in site 5 (figure 2.12).

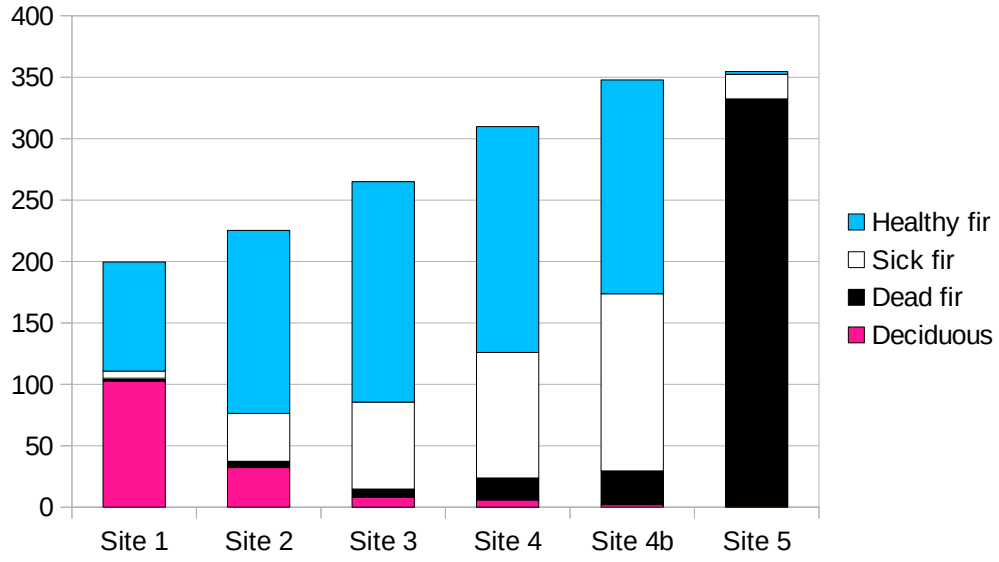

Figure 2.12: The distribution of different tree types in the study sites

2.3.2 The distribution of fir tree health according to the change of terrain

2.3.2.1 *Elevation*

The elevation of these six sites ranges from 1368 m to 1714 m (figure 2.13). The elevation 1500–1550 meters has the highest number of sick fir trees. This is also the elevation range that has

the highest number of fir trees, about 2400, followed by the elevation ranges 1450–1500 m with 2200 trees. The elevation range 1400–1450 m and 1550–1600 m have a similar number of fir trees, 800 and 900, respectively, however at the elevation range of 1550–1600 m the number of sick and dead firs are three times higher than at the elevation 1400–1450 m. At the elevation range 1600–1700 m most of the trees are dead (figure 2.14).

2.3.2.2 *Slope*

The slope with an inclination of 16.7^0–21.8^0 has the highest number of fir trees, approx. 1600 trees, followed by the slope with an inclination of 21.8^0–31^0, with 300 trees less. However, the slope with 21.8^0–31^0 has the highest number of dead fir, 528 trees and the second highest number of infested fir, 819 trees while these numbers are 471 and 870 respectively for the slope 16.7^0–21.8^0.

Other slope ranges that have more than 300 dead trees are 11.3^0–14^0, 14^0–16.7^0 and 31^0–45^0 with 344, 317 and 342 trees respectively.

Although the slope 45^0–90^0 has a low number of fir trees (534 trees), it also has a high number of dead trees (255). This is opposite in the case of slope 5.71^0–8.53^0. This slope has a higher number of fir trees than the former one, 694 trees, but it has only 94 dead trees and 175 sick trees. (figure 2.14)

2.3.2.3 *Aspect*

Aspect shows a very clear effect on the fir tree growth and infestation. Most of the fir trees grow on the west slopes, including the West, Southwest and Northwest facing slopes. The West slope has the highest number of fir trees, accounting for 2762 trees, while dead trees and sick trees

account for 1032 and 621 respectively. The Southwest and Northwest slopes have similar numbers of fir trees, 2012 and 1974 respectively, however the Southwest slope has almost 1.5 times higher number of dead trees than the Northwest slope.

In contrast with the west slopes, the east slopes (Northeast, East and Southeast) have the lowest number of fir trees at an average of approx. 250 trees on each aspect. (figure 2.14)

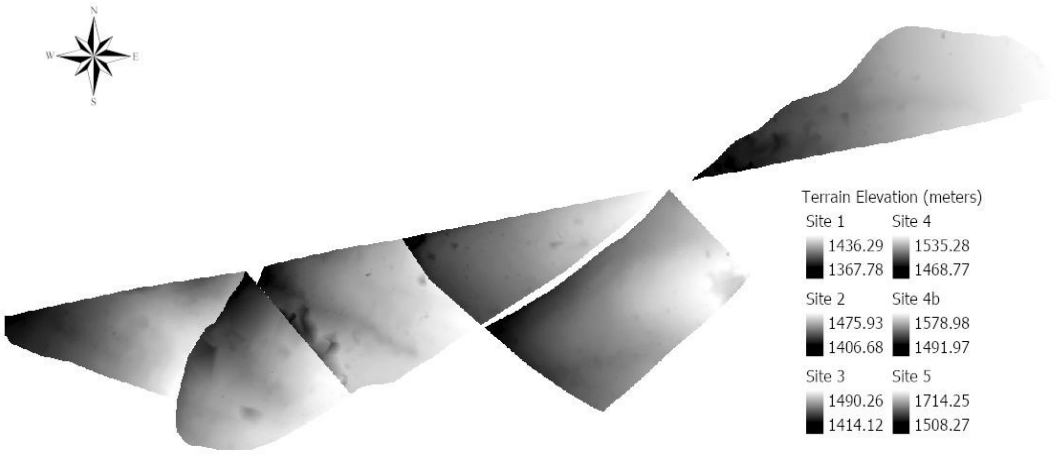

(a)

(b)

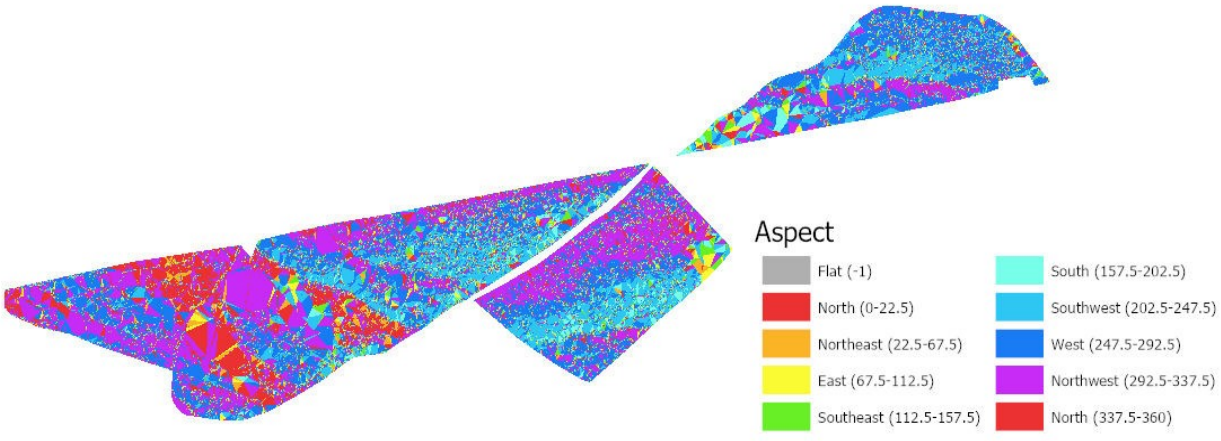

(c)

Figure 2.13: Three terrain factors (a) elevation, (b) Slope, (c) aspect

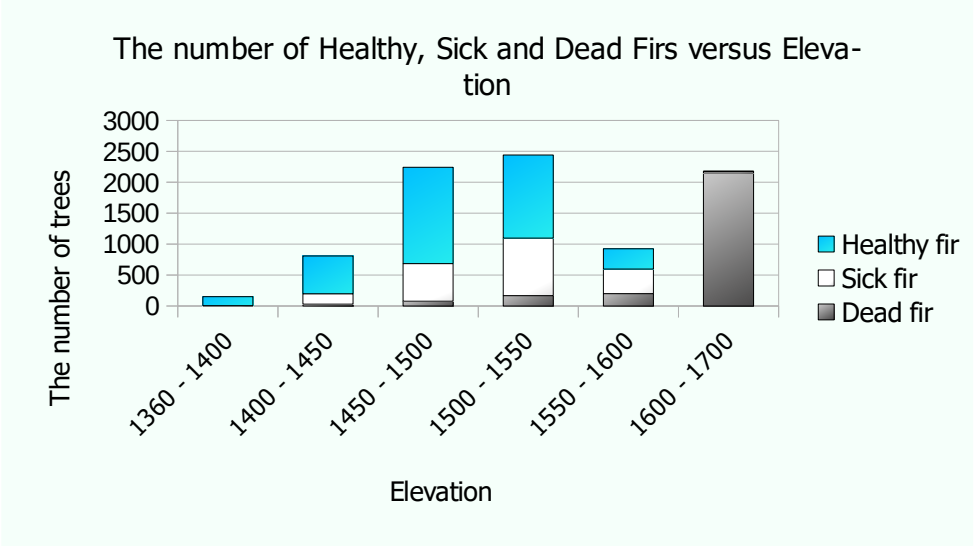

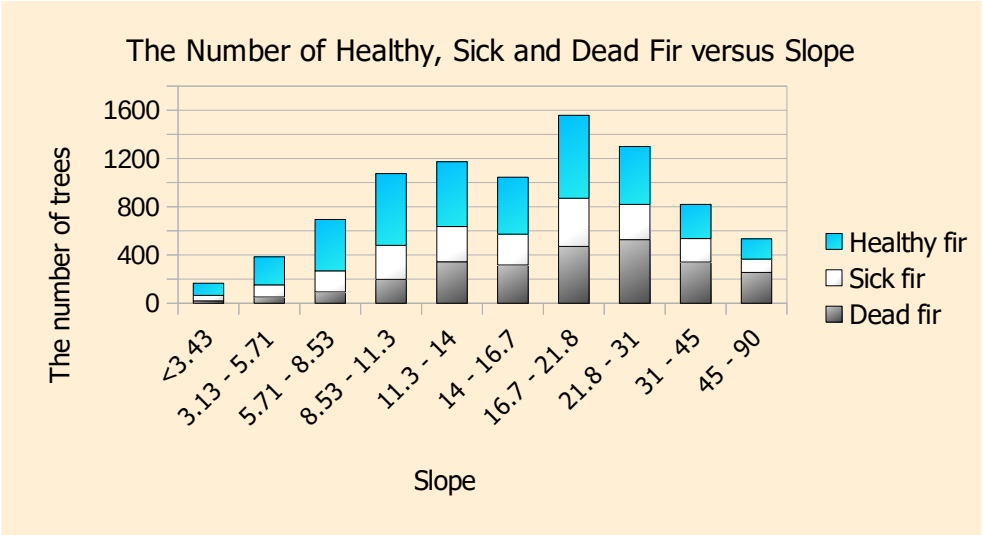

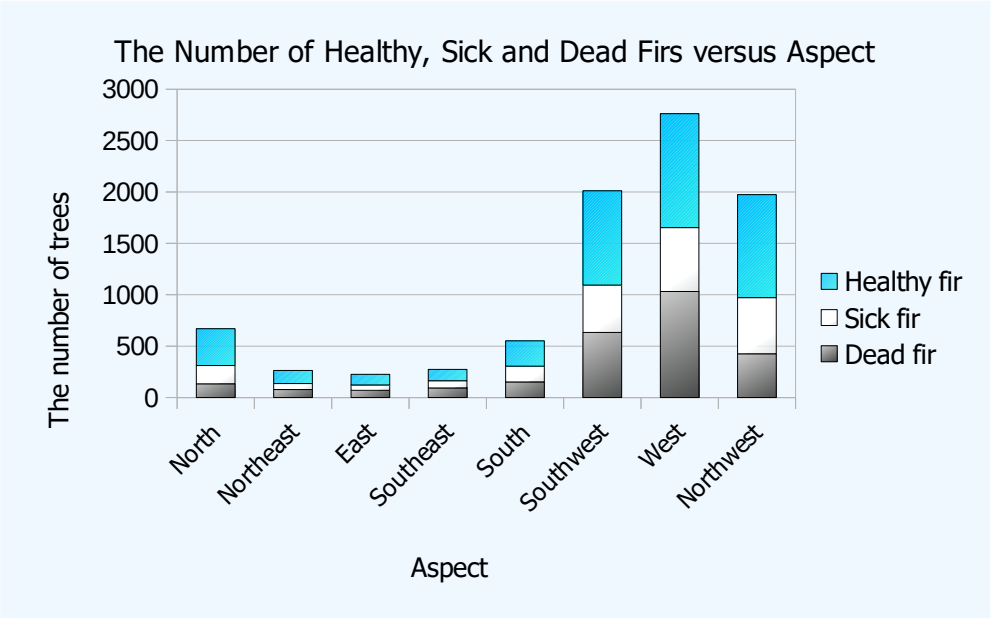

Figure 2.14: The distribution of elevation, slope and aspect in the study area

2.3.3 Hotspots of sick fir

In the hotspot analysis, the study focuses only on sick fir in order to know where the concentration of sickness is and visualize the location that the forest health will more likely be degraded in the next 2-4 years of infestation. Figure 2.15 shows the hotspot results that was calculated from sick fir density within 50 m of the vicinity.

The hotspots of sick fir are highlighted in site 4 and especially 4b. Most of the significant hotspots area (p = 0.01) are located at the elevation 1500–1550 meters (figure 2.16), mid range of slope face West direction from 8.53–21.8, especially from 16.7^0 to 21.8^0.

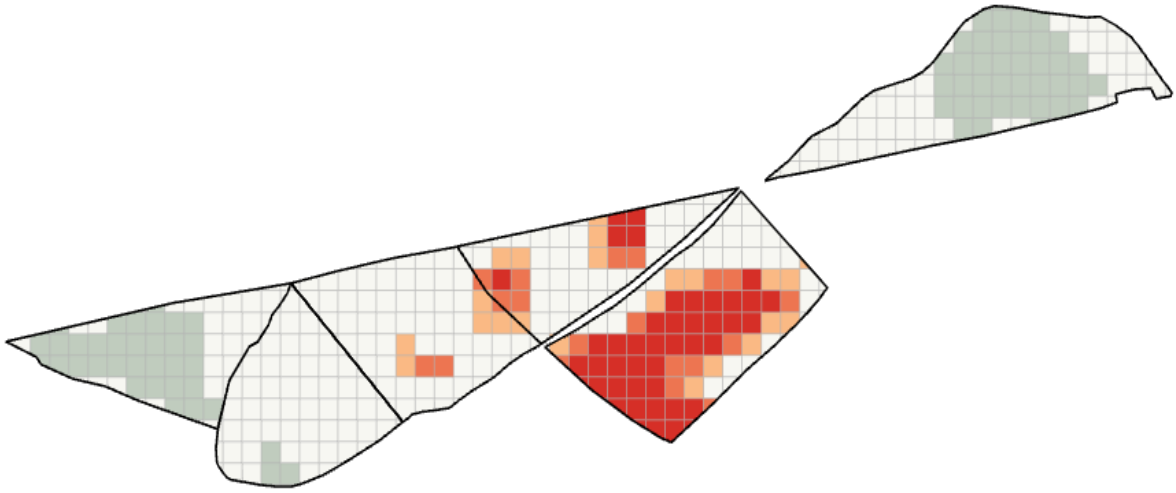

Figure 2.15: The hotspots of sick firs

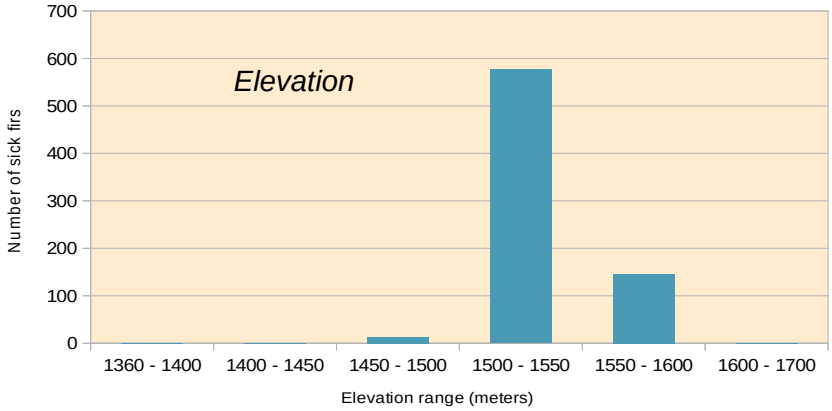

(a)

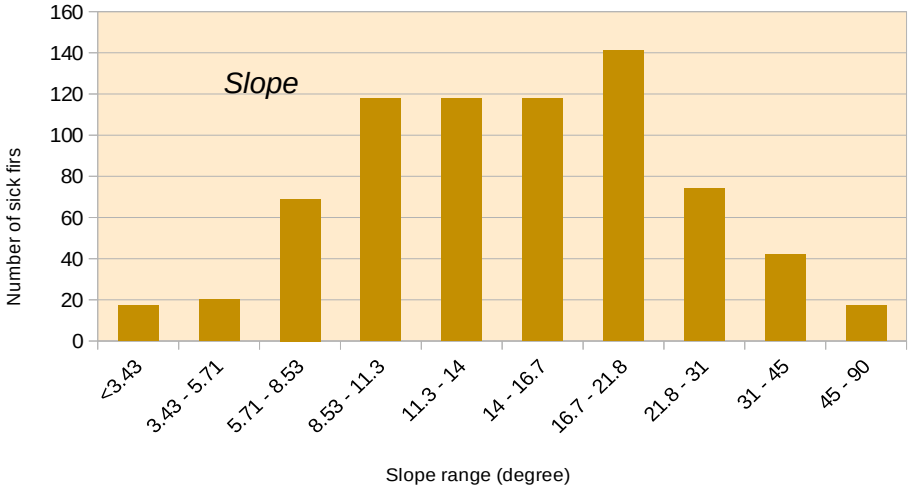

(b)

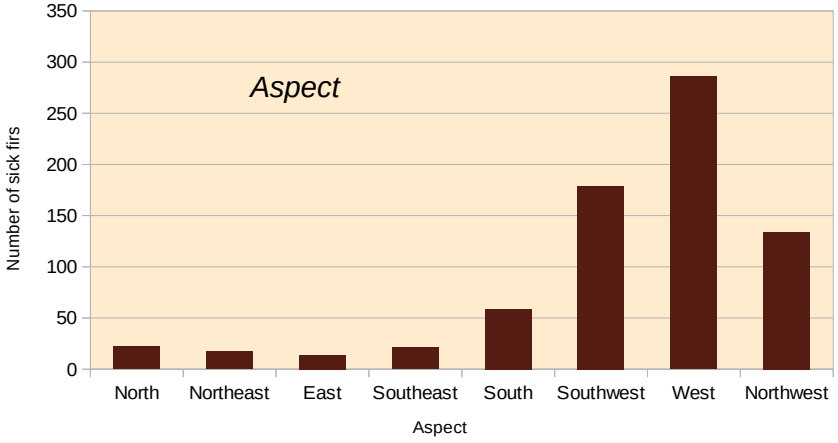

(c)

Figure 2.16: (a) Elevation, (b) slope and (c) aspect distribution of sick fir trees in hotspot area

2.3.4 Random forest for tree health prediction based on terrain factors

Scenario 1: The classification of two classes of healthy fir and infested fir

The confusion matrix shows a balance in the number of healthy fir trees and infested fir trees that was correctly predicted from the terrain factors in the RF model run in Python. Thus, the precision, recall, F1-score and accuracy values were similar. Overall, the algorithm could correctly predict 74.6% of all trees of two classes. Among all the predicted healthy and infested fir 71% and 79% are actually healthy fir and infested fir. Focusing on the recall, of all 819 healthy fir, the algorithm could correctly predict 639 trees, which accounts for 78% of the total number of trees. However, there are more infested fir mis-classified as healthy fir: 265 trees out of 932 trees. This makes the recall of this class slightly low at 72%. F1-score of two classes is balanced as 74% and 75% respectively. (table 2.10)

The RF model run in ArcGIS returns almost 10% lower in overall accuracy. There are less than 153 healthy fir trees predicted correctly compare with infested fir trees, while that number in the Python model is 28. The results show that precision, recall and F1-score are also lower than in the Python model. (table 2.10)

Among six sites, site 5 and 1 achieve the highest number of trees that were correctly predicted 98.8% and 87.5%, respectively (table 2.11). Low variation in the tree health condition in these two sites is the reason for the good results obtained. Most of the trees in site 5 are infested and most of the trees in site 1 are healthy thus it is more feasible for the algorithm to predict these two sites. The percentage reduced to 70.8% and 70% in site 2 and site 3 where the number of infested fir increased to 210 and 402 respectively.

Table 2.10: Confusion matrices for the classification of healthy fir and infested fir in (A) Python and (B) ArcGIS

A					
	Healthy fir	Infested fir	precision	recall	f1-score
Healthy fir	639	180	0.71	0.78	0.74
Infested fir	265	667	0.79	0.72	0.75
Overall accuracy: 74.6 %					
B					
	healthy fir	infested fir	precision	recall	f1-score
healthy fir	501	318	0.64	0.61	0.62
infested fir	278	654	0.67	0.7	0.68
Overall accuracy: 66 %					

The classification performance continues reducing to 59.1% and 59.7% for site 4 and site 4b where the number of infested fir keep increasing to 485 and 1211 respectively. The higher variation in tree classes, the less association between terrain and health condition, the lower the performance of prediction and vice versa.

Figure 2.17 & 2.18 show more infested were mis-classified into healthy fir in site 1, 2 and 3 and 4, while more healthy fir were mis-classified into infested fir in site 4b and 5. This is because there are more healthy fir in site 1, 2 and 3 and more infested fir in site 4b and 5.

Table 2.11: The percentage of trees correctly predicted according to sites – result obtained from the classification model ran in Python

Site	**Samples (trees)**	**Correctly predicted (trees)**	**Percent**
1	80	70	87.5
2	195	138	70.8
3	279	195	70
4	257	152	59.1
4b	454	271	59.7
5	486	480	98.8

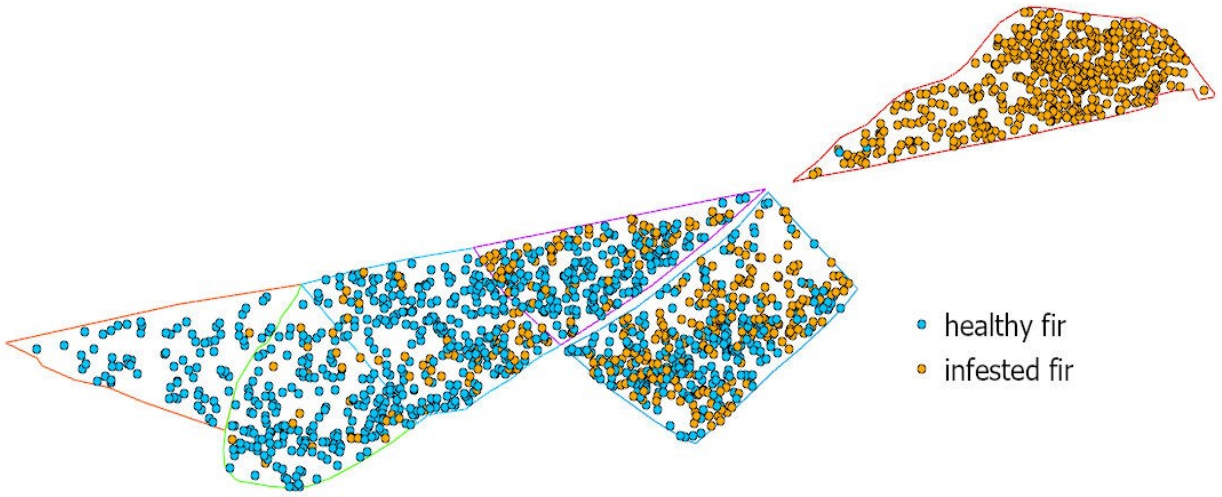

(a)

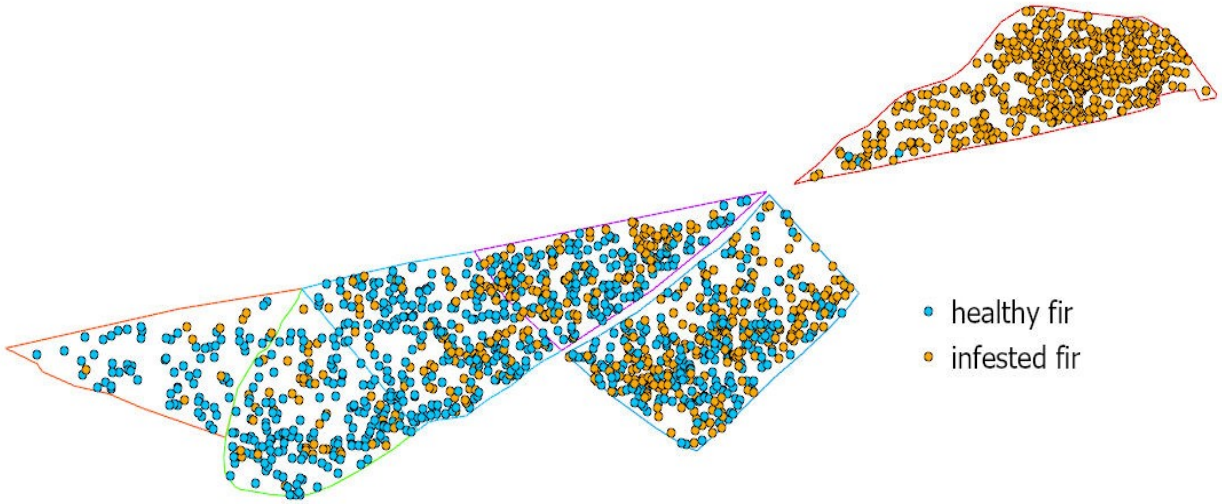

(b)

(c)

Figure 2.17: (a) classified result, (b) ground truth data (test set) and (c) mis-classified healthy to infested and infested to healthy from random forest model in python

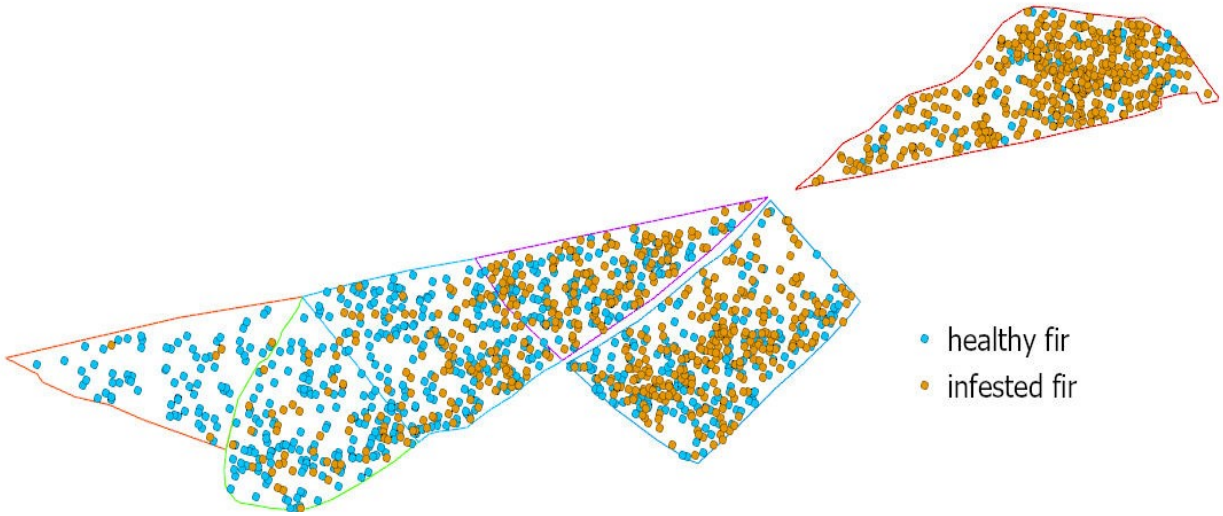

(a)

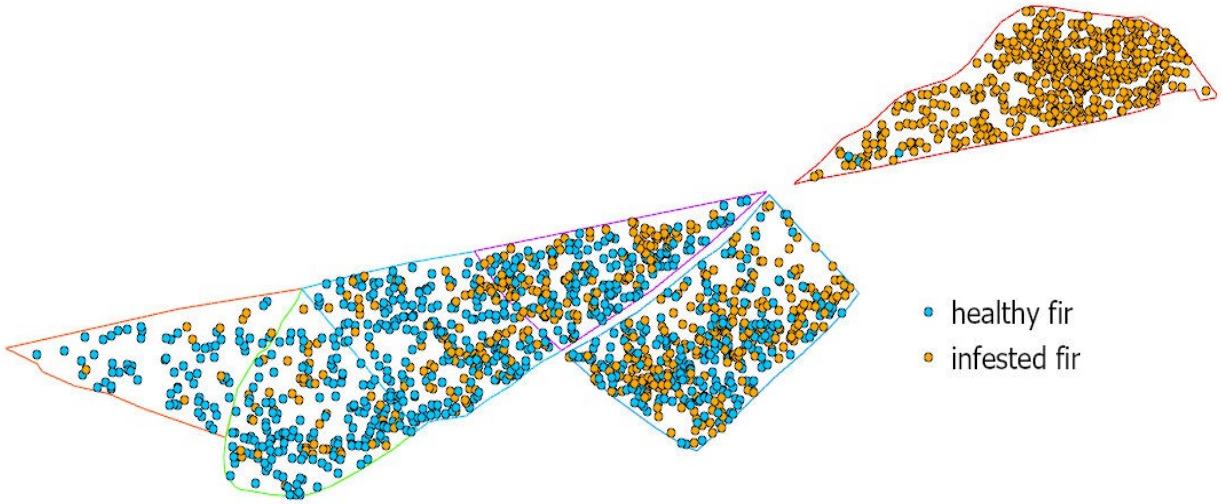

(b)

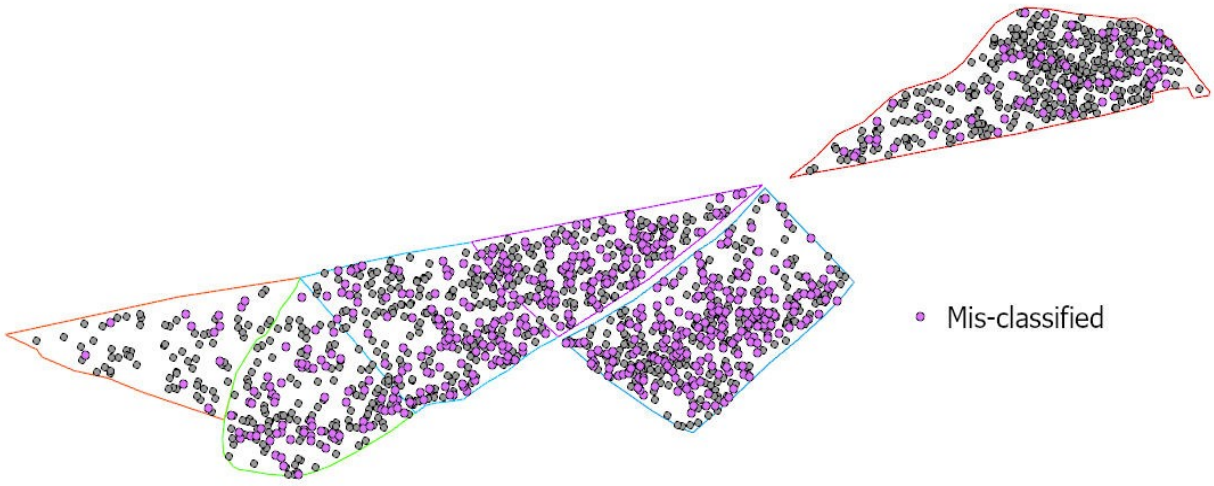

(c)

Figure 2.18: (a) classified result, (b) ground truth data (test set) and (c) mis-classified healthy to infested and infested to healthy from random forest model in ArcGIS

Scenario 2: The classification of three classes of healthy fir, sick fir and dead fir

The confusion matrix shows an imbalance in the number of healthy fir, sick fir and dead fir that were correctly predicted from the terrain factors in the RF model run in Python. This reflects in the precision, recall and F1-score results. The precision is very high for dead fir (0.94) but very low for healthy fir (0.68) and sick fir (0.45). In the recall the results are almost similar for healthy fir and dead fir (>0.80) but low for sick fir (0.34). Overall, the Python algorithm could correctly predict 71.1% of all trees (table 2.12).

The RF model run in ArcGIS returned 17% lower in overall accuracy. There were less than 293 trees that were predicted correctly compare with the model run in Python. The results show that precision, recall and F1-score were also lower than in the Python model (table 2.12).

Compared with the model of 2 classes, site 1 and site 4 showed a higher percentage of trees correctly predicted, while the other sites had lower prediction values (table 2.13), but similar to the trend obtained from the previous model, site 1 and 5 achieved the highest percentage of trees correctly predicted. From site 2 to site 4b, the percentages decreased.

There are 99% of trees in site 5 are dead fir. Thus the RF classifier (run in Python) mis-classified several sick and healthy fir trees as dead fir trees (figure 2.19). In contrast, the model run in ArcGIS perform poorer when mis-classified many dead firs as healthy firs and sick firs (figure 2.20). Likewise, in site 1 where most of the firs are healthy, the python model mis-classified several sick firs as healthy firs, but in reverse way, the ArcGIS model mis-classified more healthy fir as sick fir. From site 2 to site 4b, while python model mis-classified more dead and sick firs into healthy firs the ArcGIS model mis-classified more healthy and sick firs into dead firs.

Table 2.12: Confusion matrices for the classification of healthy fir, sick fir and infested fir in (A) Python and (B) ArcGIS

A

	Healthy fir	Sick fir	Dead fir	precision	recall	f1-score
Healthy fir	648	144	8	0.68	0.81	0.74
Sick fir	262	147	22	0.45	0.34	0.39
Dead fir	36	33	450	0.94	0.87	0.9

Overall accuracy: 71.1 %

B

	Healthy fir	Sick fir	Dead fir	precision	recall	f1-score
Healthy fir	419	261	120	0.63	0.52	0.57
Sick fir	179	179	73	0.33	0.42	0.37
Dead fir	64	101	354	0.65	0.68	0.66

Overall accuracy: 54.4 %

Table 2.13: Percentage of trees correctly classified according to sites – result obtained from the classification model ran in Python

site	**Samples**	**Correctly classified**	**Percent**
1	79	73	92.4
2	186	131	70.4
3	266	179	67.3
4	242	157	64.9
4b	485	244	50.3
5	492	461	93.7

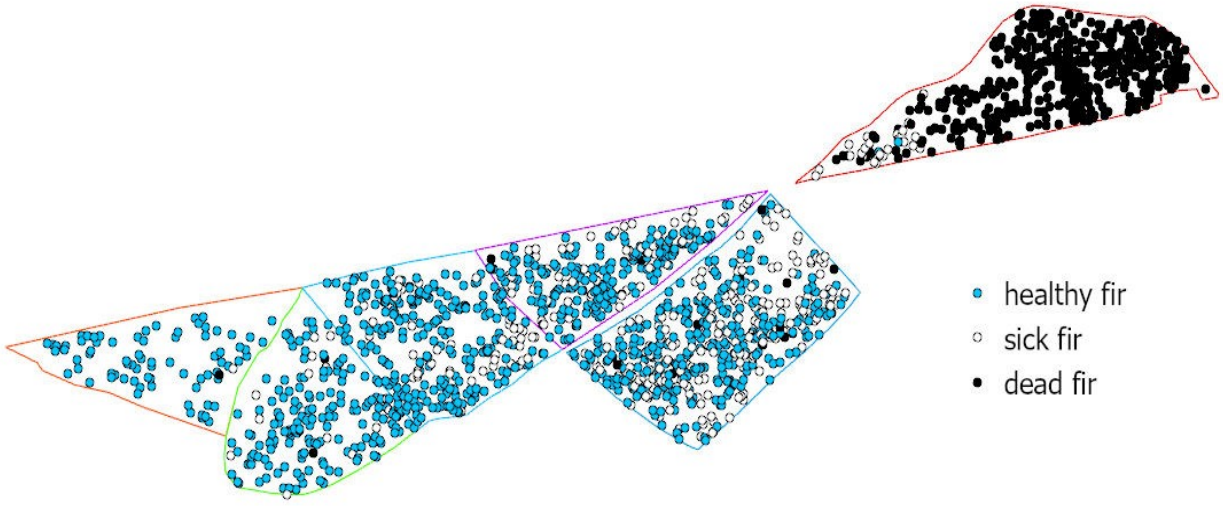

(a)

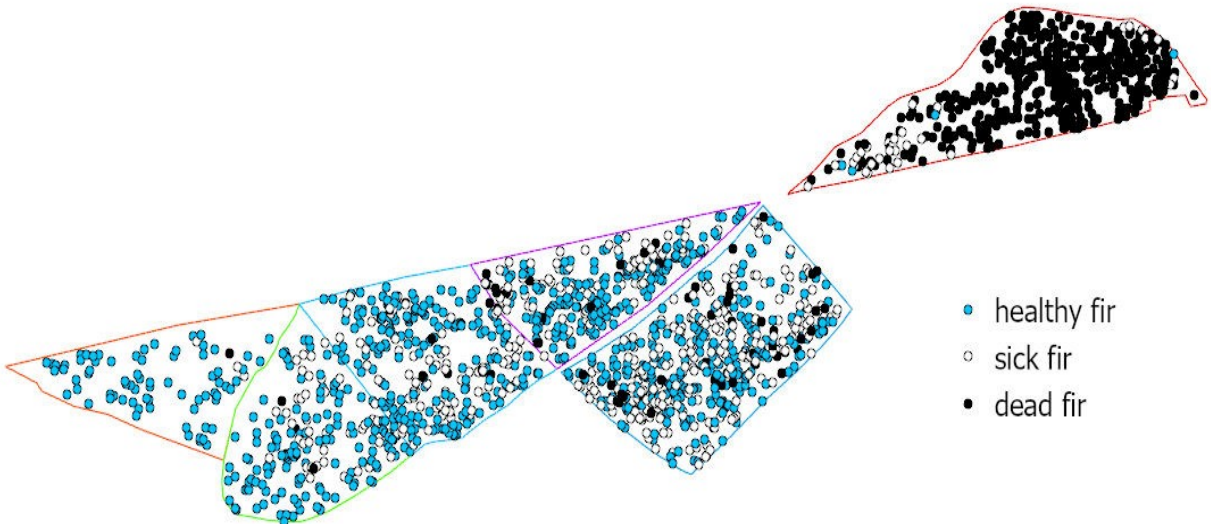

(b)

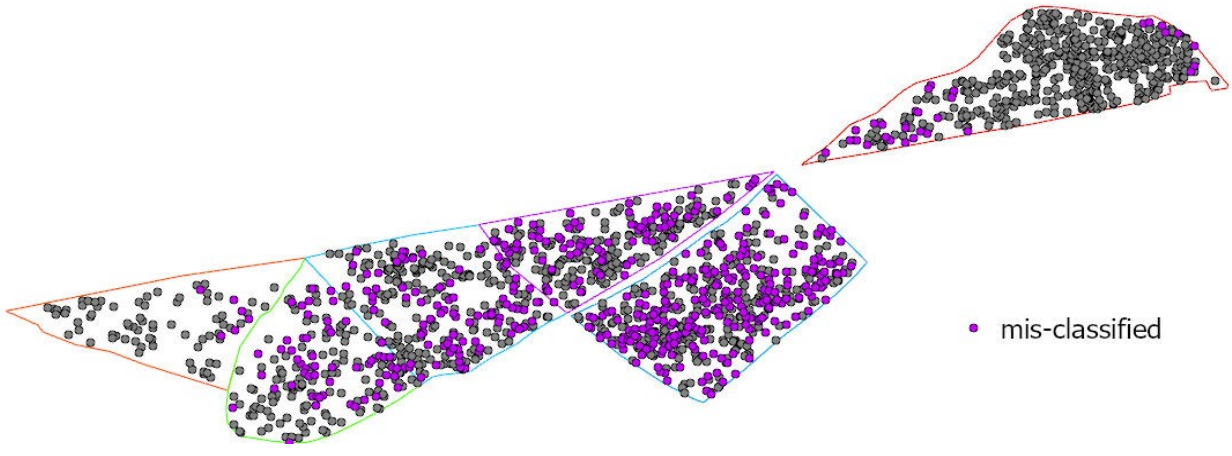

(c)

Figure 2.19: (a) classified result, (b) ground truth data (test set) and (c) mis-classified trees from random forest model in Python

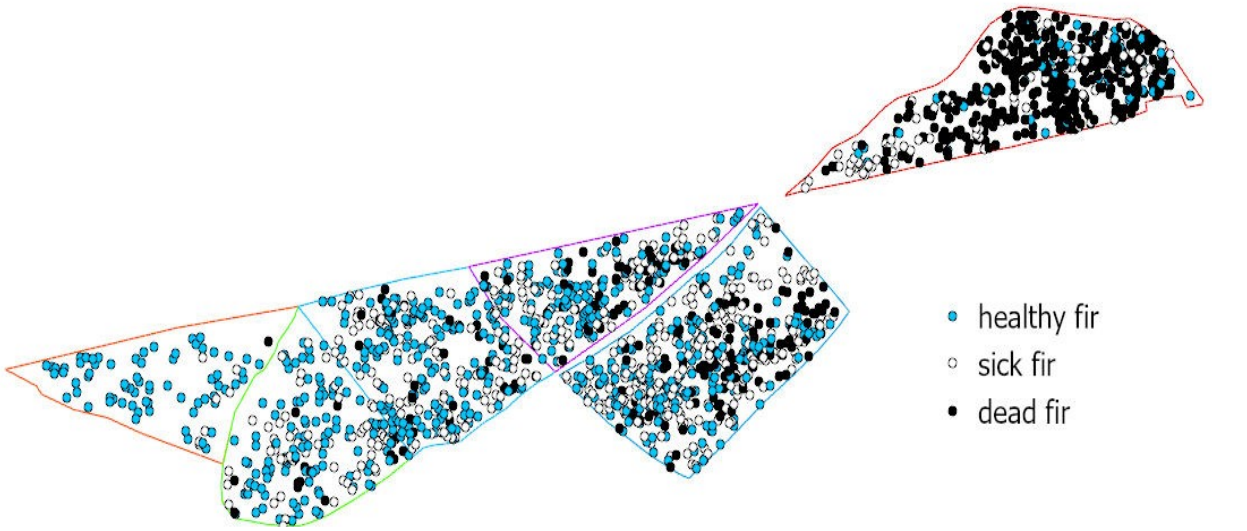

(a)

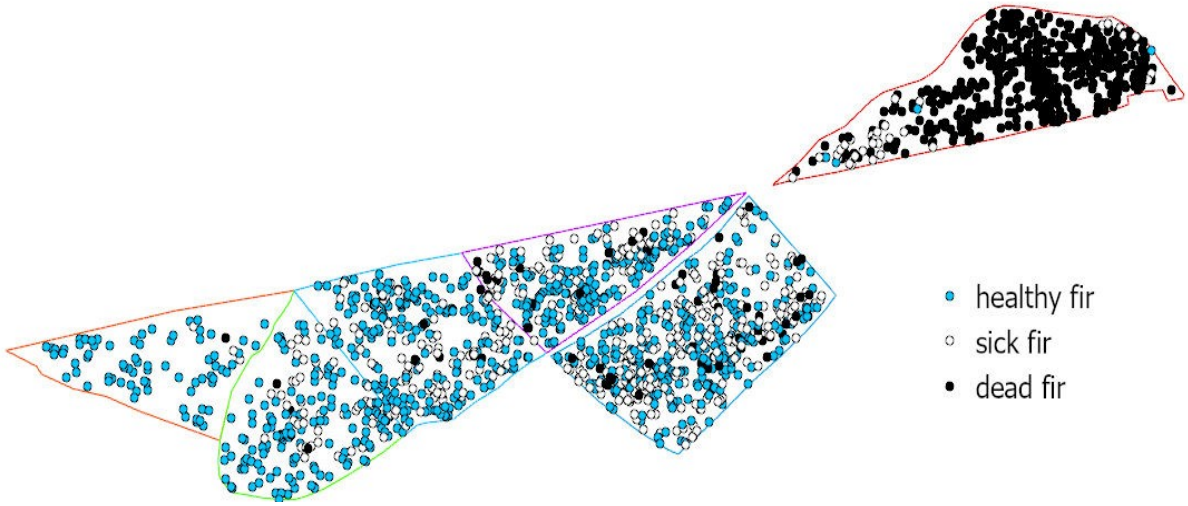

(b)

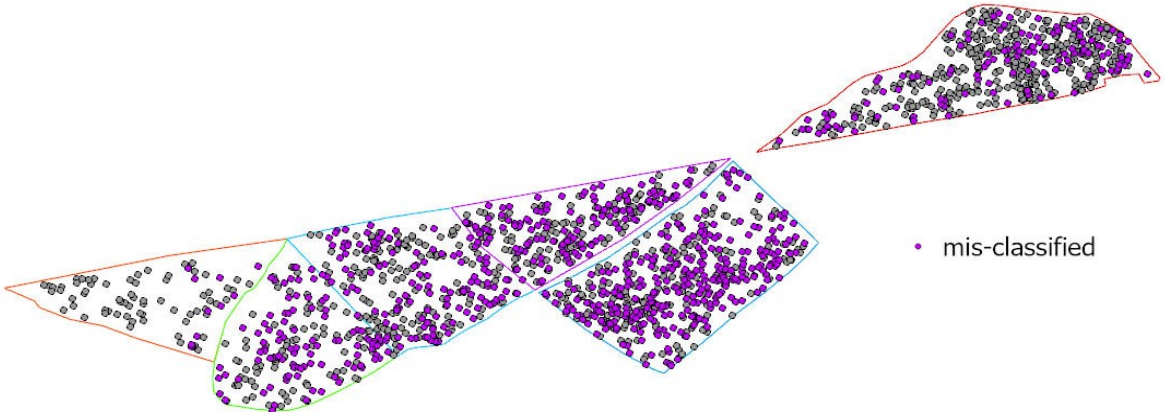

(c)

Figure 2.20: (a) classified result, (b) ground truth data (test set) and (c) mis-classified trees from random forest model in ArcGIS

2.4 Discussion

2.4.1 Variable importance

Variable importance measures the impact of each variable on the accuracy of the RF model by permuting the values of each variable and measuring how much the permutation decreases the accuracy of the model. Figure 2.21 shows the importance of elevation, slope and aspect for four different Random Forest classification models: 2 classes in Python, 3 classes in Python, 2 classes in ArcGIS and 3 classes in ArcGIS.

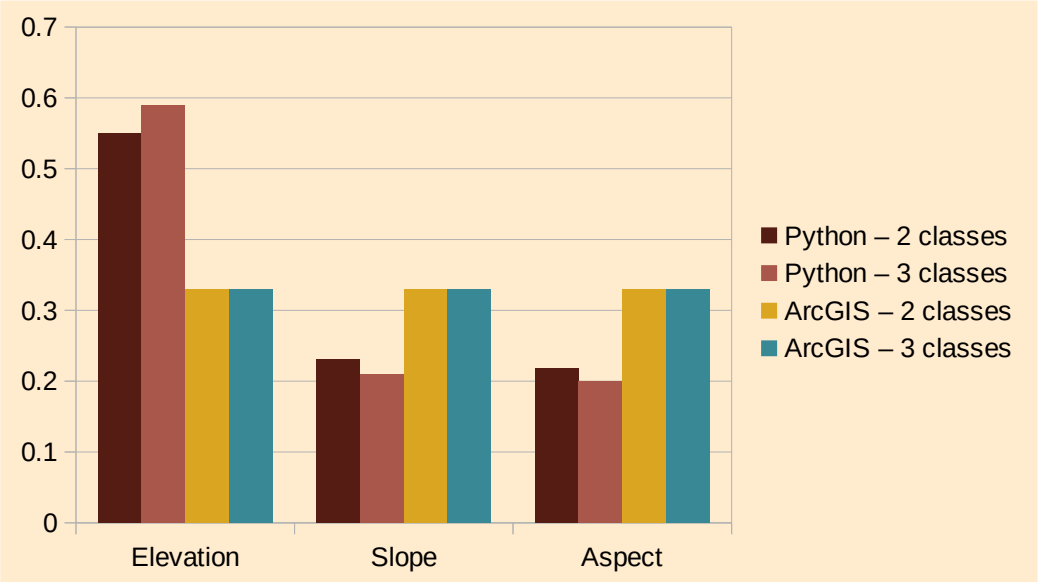

Figure 2.21: Chart shows variable importance of elevation, slope and aspect in each type of random forest mode

In the two cases of the model run in Python, the variable importance shows the elevation over weight the slope and aspect by impacting 55–58% on the accuracy of the model to predict health classes, while in ArcGIS all three variables share the same role. With higher accuracy at 75% and 71% for two classes and three classes models run in Python respectively, it suggests that the elevation has a higher impact on the abundance of fir bark beetles in the forests. In any case, the

measures show the significant impact of three terrain factors on the accuracy of predicting the tree health condition in mountainous forest. These factors have also been found to be key input variables to predict the spread of bark beetles in previous studies (Wulder et al., 2006, Lausch et al., 2011). Table 2.14 shows a distinct trend of the percentage of trees being infested in each elevation range. Almost 100% of trees on the elevation 1600-1700 m were infested, of which 98.7% were dead. Thus, only a small percentage of trees remaining at this elevation range were sick. According to table 2.14, the infestation trend is moving downhill with 64.5% and 45% of trees being infested at the elevation range of 1550-1600 m and 1450-1500 m. Of which, 42.9% and 38.1% were sick. Amman (1973) found that cold weather in elevations higher than 2130 meters is too harsh for bark beetles to survive, while the population of bark beetles increase 3 times at the elevation 1923 meters since at the infestation stage. This suggests that the lower elevation of Zao Mountains with warmer weather is a suitable habitat for bark beetles to flourish. Besides that, since the damage is more severe on higher altitude in Zao Mountain than lower altitude, it agrees with the conclusion in Krivet (2012) (cited in EFSA, 2020) that the beetles flourish in "cold areas with warm and dry summer". The altitude of 1600–1700 m of Zao Mountain, colder than lower altitudes and the temperature in the summer higher than 15^{0}C, maintains the requirement for the emergence of swarming period (EFSA, 2020) (figure 2.22). Thus the infestation began from the top of the Mountains where all the trees were dead and continued moving downhill to site 4b and 4 where there is a cluster of sick fir hotspots. Another reason the infestation begins from the top could be because the trees are smaller than the trees at lower altitudes. Takagi et al., (2018) found a significant relationship between small trunks and the intensity of *P. proximus* colonization. Bigger trees with thicker bark are more resistant to the infestation, while tree of smaller diameter tend to

be damaged more severely (Takagi et al., 2018, EFSA, 2020). Futhermore, Takagi et al., (2018) mentioned that trees with smaller trunks might be more susceptible to climatic conditions and thus make them more vulnerable to the attack of bark beetles. Although this conclusion is found to be opposite to the study of Amman (1978), about mountain pine bark beetle which prefer larger-diameter trees with thicker phloem, it is suitable to the occurrence on Zao Mountain.

Table 2.14: The percentage of infested, sick and dead trees at different elevation range

Elevation	Percent infest	Percent sick	Percent dead
1360 - 1400	3.4	2.7	0.7
1400 - 1450	24.4	21.1	3.3
1450 - 1500	30.6	27.2	3.4
1500 - 1550	45	38.1	6.8
1550 - 1600	64.5	42.9	21.6
1600 - 1700	99.9	1.2	98.7

Figure 2.21 shows a similar role of slope and aspect, approx. 20% each contribute to the accuracy of the model ran in Python. While table 2.15 shows a tendency of more infested trees on steeper slopes than on more gentle slopes, the aspect (table 2.16) presents almost the same impact from all orientation of the slope to the percentage of infestation.

There are 68.5% of trees at the steepest slope 45^0-90^0 being infested and the percentage gradually reduced to 39.2% at the flat terrain ($<3.43^0$). However, the percentage of sick trees is almost equal in all slope angles, ranging from 21% to 27% with higher percentages found at flat to gentle slope and lower percentages presented at steeper slopes. In contrast, the percentage of dead trees increase following the increase of the slope angles, from 12% to 48%. This indicates that the

steeper slopes accelerate the mortality of trees. This might be related to higher exposure by trees to the harsh winds in Zao Mountain which suppressed the trees (Iwaki & Totsuka, 1959).

Table 2.15: The percentage of infested, sick and dead trees at different slope range

Slope	Percent infested	percent sick	Percent dead
<3.43	39.2	27.1	12
3.13 - 5.71	39.5	26	13.5
5.71 - 8.53	38.8	25.2	13.5
8.53 - 11.3	44.7	26.3	18.4
11.3 - 14	54.2	25	29.3
14 - 16.7	54.8	24.5	30.3
16.7 - 21.8	55.8	25.6	30.2
21.8 - 31	63	22.4	40.6
31 - 45	65.4	23.7	41.8
45 - 90	68.5	20.8	47.8

The percentage of trees infested, sick and dead are almost the same on all aspects of the mountain with the averaging of 54% ± 5%, 25% ± 2% and 29% ± 6% respectively. The highest percentages of trees being infested and dead are found on the slope facing West at 59.8% (table 2.16).

The percentage of sick trees is similar on all aspects of the Mountains with the average 25% ± 2% (table 2.16). Despite the western aspect bing the direction of prevailing wind (Keiko Kai, 1977) and sun radiation from 11:00 to 16:00 on Zao Mountain during the summer (Appendix). This side of the slope presents the highest number of dead trees, at 37.4% of all trees on this aspect. However, this is only slightly higher than the Southeast slope (33.9%) which is not the direction of strong wind and sun. The north slope shows the lowest percentage of dead trees at 20% of all fir trees on this aspect. Light and wind are known to have a strong impact on tree stress (Iwaki & Totsuka, 1959; Maruta, & Nakano, 1999). Wind can dry the soil and suppress tree growth, thus making

thus making them more susceptible to bark beetles. However, the aspect towards strong wind and light was not found to have impacted strongly on the spread of bark beetles on Zao Mountains. The high percentage of sick firs and low percentage of dead firs on the South and Northwest slopes shows that these two aspects have a low pace of mortality. In contrast, the west slope shows a low percentage of sick fir and a high percentage of dead fir, suggesting a faster pace of tree mortality. Therefore, although the aspect does not show a strong impact on the infestation of fir trees, it may still influence the rate of forest health degradation.

Nevertheless, by permutating either aspect or slope factors in RF model, it reduces the accuracy of the model to 20%, suggesting that it is better to put aspect in the context of slope angle. The combination of west slope 21^0-90^0 would leave the trees more exposed to the challenging climate of Zao Mountains and speed up the mortality of the trees.

Table 2.16: The percentage of infested, sick and dead trees at different aspect range

Aspect	Percent infested	Percent sick	Percent dead
North	46.4	26.4	20
Northeast	51.5	22	29.5
East	54	23	31
Southeast	59.5	25.5	33.9
South	55.2	27.7	27.5
Southwest	54.4	22.9	31.5
West	59.8	22.5	37.4
Northwest	49.2	27.7	21.6

Regarding the RF model to predict infested, sick and dead trees in Zao Mountain according to the change of elevation, slope and aspect, the model run in Python provides a better result in term of validation metrics and variable importance.

RF model run in ArcGIS illustrates the equal roles of elevation, slope and aspects which do not explain well the statistical results presented above. It also shows a high number of trees that are mis-classified in site 5 and site 1 (figure 2.18 & 2.20) where present the lowest variation of tree health condition, showing a misbehavior of the model. In contrast, the model run in Python provides better accuracy, especially, in homogeneous area, where prediction are correct (more than 90%).

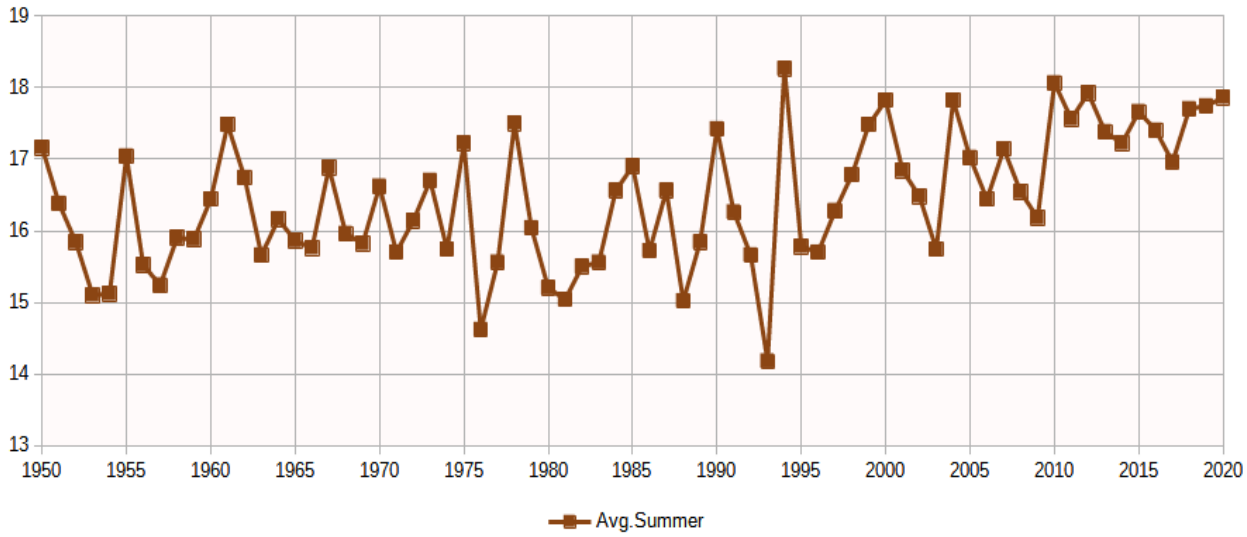

Figure 2.22: Mean summer temperature estimated for Zao Mountains at 1350 m

In the comparison between 2 classes model and 3 classes model run in Python, the model performs better when the number of classes to predict is less. The accuracy is higher and more balanced in the result of F1-score, recall and precision. In the prediction model for 3 classes, the model misclassified many sick firs with precision, recall and F1-score of 0.45, 0.34 and 0.39, while the numbers of dead firs are 0.94, 0.87 and 0.9 and for healthy firs are 0.68, 0.81 and 0.74 respectively. This is because many sick firs were misclassified into healthy firs. The proportion of training data for healthy fir, sick fir and dead fir were 45.5%, 24.5% and 30%, which shows almost equal amounts of data for sick firs and dead firs. This means that the low performance on sick fir is not only the result of imbalance data but also the spatially imbalanced. Dead trees cluster in site 5,

made it more predictable by relying on terrain factors, especially elevation. Sick trees spread heterogeneously from site 2 to site 4b, showing less terrain pattern and thus, more challenging to predict correctly. Nevertheless, with 75% and 71% accuracy achieved for the 2 classes and 3 classes models, it shows that terrains are the main factors that contribute to the spread of bark beetles in Zao Mountains, mainly because it regulate the mountainous climate which directly influence the productivity of bark beetles (Amman, 1978; Logan & Powell 2001).

Chapter 3

Individual Sick Fir Tree (*Abies mariesii*) Identification in Insect Infested Forests by Means of UAV Images and Deep Learning

3.1 Introduction

3.1.1 Background

Modern forest management demands more practical approaches on a macroscopic scale with the accuracy at tree level that can provide detailed information of tree characteristics such as crown color, tree height, diameter at breast height (DBH), tree crown area and basal area. These characteristics are essential for quantitative analysis of infestation, evaluating forest damage and monitoring forest regeneration. Traditional forest surveying on the field can acquire data of a single tree but face the challenge of seeing the forest condition as a whole and often is time-consuming and physically demanding. The satellite data can observe large area of forests but too coarse to get detailed information of a single tree. UAVs, with the ability to acquire data over a large area in high detail, can fill the gaps between field measurement and satellite observation. Using UAV to evaluate forest health has increased recent years (Nasi et al., 2015; Smigaj et al., 2015; Safonova et al., 2019). UAVs make data acquisition possible in areas where access is difficult (Pulido et al., 2020), such as Zao mountain, where field studies face challenges because of unfavorable weather, dense understory vegetation and complex terrain. UAVs open up opportunities to study mountainous natural forests where tree distributions are often heterogeneity and high variability among individual tree characteristics (size, species, and position)- by reconstructing 3D images of the forest (Diez et al., 2020; Kentsch et al., 2020; Krisanski et al., 2020). Such data present high spatial resolutions (of up to centimeters per pixel) allowing for the analysis of single tree-canopies (Michez et al., 2016; Brovkina et al., 2018). Single tree identification is essential to classify trees, to monitor their health or to estimate forest inventory, forest biomass and carbon stocks, among other forest dendrometric (Vastaranta et al., 2011; Pulido et al., 2020; Bennett et al., 2020).

Nasi et al., (2015); Smigaj et al., (2015); Dash et al., (2017) presented related methodologies on forest health evaluation, but these studies took place in plantation forests and relied on either multi-spectral or hyper-spectral cameras, which are costly and have low spatial resolutions. The low cost commercial UAV-acquired RGB images are more accessible for any forestry institution while still offer high sensor quality. Klouček et al., (2019) used RGB images and multi-spectral images to classify bark beetle infestation in forest and stated that the consumer-graded UAV performed better, especially because infested and healthy trees showed a visible distinction at red band. The first try of drone-acquired RGB images and deep learning to classify insect outbreak in natural forest was carried out by Safonova et al., (2019) on Siberian fir but the study was conducted on some regions of interest and lack of assessment of the individual tree detection algorithm.

3.1.2 Individual treetop detection

Individual tree detection is a necessary step towards identifying sick trees and monitoring the spread of tree diseases in forest (Näsi et al., 2015; Smigaj., 2015; Safonova., 2019). Various methods have been proposed to detect individual trees either through individual treetop detection (ITD) or through individual tree crown (ITC) delineation. Individual treetop detection (ITD) is to find the top of the trees while individual tree crown (ITC) delineation is to segment the boundary of a canopy, many studies have used these two terms to identify individual trees (Ke & Quackenbush, 2011) such as Holmgren & Persson, (2004); Kwak et al., (2006); Gougeon, (1998); Zhen et al., (2015). For decades, most of the studies relied on Very High Resolution (VHR) satellite images, Airbone Laser Scanning (known as Lidar), multi-spectral and hyper-spectral aerial images as medium data to detect individual trees (Chen et al., 2006; Kwak et al., 2006; Näsi et al., 2016;

Pleșoianu et al., 2020). However, satellite images are affected by cloud and the Lidar approaches are not always affordable.

Fast improvement in UAV technology has broadened the opportunities to use it in a wide range of applications. Several studies have attempted to use UAV-acquired RGB images to detect individual trees directly or indirectly, for example: Lim et al., (2015) attempted to identify 25 individual trees to measure tree height and crown diameter in an urban plantation based on Canopy Height Model (CHM) and orthomosaics; Kattenborn et al., (2014) detected individual palm trees using pouring algorithm on UAV-derived CHM in three different tree composition of plantations. They identified 69.8% of trees at flying altitude of 70m with lower overlapping and 86% of trees at flying altitude of 100m with higher overlapping; Mohan et al., (2017) developed a method to automatic detect individual coniferous trees in an open mountainous coniferous forest from UAV-derived CHM. They detected 312 trees out of 367 trees; Diez et al., (2020) experimented with six different local maxima detection and image clustering algorithms on UAV-acquired RGB images to detect treetops in 40 ha mixed natural mountainous forests and evaluated these algorithms. Their algorithms found 90% of trees with lower location accuracy and 80% with higher location accuracy. Gu et al., 2020 detected the treetops and segmented the canopy crown in a mixed forest with region growing techniques using natural color UAV. Although they did not illustrate the detection rate, they could detect 4164 trees in one experiment. Despite different forest structures, these studies have shown a possibility of using consumer grade UAV for automatic individual treetop detection in forests.

ITD in mixed mountainous natural forests faces many challenges when comparing with flat mono-cultured plantation forests. In mountainous forest, the steep slope makes the flying height to the ground non-uniform within a fly mission, thus affecting to the size of trees on captured images. Trees near to the camera are bigger size and more detailed than trees far from the camera. Trees in natural forest grow more heterogeneously with different age, size and distance between them, which is more challenging to find a uniform formula for the detection algorithm (Pouliot et al., 2002). Forest structure also affect the detection of treetops. Coniferous trees have pyramid shape with obvious treetops place at the center of the canopy which are easier to detect. In contrast, deciduous trees have large crowns, flat at the center, multiple over grown branches which often lead to over detection (Diez et al., 2020).

3.1.3 Deep Learning for tree health identification

In contrast to classical computer vision algorithms, where general expert knowledge is used as an evaluation metric, emerging technologies such as Deep Learning (DL) allow for the incorporation of that knowledge into the automatic processing of the images. To build a DL network, first an architecture or set of nodes and connections among them is defined. The type of each node, the number of nodes and the connections between them, determine the behavior of the network. Subsequently, the network is given example data, the DL algorithm learns from these examples, known as training data. The data are run through the network and the weights in all the nodes are changed following an optimization process. The ways to solve the problems learnt by the computer are, thus, directly determined by the expert input. In natural forest, the specific tree characteristics that we want to find, are sometimes few in numbers, thus creating data imbalances

for DL (which has been an important issue since the inception). For example, Dupret et al. (2001) studied the amount of resampling needed to obtain the best results in binary classification problems using neural networks based on perceptrons. Their theoretical analysis showed how resampling can indeed improve the performance of classifiers and is most indicated when the cost of misclassifying one infrequent class is high in practical terms. However, the paper also states that the ratio between class samples needs to be carefully studied for each application. In recent years, the emergence of DL networks and their dominance in computer vision (Krizhevsky et al., 2012; Simonyan et al., 2014; Iandola et al., 2016; He et al., 2016; Huang et al., 2017) has resulted in these ideas being revisited in light of new application opportunities and data resampling techniques such as data augmentation being widely used (Cabezas et al., 2020). However, most of the existing approaches use data augmentation to improve classification performance in datasets that are small but balanced (Deng et al., 2015; Shiferaw et al., 2019; Zhao et al., 2020; Masarczyk et al., 2020). In particular, we quantify to which extent a careful use of data augmentation and the choice of an adequate DL architecture, can improve the detection of sick fir trees. In relation to our current work, Onishi & Ise (2018); Natesan et al. (2019) and Safonova et al. (2019) used drone-acquired RGB data to develop algorithms for individual tree detection and classification in natural forests. Regarding the use of DL techniques to study forest health in UAV-acquired RGB images, Safonova et al. (2019) used DL to recognize the degree of damage of fir trees in a natural forest. Onishi & Ise (2018) and Natesan et al. (2019) used individual tree detection, in relatively small datasets, but the accuracy was not quantitatively evaluated in either work and only a qualitative evaluation was provided. Onishi & Ise (2018) worked with a total testing and training dataset made up of 941 tree images and achieved classification accuracies of 68-95% for the six species classified. Natesan et al. (2019)

worked with a dataset built by imaging one single site three times under different lighting conditions. This dataset contained 1786 tree images of three species and the authors used DL networks to achieve an average classification accuracy of 80%. Safonova et al. (2019) first predicted potential regions containing trees in UAV images before classifying them into four degrees of pest infestation. The authors selected RGB images manually to build a balanced training dataset that was expanded using data augmentation. Non-tree containing parts of the orthomosaic were filtered out using computer vision processing. The highest accuracy was reported for dead trees at 91% without augmentation, while the lowest accuracy values were found for infested trees at 75%. None of these studies assessed the accuracy of individual tree detection results.

3.1.4 Objectives

We have identified two main issues using UAV-acquired RGB images to detect and classify individual trees in terms of their health or types. The first one is the relatively small datasets used in most studies so far. The second is the lack of attention on the performance of treetop detection algorithms when used in conjunction with classification algorithms. This is especially relevant for natural forests where tree detection is more challenging (Diez et al., 2020). With this study we aim to contribute with a new methodology to evaluate insect infestation in forest using UAV-acquired images. Thus the objectives of this study are (1) Developing an algorithm capable of detecting treetops and evaluating its performance and (2) Applying DL networks to classify two different health conditions of Maries fir trees: (i) healthy and (ii) sick trees and a further class for (iii) deciduous trees. All the data and annotations used for this study are available at: https://doi.org/10.5281/zenodo.4054338.

3.2 Study site, data acquisition and problem definition

3.2.1 Study Sites

The study sites are located on Zao mountain, a volcano in the Southeastern part of Yamagata Prefecture (38°09'10.5"N 140°25'18.4"E). The site covers an area of 18 ha with a tree density of about 200 trees/ha. The fir trees in the areas are between 41 to 103 years old with an average age of 72 years. We divided the image acquisition area into four sites relying on the small paths within the forest. These were used to distinguish both the forest composition and the degrees of insect damage along an elevation gradient. The elevation increases from 1250 m in site 1 to 1538 m in site 4. The sites have different compositions and varying intensity of forest damage in terms of tree species—Site 1 (3.9 ha) and site 2 (5 ha) are composed of Maries fir mixed with other natural deciduous species such as: *Acer japonicum* and *Acer nipponicum, Fagus crenata, Sorbaria sorbifolia,* and *Salix*. In sites 3 (5.1 ha) and 4 (4 ha), fir is the dominant species. Fewer sick firs are observed at the lower sites while the most severely damaged trees are found at higher sites. On the top of the mountain (1551–1706 m), all fir trees are already dead. Since our study focuses on the detection of sick trees, we exclude the top of the mountain and present results related only to sites 1 to 4 (figure 3.1).

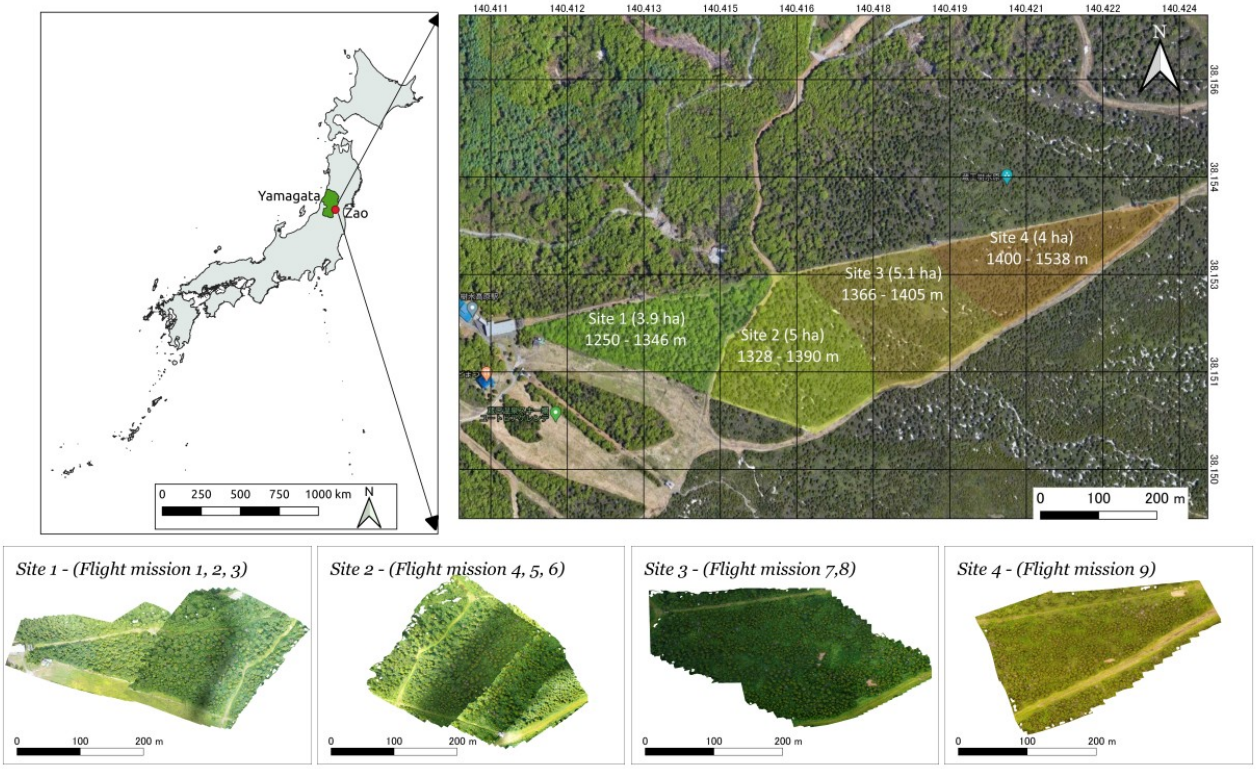

Figure 3.1: The four study sites are located in Zao Mountain, Yamagata prefecture, Japan. A gradual increase in elevation from site 1 to site 4 together with the increasing number of fir trees infested by bark beetles, followed by the decrease of mixing rate with deciduous species (background map from Google Hybrid (QGIS 3.10))

3.2.2 UAV Data Acquisition

Sets of RGB aerial photos were collected during the summer of 2019. Three flying missions in site 1 (mission 1,2,3); three in site 2 (mission 4,5,6) and two in site 3 (mission 7,8) were taken with a DJI Mavic 2 pro Hasselblad L1D-20c camera. The drone acquired 20 Megapixel images, following routes designed on DJI GS pro software (DJI Inc., Shenzhen, China). The camera sensor is a 1 inch CMOS with a fixed focal length 10 mm and aperture f/3.2. The weather on the capturing days varied but often entailed strong sun in the morning, then cloudy and windy in the afternoon. The drone flew at 70 m altitude from take-off points, nadir view, 3 m/s and shutter interval of 2 s. The photos were acquired with 90% side and front overlap. When it was strong sun and wind the

camera was set at S priority (ISO-100) with shutter speed at 1/240–1/320 s and set at 1/80–1/120 in more favourable weather. These set-ups maintained exposure values (EV) around 0 to +0.7 providing a ground sampling distance (GSD) from 1.5–2.1 cm/pixel. We had one flying mission on site 4 (mission 9) used a DJI Phantom 4 Quadcopter. The camera sensor in this UAV is 1/2.3 inch CMOS with a fixed focal length of 24 mm. The drone was pre-programmed to fly at 45 m high from take off point on a mild weather day. Photos were taken with 90% front and side overlap. The drone flew at speed 2 m/s, with a shutter interval of 2 s. The camera was set in automatic mode at a shutter speed of 1/120 s, ISO-100, EV at 0. This set up resulted in a GSD of 2.6 cm/pixel. The number of RAW images of each flight mission ranged from 150 to 390. All the photos have GPS coordinates which assist 3D reconstruction.

3.2.3 Problem Definition

We divided the trees in our study area into three classes: sick fir (SF), healthy fir (HF) and broadleaf (BL) trees (hereafter HF, SF and BL). Pest infestation has different effects on individual trees, some trees show defoliation on lower branches while in others, defoliation appears on the top branches. In order to facilitate the classification, we followed the reference on crown condition classification of the USDA (Schomaker, 2007) in which the authors classified trees based on their defoliation rates. Following this classification, we subdivided fir trees in Zao mountain in two classes: healthy, when no leafless branches were observed and sick, when leafless branches were observed (figure 3.2). Although there are several broadleaf trees, especially on site 1 and 2, we classified all of them in the single class, BL (figure 3.2).

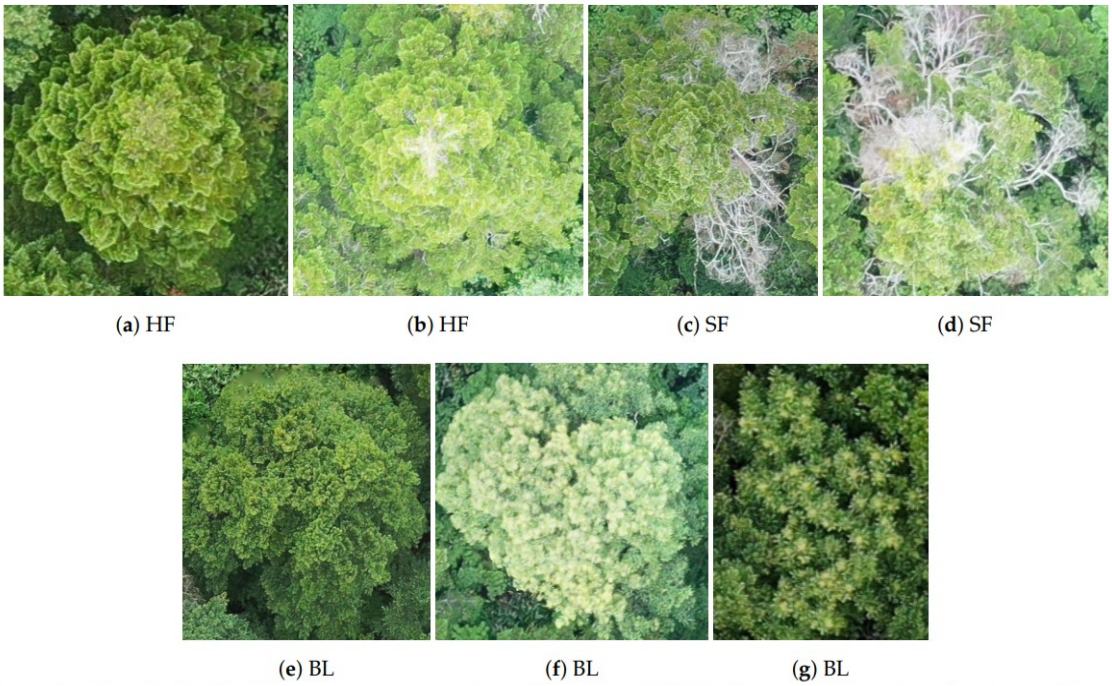

Figure 3.2: (a) healthy fir (HF) fully covered by green leaves; (b) healthy fir (HF) with minimal defoliation; (c) sick fir (SF) with some leafless branches at the bottom; (d) sick fir (SF) with majority of leafless branches (e–g) broadleaf (BL) in site 1 and 2

3.3 Methodology

3.3.1 Dense Point Cloud, DSM and Orthomosaic Generation

A Dense point cloud is a set of millions of points positioned by GNSS (Global Navigation and Satellite System) with 3 dimensional locations (X, Y, Z). It is used to generate the DSM and the orthomosaics. Orthomosaic images are composed of all raw single images of each flight and are geographically corrected to be at the true position, reducing the distortion from camera, lens and topography. An orthomosaic facilitates the labelling of trees in order to create the training and testing patches for DL. In this study, dense point clouds, DSM and orthomosaics were generated after aligning the raw RGB images of each flight using Agisoft Metashape.

The dense point cloud, DSM and orthomosaics were created in Metashape using batch procedure for the whole dataset of each flight. First, each set of RGB images was aligned without ground control points (GCP), accuracy to highest, 40,000 key point limit and 0 tie point limit were set. Then the "optimize alignment" step was set to default. In the next step, the "dense point cloud" (high quality, aggressive filtering), "mesh" and "texture" were built. The procedure was completed with DSM (interpolation enable) and orthomosaics (surface = DSM, blending mode = mosaic, hole filling = yes) (table 3.1). All the dense point clouds, DSM and orthomosaics were exported to Tokyo UTM Zone 54N. The same pixel size and extent were set for DSM and orthomosaic of each flight to overlay and process them in GIMP software and Python.

Table 3.1: Summary of image pre-processing with Metashape

Attribute	Value
Accuracy	Highest
Key point limit	40,000
Tie point limit	0
Ground control point	No
Dense point cloud	High quality, aggressive filtering
Mesh	Source data: dense cloud
Texture	Mapping mode: generic, blending mode: mosaic
DSM	Interpolation
Orthomosaic	Surface = DSM, blending mode = mosaic, hole filling = yes

3.3.2 Normalized Digital Surface Model (nDSM) Generation and Validation

A nDSM is an elevation model represented on a 2D digital grid surface to display the elevation of all features above the ground. It was generated in order to filter out the forest floor and produce elevation maps that only contained the height of trees (figure 3.3). A nDSM was created by

subtracting the Digital Terrain Model (DTM) from the dense point cloud, where the Digital Terrain Model (DTM) is an elevation model of bare-earth on a raster image. Our treetop detection algorithm is based on the local maxima method, therefore, if we use DSM for treetop detection in steep slopes, the highest point (treetop) downhill could be at the same altitude of the forest floor uphill (figure 3.3). However, when we use nDSM, the local highest points are only the treetops, as the forest floor is already normalized (removing the slope effect).

In order to generate nDSM we followed the process as described in figure 3.4. First Fusion/LDV (McGaughey, 2009) was used to define bare-earth points with the function "GROUNDFILTER" adapted from the filtering algorithm of (Kraus & Pfeifer, 1998). Then the bare-earth points were converted to plane surface digital terrain model (DTM) 0.2 m cell size with the function "GRIDSURFACECREATE". This function fitted the surface to the forest floor that was visible and interpolated the parts that were not visible under the canopies.

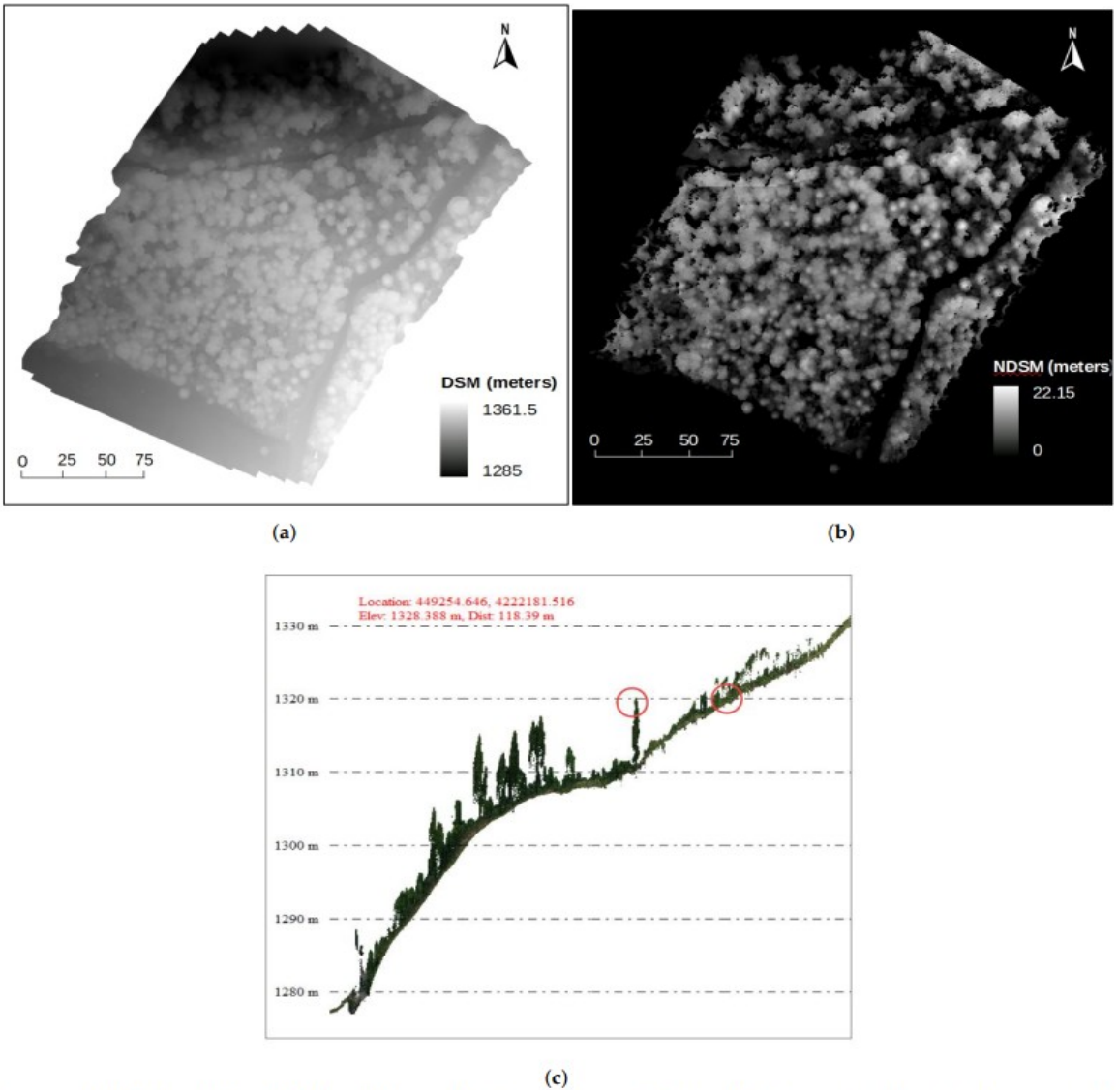

Figure 3.3: (a) DSM and (b) nDSM, the lighter (white) pixels represent high elevations and darker pixels represent low elevations, the black pixel on nDSM represents no value or the excluded ground and lower vegetation area; (c) the elevation profile of a random area on the DSM at an altitude of 1320 m as a treetop downhill is at the same altitude of the ground uphill (red circles)

The DTM was subtracted from the dense point cloud with function "CLIPDTM" to generate the normalized dense point cloud and then the terrain was normalized to 0 m. Next, the software Global Mapper was used to filter the points lower than 2 m (considered as lower vegetation) and points that belong to artefacts. The filtered points were then converted to nDSM where only tree canopies were present, with the same pixel size as that of the orthomosaic (about 0.02 m) of the

same area. Finally, QGIS 3.10 was used to convert data from tiff to jpg format for image annotation with GIMP software.

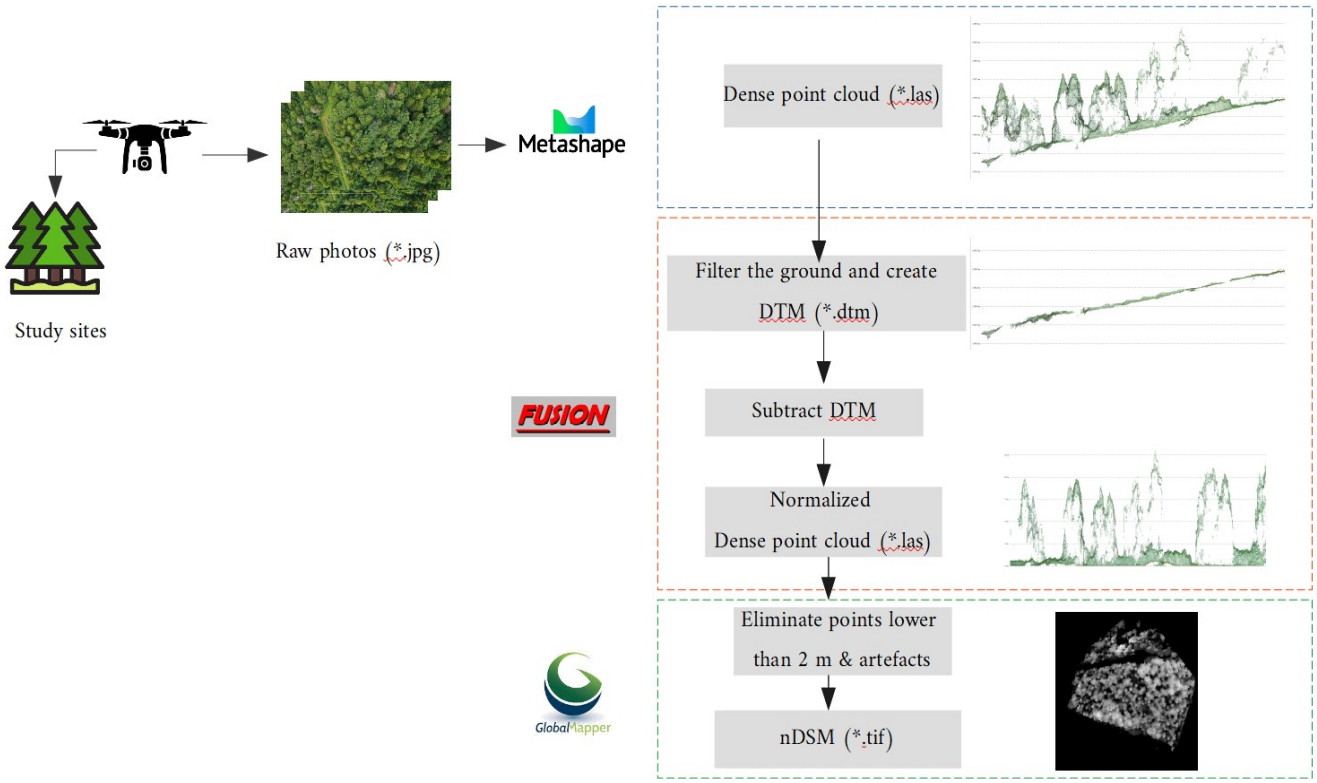

Figure 3.4: Work flow to generate nDSM

In order to perform a detailed evaluation of the results of this pre-process we would need a highly precise digital elevation model, such as the one that could be obtained with a ground based LiDAR system as well as detailed 3D annotations separating the section of the tree models corresponding to tree canopies. As such a model was not available, we focused on the visible effects that the nDSM construction step had on our ground truth. Specifically, we annotated the treetops manually on the DSM and then monitored how many of them were left out from the nDSM. A treetop was defined to be left out of the nDSM if (a) it was on a black pixel value (removed area) or (b) it had not been assigned a black value but the connected component it belonged to was smaller than a pre-defined threshold.

3.3.3 Data Annotation

Annotation is a data preparation step where all treetops and tree crowns were manually labelled on orthomosaic images and nDSM into different binary layers (black and white) including treetops, healthy fir, sick fir and deciduous. In total, 5364 treetops, 3788 healthy firs, 169 sick firs and 1407 deciduous were annotated. This is a crucial step to prepare training and testing data for the algorithms. The tree crown annotation was done on the orthomosaics by a careful work following the definition of tree health while the treetops were annotated with black dots on the DSM and nDSM in order to first, verify if all the treetops were also found on nDSM and second to evaluate the result of the treetop detection algorithm. All the annotation process was done in GIMP.

3.3.4 Treetop Detection

3.3.4.1 *Treetop Detection Algorithm*

This section describes the algorithm that are used to detect treetops in nDSM data. In order to take full advantage of the precise data representation obtained with the nDSM, a geotif data format with float components was used, allowing us to encode altitude values in millimeters. The algorithm uses computer vision techniques to find the regions in the nDSM that correspond to the tips of the treetops. A sliding window is used to process small parts of the nDSM independently. First, at each window position, only the pixels with higher intensities are considered. Then wider ranges of intensities are added iteratively. In each new iteration, connected components not containing any previously detected treetop are considered and if their areas are large enough, new treetops are assigned to them. The process continues within the window until all pixel intensities are taken into account. Subsequently, the window is shifted to a new location. Once all the positions of the sliding window have been explored, a refinement step is performed to join nearby candidate treetops.

Details of each step of the algorithm are as follows:

1. **Two-step algorithm:** We observed a large concentration of treetops at the higher intensity pixels. For example in the first orthomosaic 50% of the treetops are in the 10% higher pixels and 90% of the treetops are in the 40% higher pixels. Consequently, the algorithm runs in two key steps (which we refer to as "bands"). The first considers only pixel intensities of the nDSM from a certain threshold up and the second one considers all intensities.

2. **Sliding window:** for each of these two steps, a sliding window was passed over the nDSM. The positions of the window have a 100-pixel overlap. For each position of the window (figure 3.5), a list of candidate treetops was initialised to an empty list and a threshold value *th* was set. Then at each iteration:

• Only the upper band of intensities (larger than *th*) was considered.

• Connected components that are computed in the image are limited to the current window and band of pixel intensities. Each appearing component (if it was large enough) are assigned a new treetop that is added to the list of treetop candidates. Connected components already contained a candidate treetop do not add new candidate treetops to the list. If two connected components contain one treetop, then they are fused and both treetops are kept.

• *th* is updated and the process continues until *th* reaches the minimum intensity present in the window.

3. **Refinement:** once all the treetops are computed, they are refined to eliminate those that are too close to each other, specifically, a circle is drawn around each candidate treetop (with radius *re f*

Rad = 50 pixels) to exclude pixels higher than the candidate top (with a difference of more than 1.5 meters with the top). Then, the top point in each of the connected components is chosen as a predicted treetop. Thus, the highest treetops among those whose regions intersect are selected and the lower are discarded. An initial refinement step is done over the candidate tops resulting from considering all pixel intensities. Then, the treetop candidates corresponding to the high-intensity bands is performed. As the treetops detected in the higher-intensity band are considered more reliable, this second refinement step is less strict (the value for *re f Rad* = 35)

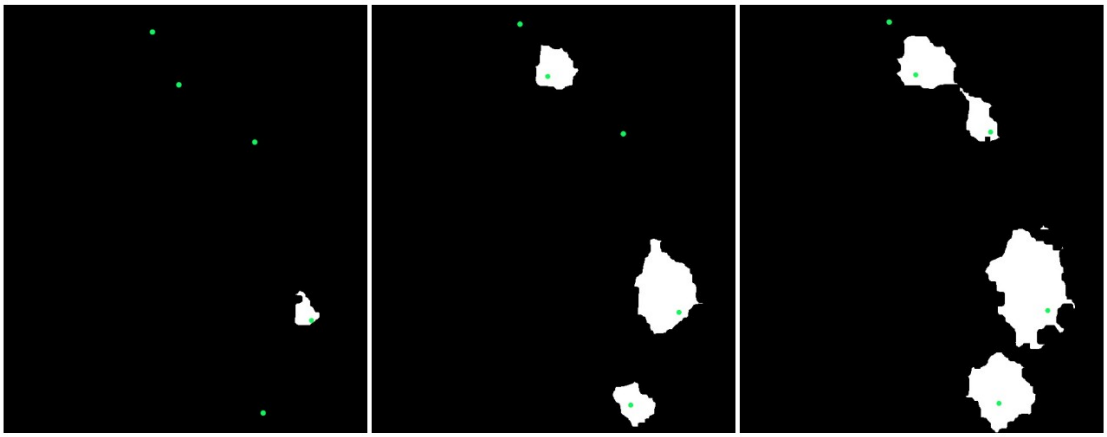

Figure 3.5: Treetop detection process: (a) step 1, one fir tree is detected, (b) in step 2, two more are detected and finally (c) in step 3, one more is detected.

3.3.4.2 *Treetop Detection Validation*

In order to evaluate the quality of the results of the treetop detection algorithm, we defined five different criteria. The output of the treetop algorithm is a set of points given as a list of 2D (x, y) coordinates. Consequently, all of these criteria considered two sets of 2D points: the set of predicted points and the set of annotated ground truth points.

Average Euclidean distance to nearest ground truth point $\left(\mathrm{d}Euc\left(PRED, GT\right)\right)$: this criterion aims to measure how close the treetops predicted are to the ground truth points. It is calculated as the average of all Euclidean distances between every ground truth point p to its nearest predicted point p

$$\mathrm{d}_{Euc}(PRED, GT) = \frac{\sum_{\hat{p} \in PRED} \left\{ \min_{\overline{p} \in GT} \mathrm{d}(\overline{p}, \hat{p}) \right\}}{|PRED|}$$

This metric, however, is somewhat vulnerable to outlier points skewing the value. Also, it does not clearly express how many predicted points are "close enough" to ground truth points. Consequently, two other metrics were provided.

Matched ground truth points percentage $(m\%)$**:** the aim of this metric is to provide an indication of how many treetops were detected. In order to implement this, a value was considered that roughly represented the radius of a tree crown. Predicted points were considered "matched" if they were within this threshold of a ground truth point $\left(d(\ \overline{p}\ ,\ \hat{p}\ ) <\ \varepsilon$ with $\hat{p}^{\ 2} \in\ PRED$ and $p \in\ GT$. After carefully examining the trees in the orthomosaic, a distance of approximately ε = 2.5 meters was used as the permissible margin of errors for two points to still be considered as the same tree crown. Given the differences in pixel resolution between sites 1, 2 and sites 3, 4, this stood for an error margin of 125 pixels for sites 1, 2 and 100 pixels for sites 3, 4. This set of thresholds make our use of this metric highly restrictive in terms of larger tree crowns which can be up to eight meters in diameter and we would only be considering a small part as valid for matching. However, we chose them to make it very difficult for a point predicted in one tree crown to be

matched to a ground truth point in a neighbouring tree crown even in the case of small trees (whose diameter is typically closer to 3 m). This addresses the issue of whether the points detected are placed correctly. During our experiments, we realised that some methods providing numerous candidate points obtained high values for this metric that did not agree with the subjective evaluation. Thus, in order to complement this metric, a simple metric based on the difference between the number of ground truth points and the number of detected points was provided.

Average Euclidean distance to closest ground truth points (correctly identified trees only): a combination of the two previous criteria, the goal in this case is to focus on the quality of the detection of correctly identified points.

Counting measure (cnt): stands for the difference of trees present in one nDSM, $cnt = (n-k)/n$ where the number of treetops detected "k" weighted over the number of trees "n". Consequently, negative values indicate that the algorithm overestimated the number of trees while positive values indicate underestimation. Reporting averages of each absolute value was taken to prevent that these two errors cancel each other.

Percentage of ground truth points detected more than once: to complement the counting criterion, we also computed the percentage of ground truth points that were matched more than once. This criterion provided us with more detail into the source of prediction overestimation. A higher number in this criterion indicated a difficulty to separate individual treetops while a lower number indicated erroneous points being detected in outer parts of tree canopies.

In order to provide a full picture, the results of the algorithm were compared to those of three previously existing methods. First two methods (clustering and extrema based methods) (Diez et al.,

2020), were used to exemplify the two families of approaches. Results for iterative Global Maxima *GMax* and Gaussian Mixture Model clustering *GMM* are, thus, presented. Additionally, results regarding the treetop detection method in Safonova et al., (2019) are also provided. This method, unlike the method in our study, works using the RGB orthomosaics to detect treetops. First, the orthomosaics are transformed into gray scale and blurred, then a thresholding step is used to work with binary images. The resulting images are then eroded and dilated repeatedly to isolate individual trees and finally a contour area calculation function is used (Dawkins implementation) to determine treetop candidates. We followed the execution of this algorithm with an additional step where predicted points that were identified as ground in the nDSM were eliminated.

3.3.5 Treetop Classification

In order to capture the distinctive characteristics of each tree type, a small square patch (100 × 100 pixels approximately 2 × 2 sq.m) around each treetop was sampled (indicated by a single point at its center). Then, each patch was assigned a class according to the manual annotation codifying the classes that could be found in the image (SF, HF and BL). Using this information, the problem was formalized in terms of DL as a classical single-label classification problem using the patches extracted around the treetops. This problem was solved using one of the following DL classifiers:

3.3.5.1 *Treetop Classification Algorithm*

In order to classify the patches representing each of the detected treetops, a series of feature extractor DL networks was used. The following architectures were considered as defined on the FastAI Library (Howard, 2020). This library uses the torchvision package from pytorch (A

description of the implementation of each model and a quantitative comparison on the ImageNet dataset can be found at https://pytorch.org/docs/stable/torchvision/models/).

1. Alexnet (Krizhevsky et al., 2012) is one of the first widely used convolutional neural networks, composed of eight layers (five convolutional layers sometimes followed by max-pooling layers and three fully connected layers). This network was the one that started the current DL trend after outperforming the current state-of-the-art method on the ImageNet data set by a large margin.

2. Squeezenet (Iandola et al., 2016) uses so-called squeeze filters, including point-wise filter to reduce the number of necessary parameters. A similar accuracy to Alexnet was claimed with fewer parameters.

3. Vgg (Simonyan & Zisserman 2014) represents an evolution of the Alexnet network that allowed for an increased number of layers (16 in the version considered in our work) by using smaller convolutional filters.

4. Resnet (He et al., 2015) is one of the first DL architectures to allow higher number of layers (and, thus, "deeper" networks) by including blocks composed of convolution, batch normalization and ReLU. In the current work a version with 50 layers was used.

5. Densenet (Huang et al., 2017) is another evolution of the Resnet network that uses a larger number of connections between layers to claim increased parameter efficiency and better feature propagation that allows them to work with even more layers (121 in this work). All these DL classifiers were initialized using Imagenet weights (Krizhevsky et al., 2012) with their final layers substituted by a linear layer with our number of classes. This final layer was followed by a sofmax activation function.

3.3.5.2 *Data Augmentation*

Data augmentation is a commonly used strategy in DL that allows to increase the size of datasets without the need to collect new data. In our case, SF is the most important category. However, this category is much less frequent than the other two. In order to increase the relative weight of sick fir trees during the training process of DL networks, we used six image transformations to augment our data: up/down and left/right flips, small central rotations with a random angle, Gaussian blurring of the images, linear and small contrast changes and localised elastic deformation. To implement these transformations we used the "imgaug" library (Jung et al., 2020).

3.3.5.3 *Treetop Classification Algorithm Training and Validation*

The treetop classification algorithm received input of treetop points. For each of these points, the algorithm:

1. Checked to which of the classes it belonged. To do so it checked the annotated class binary masks.

2. Cut a small patch of the orthomosaic around each treetop (of 100 × 100 RGB pixels, amounting approximately to a 2 m sided square).

3. Once the correct class had been identified and the patch built, the patch was stored as an image with the class name in its file name.

The set thus constructed was then passed on to a deep learning network where it was divided into training/validation and testing subsets. The treetop points used to build the sets as well as the

way the training/validation/testing subdivision was made determined what was being tested. Regarding the treetops, first we used the ground-truth treetops annotated by experts in order to assess the performance of the classification algorithm with the best possible input data. Then we used the output of the tree detection algorithm to assess how the classification algorithm performed as a part of the whole algorithmic pipeline presented. Regarding the division in validation and testing, first we used all data from all mosaics in a single dataset, dividing it randomly in 80% training/validation and 20% testing. However, as mosaics in the same sites have overlap, images from the same tree (taken in different mosaics and thus, in different flights with different lighting conditions) might have appeared in both the training and testing sets.

We considered this a problem as it put into question the generalization power of the classification algorithms. Consequently, we also used (in both experiments) a site-based leave-one-out strategy to prevent this issue as follows: The orthomosaics available were grouped into sites, all the mosaics of three of the sites were used for training/validation while all the mosaics of the remaining site were used for testing. The site used for testing was rotated, so all orthomosaics were used for testing once and no orthomosaic was used for training/validation and testing at the same time to avoid leakage between the training and testing patches.

- First fold, testing: Site 1 (orthomosaics 1,2,3) – training/validation: Sites 2,3,4 (orthomosaics 4 to 9)

- Second fold, testing: Site 2 (orthomosaics 4,5,6) – training/validation: Sites 1,3,4 (orthomosaics 1 to 3 and 7 to 9)

• Third fold, testing: Site 3 (orthomosaics 7,8) – training/validation: Sites 1,2,4 (orthomosaics 1 to 6 and 9)

• Fourth fold, testing: Site 4 (orthomosaic 9) – training/validation: Sites 1,2,3 (orthomosaics 1 to 8)

In all cases, the following measures were used to evaluate the classification accuracy: In order to target the predictive capacity of the algorithms the relation between predicted values and ground truth values was considered and expressed as: True Positives (TP), False Positives (FP), True Negatives (TN), False Negatives (FN). Furthermore, and in order to focus on the defined classes, the following measures were computed on them: True Positive Rate (TPR), also known as Sensitivity ($SENS$), False Positive Rate (FPR), also known as the probabilistic complement of Specificity ($SPEC$) and finally accuracy (ACC). Their formulae as follow:

$$TPR = SENS = \frac{\mathrm{TP}}{\mathrm{TP} + \mathrm{FN}} \qquad FPR = 1 - SPEC = \frac{\mathrm{FP}}{\mathrm{TN} + \mathrm{FP}}$$
$$ACC = \frac{\mathrm{TP} + \mathrm{TN}}{\mathrm{TP} + \mathrm{TN} + \mathrm{FP} + \mathrm{FN}}$$

3.4 Results

3.4.1 nDSM Validation

nDSM validation was expressed as the percentage of ground truth treetop found in the DSM missing in the nDSM (0% means all ground truth treetops are present) (table 3.2). The percentage of treetop missing in nDSM6 and nDSM4 were 0.0% and 6.9%, representing the lowest and highest values respectively. The mean validation value of all the nDSM was 2.14%. After a visual review of the images, we found that most of the annotated treetops missing were those of smaller deciduous trees in distorted areas of the orthomosaic boundary or were small fir trees (2–6 years old) (figure

3.6). Missing trees represent one of the limitations of this study, since only the treetops found in the nDSM are considered.

Table 3.2: Percentage of annotated treetop lost when using nDSM instead of DSM

nDSM	1	2	3	4	5	6	7	8	9	Average
% treetop lost	1.12	1.57	0.17	6.90	3.08	2.25	0.00	1.00	3.20	2.14

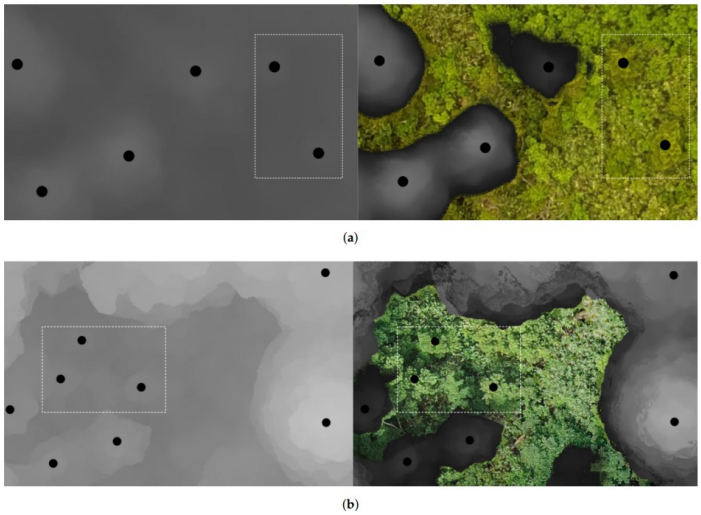

Figure 3.6: (a, b) annotated treetops on small trees that were in DSM (left) but do not appear on the nDSM (right).

3.4.2 Treetop Detection

The performance of the treetop detection algorithm was evaluated using the quality criteria and comparing it with the results of three pre-existing algorithms (Safonova et al., 2019; Diez et al., 2020). The percentage of points matched (m%) and counting measure (cnt%) obtained by each of the algorithms in each of the nDSM (table 3.3). The results showed that the method introduced in this paper obtained the best overall results both in the matching (85.7%) and counting (9.67%) criteria. Differences in the results depending on the nDSM, for example nDSM 1,3 and 9 showed higher accuracy in treetop detection ranging form 89.61% to 96.29%, while nDSM 5 and 6 obtained matching values of around 85%. The lowest values were obtained for nDSM 2,4,7 and 8 but still

were all in the range of 80%. The lower matching averages were observed in nDSM that corresponded to lower and middle areas with steep slopes and the highest rate of mixing with deciduous trees.

Table 3.3: Individual tree detection method performance. This table show the result using our data with previously reported algorithm

nDSM	1		2		3		4		5	
Methods	m%	cnt	m%	cnt	m%	cnt	m%	cnt	m%	cnt
Our approach	89.61	9.87	80.14	14.51	90.47	5.67	82.97	14.15	85.61	8.73
Dawkins (Safonova et al., 2019)	70.54	2.18	54.61	13.79	73.41	6.92	59.79	16.32	51.12	19.35
GM (Diez et al., 2020)	71.17	-9.21	60.75	-11.11	78.35	-9.82	70.09	-8.12	69.81	-9.76
FCM (Diez et al., 2020)	66.22	-9.74	61.68	-12.37	73.56	-12.25	73.21	-7.25	69.49	-9.05
nDSM	6		7		8		9		10	
Methods	m%	cnt	m%	cnt	m%	cnt	m%	cnt	m%	cnt
Our approach	85.71	8.37	80.52	7.74	80	9.24	96.29	8.78	85.7	9.67
Dawkins (Safonova et al., 2019)	50.06	22.43	70.69	1.27	71.36	8.79	92.61	3.31	66.02	10.48
GM (Diez et al., 2020)	68.85	-14.82	63.27	-9.44	72.82	-12.27	87.67	-7.41	71.42	10.22
FCM (Diez et al., 2020)	72.2	-10.18	64.71	-17.87	72.3	-7.76	90.14	-5.71	71.5	10.24

Regarding the counting criterion, our algorithm tended to slightly under-estimate the number of trees that are represented by cnt positive values. This under-estimation was kept, however, under 10% for most of the orthomosaics and with less variability as that found when using the other methods. The methods based on finding local extrema and on clustering algorithms GM and FCM obtained lower performances for matching with values around 71% and similar performances in terms of the counting criterion. The Dawkins method used before in Safonova et al., (2019) obtained poor results in terms of matching percentage with an average of 66.02% with some very low performances in the lower and middle elevation sites (around 50% for nDSMs 2,5,6) and very good performance for the nDSM in the highest elevation site (nDSM 9).

Regarding the average Euclidean distance between the sets of predicted and ground truth points, our method obtained the best value with an average of 50.29 pixels of distance (around 1

m) between each predicted point and its closest ground truth point. As this also considered unmatched points (further than 100 or 125 pixels) it illustrates the strength of the presented algorithm. The values for this criterion obtained by the other methods were: FCM 116.32, GMax 118.11, and Dawkins 178.67). The quality of the matching results is also compounded when we consider the euclidean distance for correctly matched points only. The distance drops from 50.29 to 27.42 showing correctly found points were on average about 50 cm from their corresponding ground truth point. The percentage of points detected more than once was on average 8.22% with the highest value of 15.68% for orthomosaic 1 which had the highest occurrence of deciduous trees.

3.4.3 Classification of Ground Truth Treetops Using Deep Learning

In this experiment we assessed the capacity of the DL networks to classify treetops into the healthy fir, sick fir and deciduous classes. In order to focus on the merits of the classification algorithms, annotated treetops were used (from now referred to as ground truth or GT treetops). The data remaining inside the chosen Region of Interest (ROI) of the 9 orthomosaics in the 4 sites contained 5364 trees (1407 deciduous, 3788 healthy fir and 169 sick fir). Initially, the dataset constructed considering patches corresponding to all these treetops was divided randomly into 80% training and 20% testing. Figure 3.7 contains the percentage of misclassification over all images (Error Rate, ER) values for the validation set in each of the considered DL architectures over a list of learning rate values.

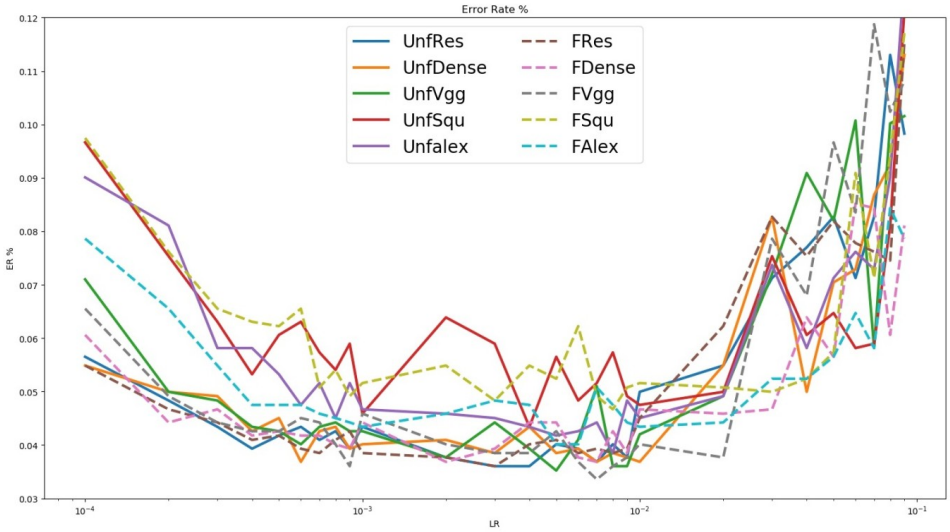

Figure 3.7: Error Rate Results for tree health classification for all learning rates and DL architectures

The best results were obtained by Vgg, with the lowest ER value of 0.03357% for FVgg and learning Rate (LR) = 0.007 (figure 3.7). The same network reached 0.03521% ER in its unfrozen version (UNFVgg, LR = 0.005). Resnet and Densenet obtained similar results (0.03603% UNFResnet, LR = 0.004 or 0.03685% UNFDense, LR = 0.007) with small difference between their frozen and unfrozen versions. Alexnet and Squeezenet obtained the lowest results with Alexnet doing slightly better with just under 0.040% ER (0.03949% for UNFAlex LR 0.008) and Squeezenet reaching an ER of 0.0434% (UNFSqu, LR = 0.004). These results show that all networks are successful at classifying the images received into the three existing classes. The results obtained presented problems in terms of their practical use: the class with the highest interest was sick fir trees, but most of the networks produce low sensitivity value for this class. Table 3.4 shows the best results obtained regarding this criterion together with the specificity, sensitivity and accuracy of the other classes (Densenet LR = 0.06).

Table 3.4: Sensitivity, specificity and accuracy values for the classification of treetop patches according to health.

	Sensitivity	Specificity	Accuracy
Deciduous	0.982	0.999	0.995
Healthy fir	0.995	0.926	0.976
Sick fir	0.513	0.996	0.980

Table 3.4 shows that even though high accuracy results were obtained in the three classes, the sick fir class obtains very low results in its sensitivity value. This stands for the classifiers miss-classifying about half of the sick fir images. The fact that this class is less frequent than the other two accounts for the high accuracy obtained regardless of this. Furthermore, the data used in this section contains images from all orthomosaics and sites. Since, the orthomosaics within a site contain an overlap of the adjacent site (1,2,3 for site 1, 4,5,6 for site 2, 7,8 for site 3 and 9 for site 4), it is possible that the validation sets contained images of trees that also appear in the training set. While this is often seen in the literature due to the difficulty of obtaining data, we assume that training the networks in this manner may contribute to a subtle form of over-fitting. In order to obtain a classification algorithm that presents improved sensitivity for the sick fir class, we used data augmentation and a leave-one-out strategy for the building site-specific training sets. In terms of DL networks and given the results presented here, our focus was set on the Unfrozen version of the Vgg, ResNet and DenseNet. While the best performances of Frozen and Unfrozen networks were very similar, the smaller variance of Unfrozen networks were valued as a sign of a more stable performance and were considered as being better suited for the use of data augmentation because of the larger number of modifiable parameters. This is expected to increase the classification accuracy of the images containing the augmented classes at the cost of decreasing that of the other classes. To avoid having images of the same tree (even if taken in different flights) both in the training and

testing set we used a site-based leave-one-out strategy and build one training/validation distribution of images for each site. In short, in each fold of the leave-one-out, the orthomosaics of one site were used as the testing set, while the orthomosaics of all the other sites conformed with the training set. The sensitivity, specificity and accuracy for the 4 sites using the three DL networks considered (Densenet, ResNet and Unfrozen Vgg) and five different data augmentation scenarios: No augmentation (row "no augm") and 2,6,10 or 20 augmented images for each original sick fir image (rows augm 2 to augm 20) were used (table 3.5).

Table 3.5: Results for the sick fir class for three DL networks and five data augmentation scenarios. Values for the LR obtaining best sensitivity are shown for all augmentation scenarios.

	DenseNet			ResNet			VGG		
	Sens	**Spec**	**Acc**	**Sens**	**Spec**	**Acc**	**Sens**	**Spec**	
no augm	0.4109	0.9959	0.9771	0.4422	0.9912	0.9738	0.4001	0.9931	0.9761
augm 2	0.6772	0.9948	0.9763	0.7199	0.9941	0.9782	0.6576	0.9921	0.9752
aumg 6	0.9382	0.9875	0.9796	0.9407	0.9863	0.9788	0.9391	0.9877	0.9787
augm 10	0.9806	0.9839	0.9834	0.9794	0.9810	0.9809	0.9792	0.981	0.9794
augm 20	0.9936	0.9769	0.9836	0.9972	0.9822	0.9880	0.9868	0.9805	0.9791

The results show that the use of data augmentation led to better sensitivity values for the sick fir class despite a decrease in specificity because of an increase in the number of False Positive detections of the sick fir class. This is mainly due to the relatively low number of sick fir trees compared to the total number of trees (sick and healthy fir plus deciduous). Comparing the three studied networks, Vgg obtained slightly lower values with DenseNet and ResNet showing similar values. In order to choose between the two networks, the average sensitivity, specificity and accuracy values in all the learning rates were considered. For example, for augm10, values of 0.97632, 0.8781, 0.9532 for DenseNet and 0.9758, 0.8908, 0.9558 for ResNet. Even though the differences remained small, ResNet obtained higher values for all datasets suggesting a more stable behaviour in this classification problem. The same indicators for the other two classes (healthy fir and deciduous)

showed similar tendencies. For example, for the same dataset (augm10) and comparing the two learning rates with better sick fir specificity values, ResNet (LR = 0.001) obtained values of 0.8953, 0.9830, 0.9601 for healthy fir, and 0.9921, 0.9720, 0.9877 for deciduous while Densenet (LR = 0.006) obtained 0.8790, 0.9431, 0.9225 for healthy fir and 0.9601, 0.9548, 0.9586 for deciduous. These values illustrate the slightly superior performance of Resnet over Densenet as well as the trade-off between the larger specificity values for the sick fir class and a decrease in percentage for the other classes. The use of data augmentation increased the impact of the sick fir class in the training step. This results in better sensitivity but also increases the number of False Positives in the healthy fir class. Considering these results, the ResNet network was used to classify the detected treetops.

3.4.4 Automatic Detection and Classification of Sick Fir trees

Finally all the algorithms presented in this paper were used together and their combined performance was evaluated. First, the pre-processing procedure was used to obtain a nDSM from the drone-acquired data. This nDSM was then used as input for the treetop detection algorithm and as a result, a list of (x, y) coordinates representing the position of each automatically detected treetop was obtained. The treetops thus detected were then classified into the three existing classes (SF, HF and BL) using the ResNet network. Regarding the training/testing sets, used for the ResNet classifier network, the site wise leave-one-out approach was used. Within each fold of the training set, we initially used the same approach where ground truth treetop points were considered and 100 × 100 pixel images were cut around them (approximately 2 × 2 sq.m). The testing set was then built by cutting 100 × 100 pixel images around the automatically detected treetop candidate points.

However, the results of this approach were not satisfactory, mainly because on the training set the trunk of the trees was always placed at the center of the image whereas in the testing set this was not always the case. In order to ameliorate this problem we considered small perturbations of the coordinates of the ground truth points so that the generated 100×100 pixels were not perfectly centered on the actual ground truth points. All the results presented in this section correspond to this training strategy.

Concerning data augmentation, for each of the scenarios considered before, we used the learning rate value that had showed the best results in the classification experiment using ground truth points. Additionally, in this experiment the practical use of the resulting classifier networks were considered and three "use cases" were summarised (figure 3.8). First in part (A) of the figure, data augmentation was not used in order to maximize the total classification accuracy of the network. Second part (B), a small amount of data augmentation was used to increase the sensitivity of the sick fir class while retaining most of the networks overall classification accuracy. Finally, part C contained information of a classifier that relied heavily on data augmentation to provide the maximum sensitivity for the sick fir class at the cost of decreasing the overall number of correctly classified trees among all classes.

Our algorithms can be used to gain valuable insight both into the tree type distribution of the studied forests as well as the health status of the fir trees. On the first case (A), the combination of our algorithms without using data augmentation provides us with a description of the location of trees and tree type distribution that automatically places and identifies correctly 78.59% of the trees. This shows that the analysis of drone-acquired images using computer vision and DL techniques

presents opportunities for forest research in a much larger scale than what was previously possible. Although there was 85.07% of trees successfully detected (80.16% for deciduous, 89.6% for healthy fir and 90.65% for sick fir), the first case had the problem that the sensitivity of the sick fir class was low with 39.64%, while 72.80% of deciduous trees and 82.07% of healthy fir trees were detected and classified correctly. The low detection + classification result for sick trees was mainly due to miss-classification. The value of approximately 40% sensitivity is coherent with the observed classification of ground truth treetops where the relatively low number of sick fir trees resulted in low sensitivity for this class. Using data augmentation in the classification part of the algorithm resulted in improved sensitivity for this class. This is achieved at the cost of decreased accuracy for the healthy fir and deciduous classes. The second case showed that using a moderate amount of data augmentation (6 synthetic images are created for each real image in the training set of each fold of the leave-one-out strategy) can increase the number of sick fir trees detected (up to 55.82%) at the cost of about a 5% loss in the percentage of trees correctly detected and classified (from 78.59% to 74.47%). This loss is better put into context by looking at the decrease in the number of False Positives produced for every positive detection. In this case, in order to detect approximately half of the sick fir trees, 2.13 False Positive predictions were detected for each True Positive. Taking into consideration, the infrequent occurrence of the sick fir class, the overall accuracy of the system is still high. Finally, a wider use of data augmentation (with 20 sick fir images created out of each original one) resulted in a percentage of correctly detected and classified sick fir treetops that rose to 73.01%. The cost of this increase is a larger FPR for sick fir (raising to 5.24 from 2.21) that resulted in a higher impact of the total performance of the system (with the percentage of deciduous

trees correctly detected and classified) slightly decreasing to 73.61% and that of healthy fir trees registering a sharp decrease down to 60.05%.

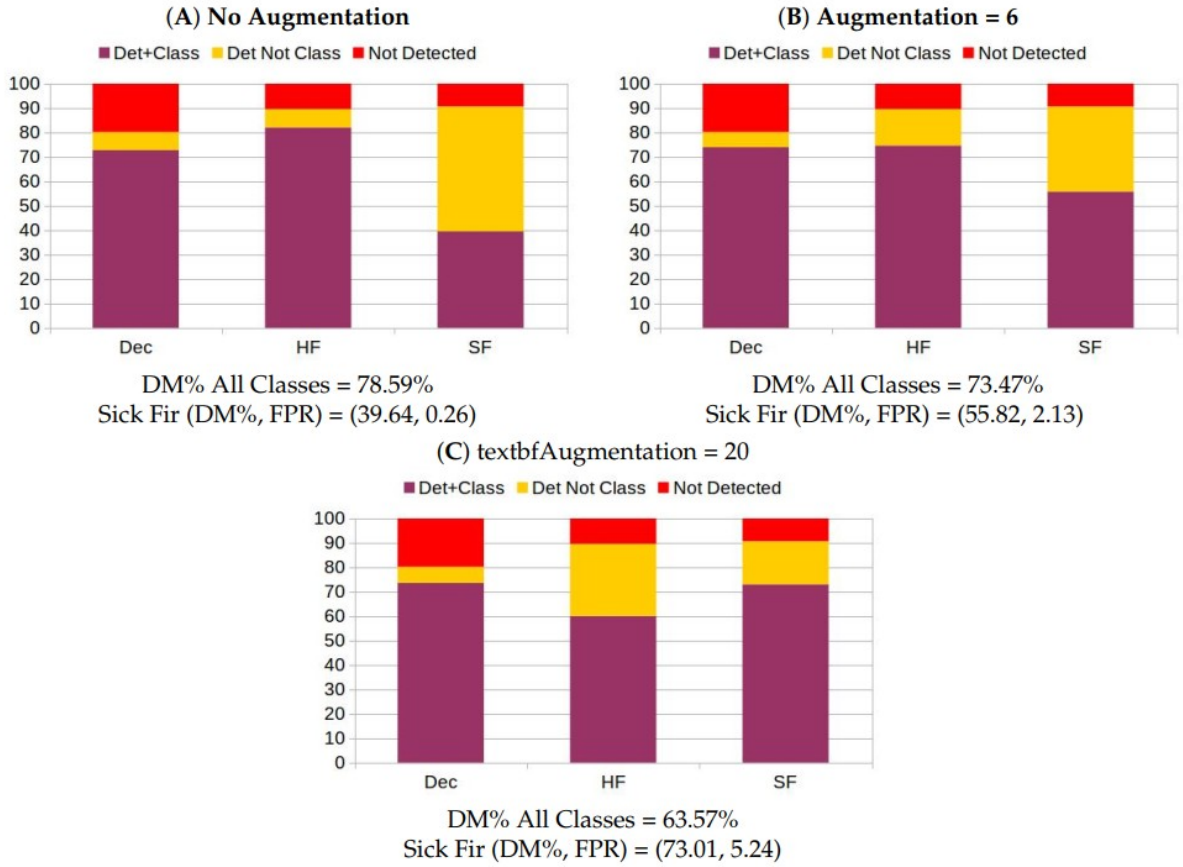

Figure 3.8: Detection and classification of trees according to species and health categories. Three graphs are presented according to three use cases of our algorithm (A) No Data Augmentation. (B) Data Augmentation = 6. (C) Data Augmentation = 20.

3.5 Discussion

3.5.1 Data Challenges

The research area is a natural mountainous forest. That presents high heterogeneity in terms of tree height, age and the tree type distribution within each of the study sites. While the use of UAV allow the collection of high-resolution data in wide extensions of this difficult-to-access area, the

data still presents some challenges. For example, after using the UAV-acquired images to build orthomosaics and DSM, the orthomosaics contained information extraneous to our purposes such as buildings, power lines or power towers. Additionally, and due to the flight pattern followed for data acquisition, the border sections of the orthomosaics contained heavy image distortions. Figure 3.9a presents examples of these two issues. In order to partially address these issues, for each orthomosaic we selected a Region Of Interest (ROI) in its central part and focused our computations within that region (figure 3.9 b). Additionally, the mountainous terrain resulted in the height values encoded in the DSM including in each pixel both the altitude of any trees present along with the terrain elevation. This severely hampered the automatic detection of treetops as the slope create the same elevation values of treetop downhill and the ground uphill. This problem was dealt by normalizing the slope with the Fusion/LDV software and having the ground removed by the software Global Mapper. Furthermore, some treetops were not distinguishable even in the nDSM. This happened particularly when larger, taller trees where very close to smaller trees with lower treetops. Figure 3.9 c, d presents an example of this. Even though 10 treetops are visible in the orthomosaic, only 4 clear distinct regions are visible in the nDSM. Although those treetops were not visible on the nDSM, they were still marked in the annotation step for the validation, but there is a high chance that they would not be found by any detection algorithm that uses elevation data to detect treetops (such as the one presented in this work).

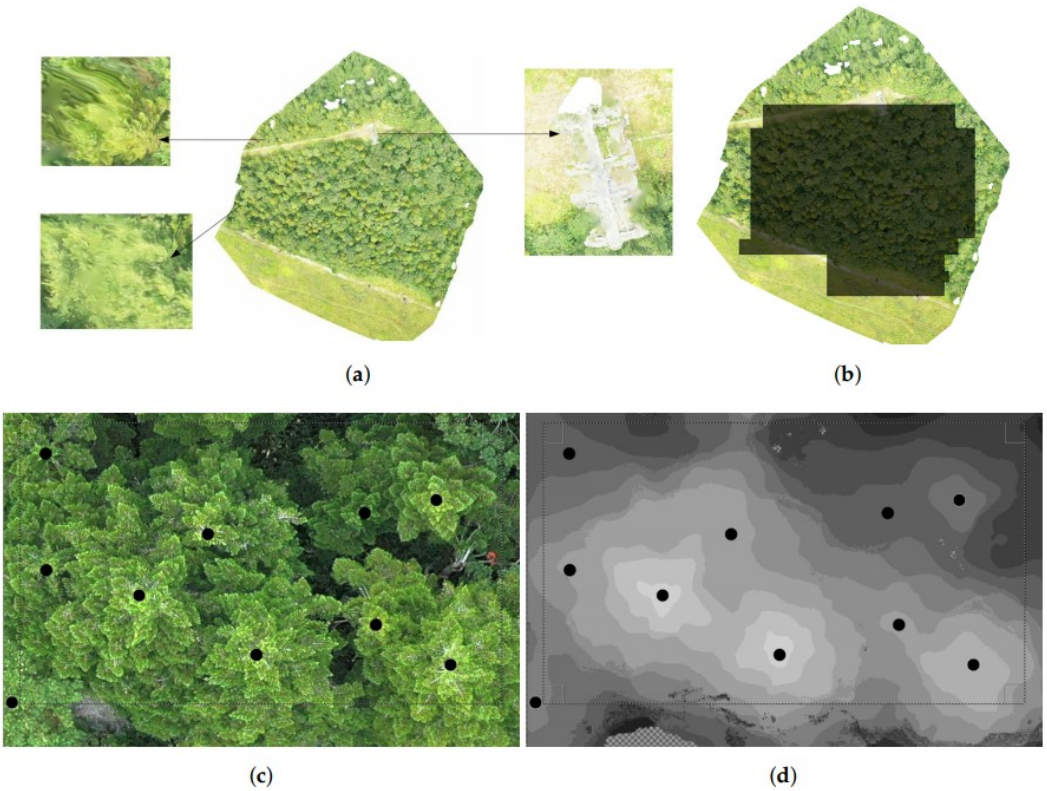

Figure 3.9: (a) artefact and distortion at the edge present in the orthomosaic; (b) ROI was applied to eliminate the artefacts and the distorted edge; (c) 10 Trees present in orthomosaics but (d) only 4 trees have clear distinct regions in nDSM.

The use of the pre-processing step allowed us to focus the detection and classification efforts in the parts of the orthomosaics and DSMs that correspond to tree canopies. Furthermore our treetop detection algorithm is based on exploring pixel altitude values starting with higher values (expected to belong to treetop tips). This makes it necessary to mitigate the distorting effect of the terrain in the elevation values by using the nDSM, which resulted in the loss of 2% of the treetops. Most of the lost treetops were located in parts of the orthomosaics that were out of the ROI. The number of treetops remain after the pre-processing step (5364 trees, with 169 sick fir trees) was larger than the number of trees considered in the other studies (336 in the testing set in Safonova et al., (2019) or 931 tree samples in the testing set in Sun et al., (2019) for example). The 85.70%

matching percentage obtained by the algorithm represents a clear improvement compared to existing methods (71.50% for the second-best method studied (Diez et al., 2020)). Most treetop detection mistakes occurred when deciduous trees were detected (80.16% matching percentage) while the fir classes presented even better performances (89.6% for healthy fir and 90.65% for sick fir). The counting criterion (cnt) results showed that the method used tends to overestimate the number of existing trees (by 9.67% on average), while other methods obtained better results in relation to the counting criterion for some sites. For example, for nDSM 1 our method obtained 89.61% matching with an overestimation of 9.87% of the number of treetops (yielding, thus, 81.56% of matched points among those predicted). On the other hand, the implementation of the Dawkins method used in Safonova et al., (2019) obtained 70.54% matching with 2.18% of treetop underestimation (representing a 72% of success). In comparison, our method found more ground truth points and made stronger predictions which can be explained by the fact that the data used in Safonova et al., (2019) was slightly different. While the tree species and the tree health problems studied in the later paper are the same, the boreal conditions in Siberia decreased the biodiversity so only fir trees are present which allows a clear visualization of individual trees. In this respect, nDSM 9, corresponding to the top site and with poor presence of deciduous trees may be more similar to the data in Safonova et al., (2019). The higher performance of our algorithm over the other algorithms considered is also supported by the average Euclidean distance metric. This method obtained a low value of just over 50 pixels (slightly under one meter) from any predicted point to the closest ground truth point. This value becomes as low as 27.42 pixels when other matched points were considered. The merits of these results are highlighted by taking into account the multiple data challenges previously mentioned. The effects of these particular conditions can be

appraised by comparing the results of the GMax (*m*%: 71.42, *cnt*: 10.22) and FCM (*m*%: 71.50, *cnt*: 10.24) methods with the data of our study to the ones they obtained in Diez et al., (2020) (*m*%: 90, *cnt*: 9). The decrease in performance is due to the differences in data as well as the more strict matching conditions expressed by the *e* parameter (3 m in Diez et al., (2020) compared to 2–2.5 in our study). We consider that these strict conditions coupled with the larger amount of data compared to other papers in the research area showcase the importance of the results achieved. The difference with previous studies also showed how this part of the algorithmic process is the most challenging and that further progress is likely possible. The performance of five existing DL networks were studied (AlexNet, Squeezenet, Vgg, ResNet and DenseNet) to classify the patches around treetops. Ground truth treetops were used to evaluate the performance of this part of our algorithmic process independently. Initial results using all data from all orthomosaics showed that all networks were able to obtain low error rates, especially Vgg (with the best value of ER = 0.03357%); ResNet and DenseNet performed well. However, the sick fir class was frequently missed and the low error rates reflected its low occurrence rate. While the numbers showed that the studied networks performed well, concerns towards their practical use arose. In order to address this issue as well as overfitting, a site-wise leave-one-out strategy was used to make sure that the training and testing sets never contained images from the same trees (even if taken in different flights and with different lighting conditions). Results showed that data augmentation succeeded in increasing the importance of the sick fir class during the training process and, thus, increase the sensitivity values obtained. This was coupled with minor decreases in specificity and accuracy for the sick fir class (0.9810, 0.9809) for the Resnet network when using 10 augmented images for each real sick fir image. The decrease in specificity produced that some images that did not contain sick fir trees were

wrongly predicted as such (False Positive detections). This resulted in slightly decreased accuracy values for the other classes (0.9601 accuracy of healthy fir). These results, even those with slightly lower accuracy, were in the higher band of the results obtained in previous studies (91.95–98.97% accuracy to classify sick fir in Safonova et al., (2019), 94.01–97% in Kentsch et al., (2020) to distinguish between deciduous and evergreen trees or 73.25% accuracy for multi-species classification (Sun et al., 2019). Finally, the performance of all the algorithms introduced in the paper was studied when applied to solve the real-life problem of classifying tree health and type classes found in forest sites. After adapting the training sets to account for the fact that the automatically detected treetops were not perfectly centered on the tree trunks, we aimed at assessing how many trees in the three categories were correctly detected and classified. After exploring different data augmentation scenarios three different use cases for our algorithms were presented. In the first case, working with the original data without data augmentation we were able to correctly detect and classify over 78% of the trees, giving a reliable description of the tree type distribution of the forest with percentages of correctly detected and classified trees of 72.80% and 82.07% for deciduous and healthy fir, respectively. The biggest downside of this case was the relatively low success rate in the classification of sick fir trees. Although 90.65% of sick fir trees were detected over all sites, only 39.64% of them were correctly classified with most of them misclassified as healthy. These results were in line with the tendency observed in the experiment where ground truth points had been used for classification, the low number of sick fir trees resulted in this class being mostly ignored in the training process and in a low specificity result. However, even in this situation, the information resulting from our algorithm was of practical use. A detailed analysis for each site showed that the algorithm found 3/20 sick fir trees in site 1, 13/49 in site 2, 7/20 in site

3 and 44/80 in site 4. The results missed a small cluster containing 4 trees in the orthomosaic 1 but otherwise found sick trees in all other affected regions (including one in a region containing only three sick trees in orthomosaic 3). The algorithm tended to underestimate the extent of the regions affected by classifying the less affected trees as healthy but correctly identified the affected regions. As mentioned before, the definition of "sick" fir is slightly open to interpretation, especially, when trees presenting slight defoliation (figure 3.2b) are considered healthy while others with slightly more defoliation, sometimes obscured by top branches with green leaves (Figure 3.2c) are considered sick. Because of this, in practice any cluster of sick trees detected using the algorithm would need to be confirmed by expert analysis of the drone images and, if at all possible, with observations on the ground. Nevertheless, the results presented here show that this version of the algorithms can be used as an automatic early warning tool to detect even minor bark beetle outbreaks. In the other two cases presented, data augmentation was used to increase the importance of the sick fir class during training in order to increase its specificity. This was achieved at the cost of producing a number of False Positive detections, mostly by classifying healthy fir trees as sick. In the "balanced" case (augm 6) we could detect 55.82% of the sick fir trees producing 2.13 extra False Positive detections for each correct one (FPR 2.23) and in the case where we focused in the detection of sick fir trees (augm 20) we detected 73.01% of them at the cost of an FPR of 5.24. Both of these approaches correctly detected and classified trees in all outbreak regions at the price of overestimating their extension. The somewhat difficult distinction between sick and healthy fir played a reverse role to the first use case with most of the False Positive sick fir detections being found in areas close to outbreaks but marked as healthy. Although this may provide users with

wrong information and exaggerating the extent of the outbreaks it can also be seen as a way to point out possible areas of outbreak development.

3.6 Conclusions

The study presented algorithms for the automatic detection and classification of fir trees (healthy and sick in terms of a bark beetle infestation) as well as deciduous trees. The detection of individual treetops was found to be a key part of the process that had not been studied in enough detail so far. Our results, including the comparison of three state of the art methods showed that the algorithm for treetop detection introduced in the current work was able to detect 85.70% of existing trees, outperforming existing methods in experiments that were challenging both in terms of the data used and the quality criteria considered. We then moved on to show how, as seen in other application domains, DL networks can successfully learn to classify the classes present in our problem (obtaining over 98% accuracy on average over the three classes). However, in this case a careful use of data augmentation was needed to obtain results that not only presented good classification metrics but were also meaningful in practice. We have also presented what is, to the best of our knowledge, a detailed study of the performance of all the algorithms presented when used together, paying special attention to the sources of error and to their practical implications. In terms of the detection of sick fir trees, the main goal of our study, we showed how just under 10% of the points were not detected and how the amount of remaining points correctly classified depended on how data augmentation was used. In one use case, our algorithms were able to detect and classify correctly 78% of the trees in all species. This algorithm was also able to detect all but one of the existing outbreak clusters (composed of 4 sick trees) where it detected only about 40%

of the existing sick trees. This percentage was increased to 73.01% at the price of producing a large number of false positive detections. Consequently, we have shown how computer vision and DL networks when used to process UAV-acquired images, already provide a valuable tool for the automatic detection and monitoring of sick fir trees with tangible benefits in terms of study time, human resources needed and extent of land area required for study. Regarding future research directions, the treetop detection algorithm could be improved by considering the detection of treetops of each separate species individually since a 10% discrepancy in the percentage of successfully detected trees was observed between fir and deciduous trees. Regarding the classification algorithm, collecting datasets with a larger number of sick tree examples would reduce the need to use data augmentation and, with it, the number of false positive detections. This would also open the possibility to DL networks with a larger number of layers and optimizable parameters.

Chapter 4 Conclusion

The results of this study have shown the potential of UAV technology and AI to solve problems in forest research. The use of UAV in forestry closes the gap between the single tree and the whole forest level analysis. The very high resolution UAV-acquired images open a new window on the level of detail with which we can observe tree spatial and temporal changes in their health condition. In this study, we have focused on the health condition of *Abies mariesii* trees in Zao Mountains in northeastern Japan and have obtained an understanding of the tree health condition at individual level and the distribution of these health categories within the fir forest ecosystem. Furthermore, the large areas of around 20-30 hectares that we covered with the UAV and their different geographical conditions (altitude, slope steepness, aspect, and forest composition) within the research site has allowed us to infer the possible factors affecting the spread of bark beetles or the mitigation factors that prevent it. The validation of the results obtained from the RGB images by means of field survey has been an important part of this study.

Maries fir trees are found as north as Aomori prefecture and as south as Gifu prefecture comprising a latitudinal range of approximately 700 km, however, the virulence of the attack has only been observed in Zao Mountains. Therefore, the methodology we have applied in our study, gave us an understanding of the damage caused in this area and establish a solid base for studying the process involved in the weakening of fir forest that has served as an ideal host for bark beetle outbreak.

In this study, the role of terrain properties or characteristics in the spread of bark beetles have been evaluated by using Random Forest (RF) to predict the infestation and tree health status using

elevation, slope, and aspect as the possible drivers. The model accuracy gained 75% for the prediction on the occurrence of bark beetles (healthy and infested classes) and 71% for the prediction on tree health categories (healthy, sick and dead). This proves that terrain has played a major role on the spread of bark beetles in Zao Mountains. The feature importance function in the RF has also provided an insight into each terrain factor. Elevation controls 60% of the accuracy of the model while slope and aspect each share 20% role each. This is mainly because terrain regulates the mountainous climate which is important for suitable conditions of outbreak of bark beetles (Amman, 1973) while slope and aspect enhance the effect of strong wind and light which stress the trees (Iwaki & Totsuka, 1959; Maruta, & Nakano, 1999). However, further studies should be conducted in the other prefectures where also has the distribution of fir trees in order to verify if the finding in this study can also be applied to explain the situation in the other Mountain across Japan.

Regarding the automatic tree detection, the study could detect about 90% of fir trees and more than 80% of deciduous trees, outperforming the methods of previous studies (Safonova et al., 2019; Diez et al., 2020) when applied on our data. The complex terrain is found as one of the major challenges for the data analysis. It is solved by using nDSM (or CHM) to normalize the terrain. However the quality of the nDSM also affects the accuracy of the detection. According to the results, Phantom 4 provided better quality of DSM and nDSM in comparison with Mavic 2 pro, presenting better detection result on site 4 (87.9%) than site 2 (84.4%) and 3 (79.8%). Site 1 with the lowest number of trees (approx. 800 trees) achieved the highest percentage of trees detected (88.7%). The missing fir trees were found on the distorted edges or not appeared on the nDSM. Besides the constraint of UAV platform, the flying height also affects the quality of nDSM. All the data in this

study were collected within 60 m – 70 m flying height above the take off points. In steep slope mountains, this created heterogeneous heights from the UAV to the trees. The trees that are farther from the UAV will have less detail, thus, appear smaller and vague on the nDSM. Flying the UAV following the terrain is recommended in the future to maintain the same distance from it to the trees, so does the tree size and the amount of details of all trees by increasing the number of dense points.

This study has also successfully classified two classes of fir: healthy and sick, using DL, with the accuracy of nearly 98% for each class. Focusing on the true positive (correctly predicted) result, the healthy class achieved 99.5% of sensitivity while it was only 51.3% for sick class using the DenseNet model, due to the imbalance of the data (much more healthy fir than sick fir presented in the images). The performance of sick fir was maximized to 99.7% by using augmentation techniques on ResNet model. Beside the amount of data that affected the performance of the DL model, the annotation was found to be crucial for the classification quality. Since the number of sick trees classification was done based on the level of defoliation and the different patterns of defoliation that infested fir trees can show, it was not always straight forward to define how sick one tree is. Therefore in this study, in order to create a strong definition for the DL to recognize sick trees, I only focused on one type of sick (when there is at least one branch totally defoliated). Thus, in order to develop a classification system that is able to identify different degrees of sickness based on the defoliation (Ferracini, 2020), a mathematical system is recommended to standardize the manual annotation. This will also benefit the annotation process in term of time saving as the amount of annotated data required for DL is large.

Bibliography

Agisoft, L. Agisoft Metashape, Professional Edition, Version 1.5.5. Available online: http://agisoft.com/ (accessed on 19 March 2020)

Agne, M. C., Beedlow, P. A., Shaw, D. C., Woodruff, D. R., Lee, E. H., Cline, S. P., & Comeleo, R. L. (2018). Interactions of predominant insects and diseases with climate change in Douglas-fir forests of western Oregon and Washington, USA. *Forest Ecology and Management*, 409, 317-332.

Amman, G. D. (1973). Population changes of the mountain pine beetle in relation to elevation. *Environmental Entomology*, 2(4), 541-548.

Amman, G. D. (1978, April). Biology, ecology, and causes of outbreaks of the mountain pine beetle in lodgepole pine forests. In *Theory and practice of mountain pine beetle management in lodgepole pine forests: proceedings of the symposium* (pp. 25-27).

Arno, S. F., & Hoff, R. J. (1990). Pinus albicaulis Engelm. whitebark pine. *Silvics of North America*, 1, 268-279.

Baranchikov, Y., Akulov, E. and Astapenko, S., (2010). *Bark beetle Polygraphus proximus: a new aggressive far eastern invader on Abies species in Siberia and European Russia. USDA Research Forum on Invasive Species*. GTR-NRS-P-75.

Baranchikov, Y., Akulov, E. and Astapenko, S., 2011. Bark beetle Polygraphus proximus: a new aggressive Far Eastern invader on Abies species in Siberia and European Russia. In In: McManus, Katherine A; Gottschalk, Kurt W., eds. 2010. Proceedings. 21st US Department of Agriculture interagency research forum on invasive species 2010; 2010 January 12-15; Annapolis, MD. Gen. Tech. Rep. NRS-P-75. Newtown Square, PA: US Department of Agriculture, Forest Service, Northern Research Station: pp. 64-65.

Brandtberg, T., & Walter, F. (1998). Automated delineation of individual tree crowns in high spatial resolution aerial images by multiple-scale analysis. *Machine Vision and Applications*, 11(2), 64-73.

Breiman, L. (2001). Random forests. *Machine learning*, 45(1), 5-32.

Brieger, F., Herzschuh, U., Pestryakova, L. A., Bookhagen, B., Zakharov, E. S., & Kruse, S. (2019). Advances in the derivation of Northeast Siberian forest metrics using high-resolution UAV-based photogrammetric point clouds. *Remote Sensing*, 11(12), 1447.

Cabezas, M., Kentsch, S., Tomhave, L., Gross, J., Caceres, M. L. L., & Diez, Y. (2020). Detection of Invasive Species in Wetlands: Practical DL with Heavily Imbalanced Data. *Remote Sensing*, 12(20), 3431.

Chen, Q., Baldocchi, D., Gong, P., & Kelly, M. (2006). Isolating individual trees in a savanna woodland using small footprint lidar data. *Photogrammetric Engineering & Remote Sensing*, 72(8), 923-932.

Chiba, S., Kawatsu, S., Hayashida, M., (2020). Large-area Mapping of the Mass Mortality and Subsequent Regeneration of *Abies mariesii* Forests in the Zao Mountains in Northern Japan. J Jpn For Soc 102: 108-114.

Chilahsaeva EA. (2008). First record of Polygraphus proximus (Coleoptera, Scolytidae) in Moscow Province. *Bulletin of the Moscow Society of Naturalists* 113(6), 39-42. [In Russian]

Chilakhsaeva, E.A. (2008). First find of Polygraphus proximus Blandford, 1894 (Coleoptera, Scolytidae) in Moscow oblast, Byull. Mosk. Ova. Ispyt. Prir., Otd. Biol., vol. 113, no. 6, pp. 39–42.

Ciesla, W.M. (2001). Protecting plantations from pests and diseases. Forestry Department. Food and Agriculture Organization of the United Nations. Forest Plantations Thematic Papers.

Cole, D. N. (1990). Recreation In Whitebark Pine. In *Proceedings--Symposium on Whitebark Pine Ecosystems*: *Ecology and Management of a High-Mountain Resource, Bozeman, MT, March* 29-31 (Vol. 270, p. 305). US Department of Agriculture, Forest Service, Intermountain Research Station.

Cole, W. E., & Amman, G. D. (1980). Mountain pine beetle dynamics in lodgepole pine forests, Part 1: course of an infectation. *The Bark Beetles, Fuels, and Fire Bibliography*, 72.

Dash, J. P., Watt, M. S., Pearse, G. D., Heaphy, M., & Dungey, H. S. (2017). Assessing very high resolution UAV imagery for monitoring forest health during a simulated disease outbreak. *ISPRS Journal of Photogrammetry and Remote Sensing*, 131, 1-14.

Deng, L., & Yu, R. (2015, December). Pest recognition system based on bio-inspired filtering and LCP features. In 2015 12*th International Computer Conference on Wavelet Active Media Technology and Information Processing* (*ICCWAMTIP*) (pp. 202-204). IEEE.

Diez, Y., Kentsch, S., Caceres, M. L. L., Nguyen, H. T., Serrano, D., & Roure, F. (2020, February). Comparison of algorithms for Tree-top detection in Drone image mosaics of Japanese Mixed Forests. In *ICPRAM* (pp. 75-87).

Dupret, G., & Koda, M. (2001). Bootstrap re-sampling for unbalanced data in supervised learning. *European Journal of Operational Research*, 134(1), 141-156.

EFSA - European Food Safety Authority, de la Peña, E., Kinkar, M. and Vos, S., 2020. Pest survey card on Polygraphus proximus. *EFSA Supporting Publications*, 17(1), p.1780E.

Emiko Maruta, & Takashi Nakano. (1999). The effects of environmental stresses on conifers in the subalpine area of the Central Japan (Current status and future of plant communities in the alpine and subalpine zones of the central mountainous region). *Journal of the Ecological Society of Japan,* 49 (3), 293-300.

EPPO. (2014). Pest Risk Analysis for Polygraphus Proximus.

FAO. (2011). Guide to implementation of phytosanitary standards in forestry. FAO Forestry Paper no. 164. Rome

Ferracini, C., Saitta, V., Pogolotti, C., Rollet, I., Vertui, F., & Dovigo, L. (2020). Monitoring and management of the pine processionary moth in the North-Western Italian Alps. *Forests*, 11(12), 1253.

Franklin, J. F., Maeda, T., Ohsumi, Y., Matsui, M., Yagi, H., & Hawk, G. M. (1979). Subalpine coniferous forests of central Honshu, Japan. Ecological monographs, 49(3), 311-334.

Frey, J., Kovach, K., Stemmler, S., & Koch, B. (2018). UAV photogrammetry of forests as a vulnerable process. A sensitivity analysis for a structure from motion RGB-image pipeline. *Remote Sensing*, 10(6), 912.

Gninenko, U.I., Czilaszajeva, E.A., and Klukin, M.S. Nowe zagro enie dla lasów Europy kornik ussuryjski (Polygraphus proximus), Gospodarka Le na, GOSLASU, 2012, vol. 9, p. 19.

Gougeon, F. A. (1998, February). Automatic individual tree crown delineation using a valley-following algorithm and rule-based system. In *Proc. International Forum on Automated Interpretation of High Spatial Resolution Digital Imagery for Forestry, Victoria, British Columbia, Canada* (pp. 11-23).

Gu, J., Grybas, H., & Congalton, R. G. (2020). Individual tree crown delineation from UAS imagery based on region growing and growth space considerations. *Remote Sensing*, 12(15), 2363.

Hansen, M. M., Jones, R., & Tocchini, K. (2017). Shinrin-yoku (forest bathing) and nature therapy: A state-of-the-art review. *International journal of environmental research and public health*, 14(8), 851.

Hara, H., Miyoshi, H. and Tokuda, S. (2008). Forest decline after the damage by a typhoon in the Kubo thinning experiment forest [Japan] of Todo-fir, Abies sachalinensis, and the occurrence of a fir bark beetle, Polygraphus proximus. Bulletin of the Hokkaido Forestry Research Institute (Japan).

He, K., Zhang, X., Ren, S., & Sun, J. (2016). Deep residual learning for image recognition. In *Proceedings of the IEEE conference on computer vision and pattern recognition* (pp. 770-778).

Holmgren, J., & Persson, Å. (2004). Identifying species of individual trees using airborne laser scanner. *Remote Sensing of Environment*, 90(4), 415-423.

Howard, J., & Gugger, S. (2020). Fastai: a layered API for deep learning. *Information*, 11(2), 108.

Huang, G., Liu, Z., Van Der Maaten, L., & Weinberger, K. Q. (2017). Densely connected convolutional networks. In *Proceedings of the IEEE conference on computer vision and pattern recognition* (pp. 4700-4708).

Iandola, F. N., Han, S., Moskewicz, M. W., Ashraf, K., Dally, W. J., & Keutzer, K. (2016). SqueezeNet: AlexNet-level accuracy with 50x fewer parameters and < 0.5 MB model size. *arXiv preprint arXiv*:1602.07360.

Iwaki, H., & Totsuka, T. (1959). Ecological and physiological studies on the vegetation of Mt. Shimagare. II. On the crescent-shaped "dead trees strips" in the Yatsugatake and the Chichibu Mountains. *Bot. Mag. Tokyo*, 72, 255-260.

Jactel, H., Koricheva, J., & Castagneyrol, B. (2019). Responses of forest insect pests to climate change: not so simple. *Current opinion in insect science*, 35, 103-108.

Jayathunga, S., Owari, T., & Tsuyuki, S. (2019). Digital aerial photogrammetry for uneven-aged forest management: Assessing the potential to reconstruct canopy structure and estimate living biomass. *Remote Sensing*, 11(3), 338.

JMA, Japan Meteorological Agency website, https://www.jma.go.jp/jma/indexe.html (accessed on 1 October 2021)

Jung, A. B., Wada, K., Crall, J., Tanaka, S., Graving, J., Reinders, C., ... & Laporte, M. (2020). *Imgaug*. 2020.

Kai, K. (1977). Regional division of the Honshu Mountains by predominant wind direction estimated from Polarimetric Trees. *Geographical Review of Japan,* 50 (1), 45-54.

Kandler, O., Development of the recent episode of Tannensterben (fir decline) in Eastern Bavaria and the Bavarian Alps, in Forest Decline in the Atlantic and Pacific Region, Berlin: Springer-Verlag, 1993, pp. 216–226.

Kattenborn, T., Sperlich, M., Bataua, K., & Koch, B. (2014). Automatic single tree detection in plantations using UAV-based photogrammetric point clouds. *The International Archives of Photogrammetry, Remote Sensing and Spatial Information Sciences*, 40(3), 139.

Ke, Y., & Quackenbush, L. J. (2011). A comparison of three methods for automatic tree crown detection and delineation from high spatial resolution imagery. *International Journal of Remote Sensing*, 32(13), 3625-3647.

Keane, R. E. (2000). The importance of wilderness to whitebark pine research and management. In *Proceedings of the symposium*: *Wilderness Science*: *In a time for change* (Vol. 3, pp. 84-93).

Keane, R. E., & Arno, S. F. (1993). Rapid decline of whitebark pine in western Montana: evidence from 20-year remeasurements. *Western Journal of Applied Forestry*, 8(2), 44-47.

Kerchev IA and Torchkova DA. (2018). Assessment of the flight activity of the Four-eyed fir bark beetle Polygraphus proximus Blandf. (Coleoptera, Curculionidae: Scolytinae) in dark coniferous stands using UAV technology. *All-Russian Conference and X Annual Kataev Memorial Reading, St-Peterburg, Russia, pp.* 45. [In Russian].

Kerchev, I.A. (2014). Ecology of four-eyed fir bark beetle Polygraphus proximus Blandford (Coleoptera; Curculionidae, Scolytinae) in the west Siberian region of invasion. Russian journal of biological invasions, 5(3), pp.176-185.

Kobayashi, K. and Takagi, E. (2020). Mating Systems of the Tree-Killing Bark Beetle Polygraphus proximus (Coleoptera: Curculionidae: Scolytinae). *Journal of Insect Science*, 20(6), p.38.

Kononov, A., Ustyantsev, K., Blinov, A., Fet, V., & Baranchikov, Y. N. (2016). Genetic diversity of aboriginal and invasive populations of four-eyed fir bark beetle P olygraphus proximus B landford (Coleoptera, C urculionidae, S colytinae). *Agricultural and Forest Entomology*, 18(3), 294-301.

Kraus, K., & Pfeifer, N. (1998). Determination of terrain models in wooded areas with airborne laser scanner data. *ISPRS Journal of Photogrammetry and remote Sensing,* 53(4), 193-203.

Krivets SA. (2012) Notes on the ecology of the fir bark beetle *Polygraphus proximus* Blandf. (Coleoptera, Scolytidae) in West Siberia. Izvestiya Sankt-Peterbugskoy Lesoteknicheskoy Akademii [*Proc. Sant-Petersburg Forest-Tecknical Academy*], 2012. No. 200:94-105 [in Russian]

Krivets, S. A., Bisirova, E. M., Kerchev, I. A., Pats, E. N., & Chernova, N. A. (2015). Transformation of taiga ecosystems in the Western Siberian invasion focus of four-eyed fir bark beetle Polygraphus proximus Blandford (Coleoptera: Curculionidae, Scolytinae). *Russian Journal of Biological Invasions*, 6(2), 94-108.

Krivets, S. A., Kerchev, I. A., Bisirova, E. M., Debkov, N. M., Chernova, N. A., & Pats, E. N. 3.2. (2019) Four-eyed fir bark beetle Polygraphus proximus Blandford, 1894 (Coleoptera, Curculionidae: Scolytinae) in Western Siberia: review of a ten years of research of the invasion. *Invasive Dendrophilous Organisms*: *Challenges And Protection Operations*, 87.

Krizhevsky, A., Sutskever, I., & Hinton, G. E. (2012). Imagenet classification with deep convolutional neural networks. *Advances in neural information processing systems*, 25, 1097-1105.

Krokene, P., & Solheim, H. (1998). Pathogenicity of four blue-stain fungi associated with aggressive and nonaggressive bark beetles. *Phytopathology*, 88(1), 39-44.

Kurz, W. A., Dymond, C. C., Stinson, G., Rampley, G. J., Neilson, E. T., Carroll, A. L., ... & Safranyik, L. (2008). Mountain pine beetle and forest carbon feedback to climate change. *Nature*, 452(7190), 987-990.

Kwak, D. A., Lee, W. K., & Lee, J. H. (2006, November). Predicting forest stand characteristics with detection of individual tree. In *Proceedings of the MAPPS/ASPRS* 2006 *fall conference*.

Lanner, R. M. (1996). *Made for each other*: *a symbiosis of birds and pines*. Oxford University Press on Demand.

Lausch, A., Fahse, L., & Heurich, M. (2011). Factors affecting the spatio-temporal dispersion of Ips typographus (L.) in Bavarian Forest National Park: A long-term quantitative landscape-level analysis. *Forest Ecology and management*, 261(2), 233-245.

Lim, Y. S., La, P. H., Park, J. S., Lee, M. H., Pyeon, M. W., & Kim, J. I. (2015). Calculation of tree height and canopy crown from drone images using segmentation. *Journal of the Korean Society of Surveying, Geodesy, Photogrammetry and Cartography*, 33(6), 605-614.

Lin, J., Wang, M., Ma, M., & Lin, Y. (2018). Aboveground tree biomass estimation of sparse subalpine coniferous forest with UAV oblique photography. *Remote Sensing*, 10(11), 1849.

Linnakoski R and Forbes KM. (2019) Pathogens—The Hidden Face of Forest Invasions by Wood-Boring Insect Pests. Front. Plant Sci. 10:90.

Logan, J. A., & Powell, J. A. (2001). Ghost forests, global warming, and the mountain pine beetle (Coleoptera: Scolytidae). *American Entomologist*, 47(3), 160-173.

Masarczyk, W., Głomb, P., Grabowski, B., & Ostaszewski, M. (2020). Effective training of deep convolutional neural networks for hyperspectral image classification through artificial labeling. *Remote Sensing*, 12(16), 2653.

Masaya Saito & Sho Chiba. (2017) - Understanding the current situation of the damaged forest of Zao Abies mariesii, efforts for regeneration - 蔵王オオシラビソ 被害林の現況把握と再生に向けた取り組つみにいて (In Japanese)

McGaughey, R. J. (2009). Software for LIDAR data analysis and visualization (No. 123). Report.

Mead, D. J., & Ciesla, W. M. (2001). Protecting plantations from pests and diseases. *Forest Plantations Thematic Papers. Working Paper (FAO)*.

Mlambo, R., Woodhouse, I. H., Gerard, F., & Anderson, K. (2017). Structure from motion (SfM) photogrammetry with drone data: A low cost method for monitoring greenhouse gas emissions from forests in developing countries. *Forests*, 8(3), 68.

Mohan, M., Silva, C., Klauberg, C., Jat, P., Catts, G. and Cardil, A. (2017). Individual Tree Detection from Unmanned Aerial Vehicle (UAV) Derived Canopy Height Model in an Open Canopy Mixed Conifer Forest. *Forests.* 8: 340.

Näsi, R., Honkavaara, E., Lyytikäinen-Saarenmaa, P., Blomqvist, M., Litkey, P., Hakala, T., ... & Holopainen, M. (2015). Using UAV-based photogrammetry and hyperspectral imaging for mapping bark beetle damage at tree-level. *Remote Sensing*, 7(11), 15467-15493.

Natesan, S., Armenakis, C., & Vepakomma, U. (2019). Resnet-based tree species classification using uav images. *International Archives of the Photogrammetry, Remote Sensing & Spatial Information Sciences*.

Nobuchi, A. (1979). Studies on Scolytidae. XVIII. Bark beetles of tribe Polygraphini in Japan (Coleoptera, Scolytidae). *Bull Gov For Exp Stat*, 308, pp.1-16.

Okitsu, S. (2003). Forest vegetation of northern Japan and the southern Kurils. *In Forest Vegetation of Northeast Asia* (pp. 231-261). Springer, Dordrecht.

Onishi, M., & Ise, T. (2018). Automatic classification of trees using a UAV onboard camera and deep learning. *arXiv preprint arXiv*:1804.10390.

Pavlov, I.N., Litovka, Y.A., Golubev, D.V., Astapenko, S.A., Chromogin, P.V., Usoltseva, Y.V., Makolova, P.V. and Petrenko, S.M. (2020). Mass Reproduction of Polygraphus proximus Blandford in Fir Forests of Siberia Infected with Root and Stem Pathogens: Monitoring, Patterns, and Biological Control. *Contemporary Problems of Ecology*, 13(1), pp.71-84.

Pedregosa, F., Varoquaux, G., Gramfort, A., Michel, V., Thirion, B., Grisel, O., ... & Duchesnay, E. (2011). Scikit-learn: Machine learning in Python. *the Journal of machine Learning research*, 12, 2825-2830.

Pleșoianu, A. I., Stupariu, M. S., Șandric, I., Pătru-Stupariu, I., & Drăguț, L. (2020). Individual tree-crown detection and species classification in very high-resolution remote sensing imagery using a deep learning ensemble model. *Remote Sensing*, 12(15), 2426.

Przepióra, F., Loch, J., & Ciach, M. (2020). Bark beetle infestation spots as biodiversity hotspots: Canopy gaps resulting from insect outbreaks enhance the species richness, diversity and abundance of birds breeding in coniferous forests. *Forest Ecology and Management*, 473, 118280.

Qiu, L., Jing, L., Hu, B., Li, H., & Tang, Y. (2020). A new individual tree crown delineation method for high resolution multispectral imagery. *Remote Sensing*, 12(3), 585

Raffa, K. F., Grégoire, J.-L., and Lindgren, B. S. (2015). "Natural history and ecology of bark beetles," in Bark beetles: Biology and Ecology of Native and Invasive Species, eds F. Vega and R. Hofstetter (London: Academic Press), 1–40

Rasmussen, L. A. (1974). Flight and attack behavior of mountain pine beetles in lodgepole pine of northern Utah and southern Idaho (Vol. 180). *US Department of Agriculture, Forest Service*, Intermountain Forest & Range Experiment Station.

Reid, R. W. (1962). Biology of the Mountain Pine Beetle, Dendroctonus monticolae Hopkins, in the East Kootenay Region of British Columbia I. Life Cycle, Brood Development, and Flight Periods1. *The Canadian Entomologist*, 94(5), 531-538.

Rice, A. V., Thormann, M. N., & Langor, D. W. (2007). Mountain pine beetle associated blue-stain fungi cause lesions on jack pine, lodgepole pine, and lodgepole× jack pine hybrids in Alberta. *Botany*, 85(3), 307-315.

Safonova, A., Tabik, S., Alcaraz-Segura, D., Rubtsov, A., Maglinets, Y., & Herrera, F. (2019). Detection of fir trees (Abies sibirica) damaged by the bark beetle in unmanned aerial vehicle images with deep learning. *Remote sensing*, 11(6), 643.

Safranyik, L., & Carroll, A. L. (2007). The biology and epidemiology of the mountain pine beetle in lodgepole pine forests. *The mountain pine beetle*: *a synthesis of biology, management and impacts on lodgepole pine*, 3-66.

Sasaki, A (2015). Year-round observation of temperature in the subalpine zone of Zao volcano. Kokushikan University Geography Report No.23 (*In Japanese*).

Shiferaw, H., Bewket, W., & Eckert, S. (2019). Performances of machine learning algorithms for mapping fractional cover of an invasive plant species in a dryland ecosystem. *Ecology and evolution*, 9(5), 2562-2574.

Simonyan, K., & Zisserman, A. (2014). Very deep convolutional networks for large-scale image recognition. *arXiv preprint arXiv*:1409.1556.

Six, D. L., & Paine, T. D. (1998). Effects of mycangial fungi and host tree species on progeny survival and emergence of Dendroctonus ponderosae (Coleoptera: Scolytidae). *Environmental Entomology*, 27(6), 1393-1401.

Smigaj, M., Gaulton, R., Barr, S. L., & Suárez, J. C. (2015). Uav-Borne Thermal Imaging For Forest Health Monitoring: Detection Of Disease-Induced Canopy Temperature Increase. *International Archives of the Photogrammetry, Remote Sensing & Spatial Information Sciences*, 40.

Sun, Y., Huang, J., Ao, Z., Lao, D., & Xin, Q. (2019). Deep learning approaches for the mapping of tree species diversity in a tropical wetland using airborne LiDAR and high-spatial-resolution remote sensing images. *Forests*, 10(11), 1047.

Suyama, Y. (2014). Geographical genetic structure of Japanese forest trees (7) - Abies mariesii (Pinaceae, Fir genus). Forest Genetic Breeding Volume 3 (*In Japanese*).

Takagi, E., Masaki, D., Kanai, R., Sato, M., & Iguchi, K. (2018). Mass mortality of Abies veitchii caused by Polygraphus proximus associated with tree trunk diameter in Japan. *Forest Ecology and Management*, 428, 14-19.

Tanaka, N. and Matsui, T. (2007) PRDB: Phytosociological Relevé Database, *Forestry and Forest Products Research Institute*. URL: http://www.ffpri.affrc.go.jp/labs/prdb/index.html

Tokuda, M., Shoubu, M., Yamaguchi, D., & Yukawa, J. (2008). Defoliation and dieback of Abies firma (Pinaceae) trees caused by Parendaeus abietinus (Coleoptera: Curculionidae) and Polygraphus proximus (Coleoptera: Scolytidae) on Mount Unzen, Japan. *Applied entomology and zoology*, 43(1), 1-10.

van Lierop, P., Lindquist, E., Sathyapala, S. and Franceschini, G. (2015). Global forest area disturbance from fire, insect pests, diseases and severe weather events. *Forest Ecology and Management*, 352, pp.78-88.

Watanabe Koya. (2015). From 1933 to 2015 Monthly average temperature change on Mt. Zao. Yamagata University Faculty of Science Department of Global Environment. Report (*In Japanese*).

Westoby, M. J., Brasington, J., Glasser, N. F., Hambrey, M. J., & Reynolds, J. M. (2012). 'Structure-from-Motion'photogrammetry: A low-cost, effective tool for geoscience applications. *Geomorphology*, 179, 300-314.

Wichmann, L., & Ravn, H. P. (2001). The spread of Ips typographus (L.)(Coleoptera, Scolytidae) attacks following heavy windthrow in Denmark, analysed using GIS. *Forest Ecology and Management*, 148(1-3), 31-39.

Wulder, M. A., White, J. C., Bentz, B., Alvarez, M. F., & Coops, N. C. (2006). Estimating the probability of mountain pine beetle red-attack damage. *Remote Sensing of Environment*, 101(2), 150-166.

Wulder, MA, Skakun, RS, Franklin, SE, & White, JC. (2005). Enhancing forest inventories with mountain pine beetle infestation information. *The Forestry Chronicle*, 81 (1), 149-159.

Yamaguchi, H. (1963). Survey and population studies of beetles in windswept areas in Hokkaido (II). Beetle infestations on windthrown trees in the second year, in 1955, Bull. Gov. For. Exp. Sta., vol. 151, pp. 53–73.

Yatoh, K. (1958). Collecting and Breeding 20: 258.

Zarco-Tejada, P. J., Diaz-Varela, R., Angileri, V., & Loudjani, P. (2014). Tree height quantification using very high resolution imagery acquired from an unmanned aerial vehicle (UAV) and automatic 3D photo-reconstruction methods. *European journal of agronomy*, 55, 89-99.

Zhao, X., Zhang, J., Tian, J., Zhuo, L., & Zhang, J. (2020). Residual dense network based on channel-spatial attention for the scene classification of a high-resolution remote sensing image. *Remote Sensing*, 12(11), 1887.

Zhen, Z., Quackenbush, L. J., Stehman, S. V., & Zhang, L. (2015). Agent-based region growing for individual tree crown delineation from airborne laser scanning (ALS) data. *International Journal of Remote Sensing*, 36(7), 1965-1993.

Appendix

A. Random Forest code for tree types and health prediction

```
import numpy as np
import matplotlib.pyplot as plt
import pandas as pd
from sklearn.preprocessing import StandardScaler
from sklearn.ensemble import RandomForestClassifier
from sklearn import metrics
import seaborn as sns
import csv

#import training dataset
train_set = pd.read_csv('Training_set.csv')
x_train = train_set.iloc[:, 4:-1].values
y_train = train_set.iloc[:, -1].values

#import testing dataset
test_set = pd.read_csv('Test_Set.csv')
x_test = test_set.iloc[:, 4:-1].values
y_test = test_set.iloc[:, -1].values

# feature scaling
sc = StandardScaler()
x_train = sc.fit_transform(x_train)
x_test = sc.transform(x_test)

#RF classifier with training dataset
clf = RandomForestClassifier(bootstrap=True, n_estimators = 1000, criterion = 'gini',
random_state = 0, min_samples_split=2)
clf.fit(x_train, y_train)

#generate prediction
y_pred = clf.predict(x_test)

# save to file
```

```
with open('E:/python/ML/Chapter3_RF/Y_pred.csv', 'w', newline = '') as f:
    my_writer = csv.writer(f)
    #write the data into column
    for value in y_pred:
        my_writer.writerow([value])


#confusion matrix and calculate accuracy score
labels = np.unique(y_test)
cm = metrics.confusion_matrix(y_test, y_pred, labels= labels)
print(pd.DataFrame(cm, index=labels, columns=labels))
print("Accuracy:",metrics.accuracy_score(y_test, y_pred))

#feature important
feature_imp = pd.Series(clf.feature_importances_)
print(feature_imp)

#visualizing the feature importance
#%matplotlib inline
# Creating a bar plot
sns.barplot(x= feature_imp.index, y= feature_imp)
# Add labels to your graph
plt.xlabel('Features')
plt.ylabel('Feature Importance Score')
plt.title("Visualizing Important Features")
plt.legend()
plt.show()
```

B. Three classes of tree types and health in Python

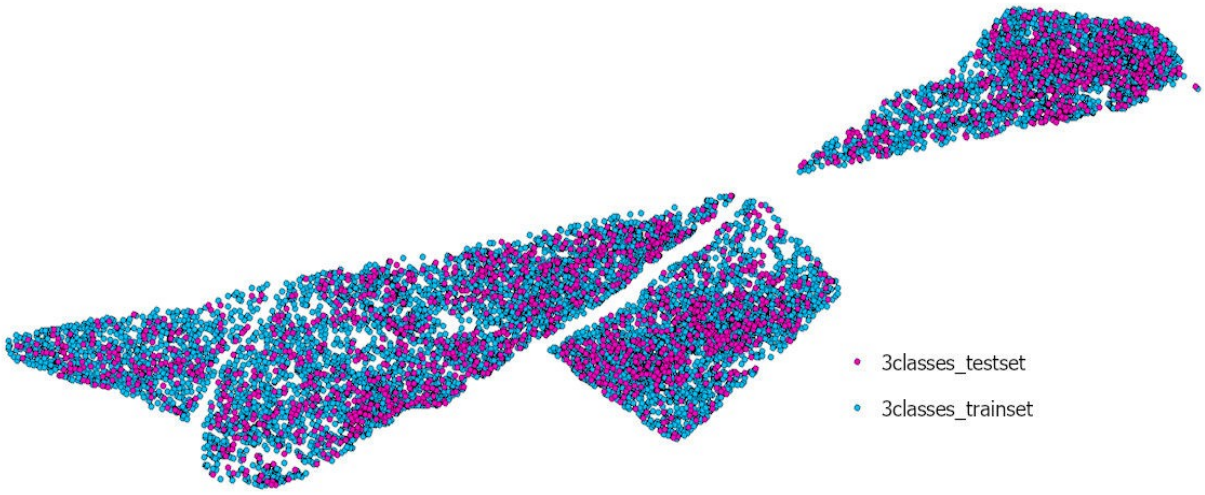

Figure 1: The distribution of training dataset and testing dataset for three classes of tree types and health

Table 1: The percentage of each tree type contribute into training set and test set

	Training set	**Test set**
Healthy fir	3191 (42.5 %)	790 (42 %)
Infested fir	3806 (50.6 %)	960 (51 %)
Deciduous	520 (6.9 %)	132 (7 %)
Total	**7517**	**1882**

Result

Table 2: Confusion matrix for the classification of only fir health

	healthy fir	infested fir	Deciduous
Healthy fir	579	169	42
Infested fir	284	668	8
Deciduous	74	5	53

Overall accuracy: 69.1 %

Table 3: Classification validation metrics

	precision	recall	f1-score
Healthy fir	0.62	0.73	0.67
Infested fir	0.79	0.70	0.74
Deciduous	0.51	0.40	0.45

Feature importance:

Aspect 0.224333

Elevation 0.545925

Slope 0.229742

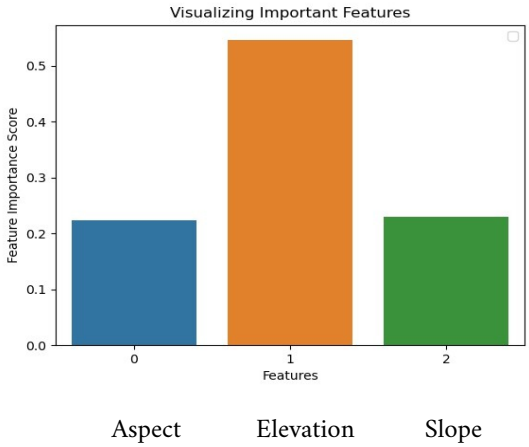

Figure 2: Feature importance of aspect, elevation and slope in the classification of tree types and health

C. Climate data

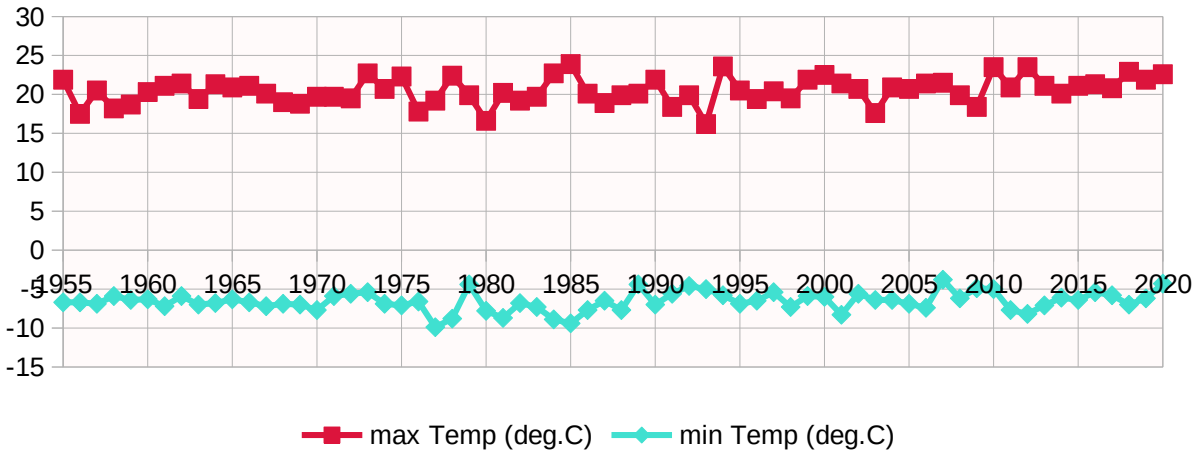

Figure 3: maximum and minimum temperature from 1954 to 2020 calculated for Zao Mountain at 1350 m

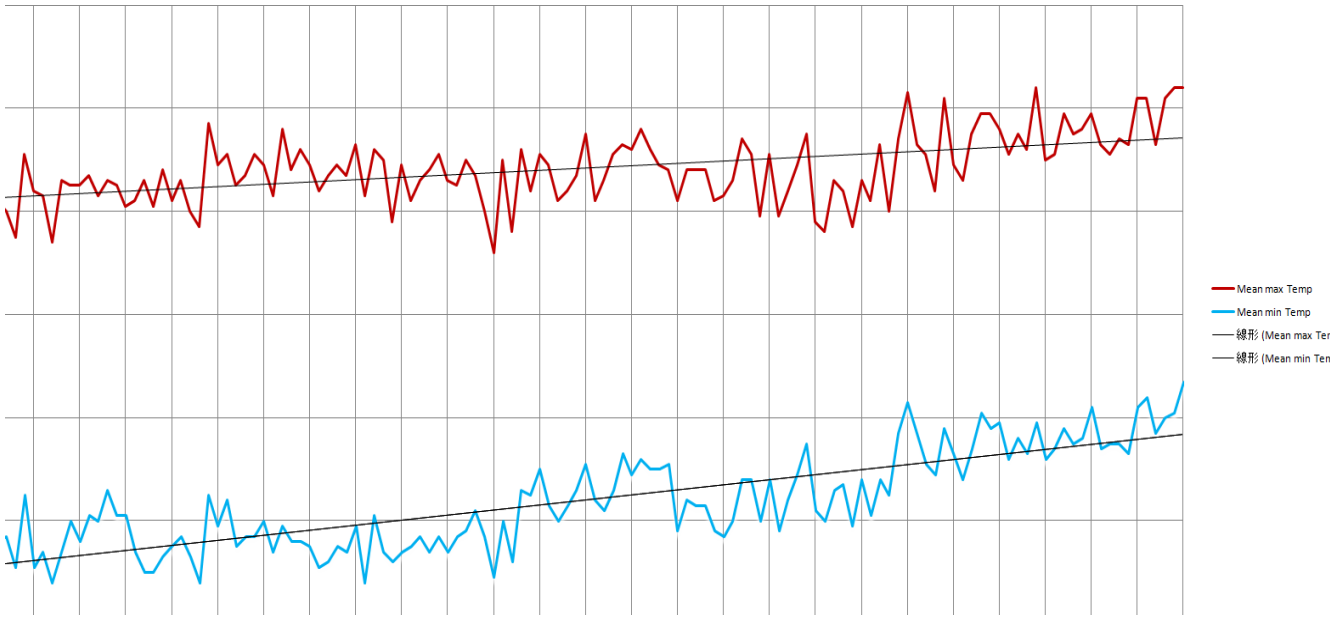

Figure 4: Mean maximum and minimum temperature trend from 1890 to 2020

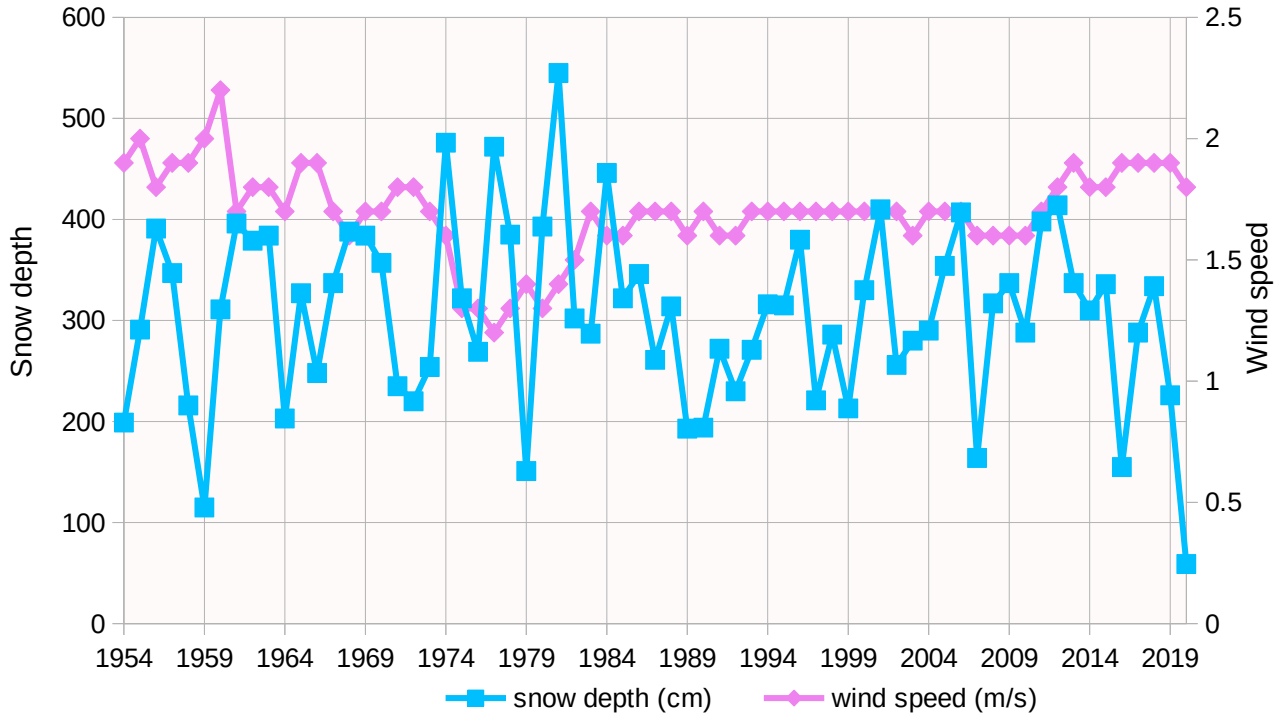

Figure 5: Snow depth and Wind speed observed at Yamagata station from 1954 to 2020